Cell Metabolism

Article

Downregulation of the kidney glucagon receptor, essential for renal function and systemic homeostasis, contributes to chronic kidney disease

Graphical abstract

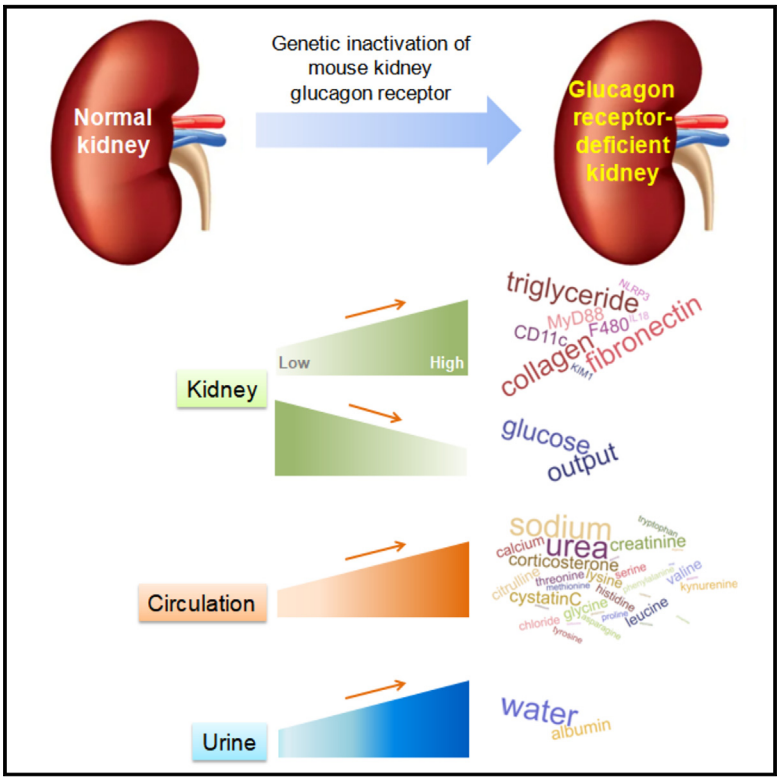

Highlights

- Kidney GCGR deficiency causes hyperaminoacidemia with reduced renal glucose output
- Kidney GCGR deficiency promotes renal lipid deposition, inflammation, and fibrosis
- Kidney GCGR deficiency induces systemic nitrogen, water, and electrolyte imbalances
- Kidney GCGR deficiency elicits hypertension

Authors

May-Yun Wang, Zhuzhen Zhang, Shangang Zhao, ..., Ruth Gordillo, Daniel J. Drucker, Philipp E. Scherer

Correspondence

philipp.scherer@utsouthwestern.edu

In brief

Wang et al. show that kidney glucagon receptor (GCGR)-deficient mice exhibit renal metabolic anomalies and homeostatic dysfunctions. These mice recapitulate several features of human chronic kidney disease (CKD), often associated with attenuated renal GCGR. Their study thus highlights a likely causative role of GCGR downregulation in the development of CKD.

Wang et al., 2024, Cell Metabolism *36*, 1–23
March 5, 2024
https://doi.org/10.1016/j.cmet.2023.12.024

CellPress

Cell Metabolism

CellPress

Article

Downregulation of the kidney glucagon receptor, essential for renal function and systemic homeostasis, contributes to chronic kidney disease

May-Yun Wang,[1] Zhuzhen Zhang,[1] Shangang Zhao,[1,2] Toshiharu Onodera,[1] Xue-Nan Sun,[1] Qingzhang Zhu,[1] Chao Li,[1] Na Li,[1] Shiuhwei Chen,[1] Megan Paredes,[1] Laurent Gautron,[3] Maureen J. Charron,[4] Denise K. Marciano,[5,6] Ruth Gordillo,[1] Daniel J. Drucker,[7,8] and Philipp E. Scherer[1,9,*]

[1]Touchstone Diabetes Center, University of Texas Southwestern Medical Center, Dallas, TX 75390, USA
[2]Sam and Ann Barshop Institute for Longevity and Aging Studies, Division of Endocrinology, Department of Medicine, University of Texas Health Science Center at San Antonio, San Antonio, TX 78229, USA.
[3]Center for Hypothalamic Research, Department of Internal Medicine, University of Texas Southwestern Medical Center, Dallas, TX 75390, USA
[4]Department of Biochemistry, Albert Einstein College of Medicine, Bronx, NY 10461, USA
[5]Division of Nephrology, Department of Internal Medicine, University of Texas Southwestern Medical Center, Dallas, TX 75390, USA
[6]Department of Cell Biology, University of Texas Southwestern Medical Center, Dallas, TX 75390, USA
[7]LunenfeldTanenbaumResearchInstitute, Mt. Sinai Hospital, Toronto, ON M5G1X5, Canada
[8]Department of Medicine, University of Toronto, Toronto, ON M5G 1X5, Canada
[9]Lead contact
*Correspondence: philipp.scherer@utsouthwestern.edu
https://doi.org/10.1016/j.cmet.2023.12.024

SUMMARY

The glucagon receptor (GCGR) in the kidney is expressed in nephron tubules. In humans and animal models with chronic kidney disease, renal GCGR expression is reduced. However, the role of kidney GCGR in normal renal function and in disease development has not been addressed. Here, we examined its role by analyzing mice with constitutive or conditional kidney-specific loss of the *Gcgr*. Adult renal *Gcgr* knockout mice exhibit metabolic dysregulation and a functional impairment of the kidneys. These mice exhibit hyperaminoacidemia associated with reduced kidney glucose output, oxidative stress, enhanced inflammasome activity, and excess lipid accumulation in the kidney. Upon a lipid challenge, they display maladaptive responses with acute hypertriglyceridemia and chronic proinflammatory and profibrotic activation. In aged mice, kidney *Gcgr* ablation elicits widespread renal deposition of collagen and fibronectin, indicative of fibrosis. Taken together, our findings demonstrate an essential role of the renal GCGR in normal kidney metabolic and homeostatic functions. Importantly, mice deficient for kidney *Gcgr* recapitulate some of the key pathophysiological features of chronic kidney disease.

INTRODUCTION

Chronic kidney disease (CKD) is a common disease characterized by the deterioration of kidney function over time, ultimately advancing to end-stage renal failure.[1] It constitutes a major global public health problem, since the prevalence of this disease is high. In 2017, 9.1% of the general population worldwide showed evidence of CKD.[2] Individuals with risk factors, such as diabetes mellitus, hypertension, or recurrent acute kidney injury, are susceptible to developing CKD. Furthermore, the risk of a negative impact on kidney outcomes is frequently increased for patients who survived COVID-19, even in the post-acute phase of the disease.[3] Patients with CKD exhibit a reduction of the renal glomerular filtration rate and/or signs of kidney damage (e.g., proteinuria), accompanied by a spectrum of pathophysiological derangements, ranging from fibrosis to microvascular rarefaction during disease progression. These individuals are also at a 2- to 4-fold higher risk of developing cardiovascular complications, resulting in increased morbidity and mortality.[4] Although enormous progress has been made toward a better understanding of the pathophysiology of CKD, the underlying mechanistic aspects of CKD pathogenesis and progression remain only partially understood.

Glucagon receptors (GCGRs) in the kidney are expressed mainly in the nephron segments of the thick ascending limb of the loop of Henle, the distal convoluted tubule, the connecting tubule, and the collecting duct, as determined by RNA sequencing (RNA-seq) and proteomic analysis.[5–7] GCGR expression is also detectable in the proximal tubule (the site of renal gluconeogenesis), the descending and thin ascending limbs of Henle's loop, the glomerulus (including podocytes and endothelial cells), and interstitial immune cells, even though the

Please cite this article in press as: Wang et al., Downregulation of the kidney glucagon receptor, essential for renal function and systemic homeostasis, contributes to chronic kidney disease, Cell Metabolism (2023), https://doi.org/10.1016/j.cmet.2023.12.024

expression levels are relatively low. The segmental regions with relatively high GCGR abundance have specific glucagon binding sites and exhibit glucagon-stimulated adenylyl cyclase activation and phospholipase C-dependent intracellular calcium mobilization.[8,9] Thus, these findings support the presence of a functionally active GCGR signaling cascade in the kidney.

However, in contrast to the extensive analysis of the function of the hepatic GCGRs, the role(s) of the kidney GCGRs has not been subjected to in-depth characterization. The precise physiological functions of renal GCGRs remain largely elusive. Nevertheless, numerous studies have shown the effects of glucagon on various aspects of kidney function, either directly through renal GCGR signaling or indirectly through other humoral factors.[10] First, administration of exogenous glucagon via infusion increases the renal glomerular filtration rate in humans and rodents,[11,12] indicating glucagon-induced renal vasodilation. In subjects with type 2 diabetes, the increment of blood glucose induced by glucagon infusion is positively correlated with present and future estimated glomerular filtration rates,[13] reflecting a relationship between reduced GCGR activity and overall nephron dysfunction. Second, glucagon modulates renal excretion of different filtered electrolytes, e.g., sodium, potassium, calcium, chloride, and phosphate ions,[14,15] suggesting a regulatory role of glucagon in renal handling of the systemic salt balance. Third, glucagon promotes urea excretion and urine concentration by the kidneys,[15,16] supporting a role in the maintenance of nitrogen and water balance system wide. Fourth, glucagon alters bicarbonate absorption by nephron segments,[17,18] suggesting a role in body fluid acid-base balance.

GCGRs in the liver play a critical role in the regulation of hepatic carbohydrate, lipid, and protein metabolism, as well as in liver metabolic zonation.[19–22] However, the regulatory action of kidney GCGRs on renal metabolism is less well defined. For example, it remains uncertain whether glucagon via GCGR regulates gluconeogenesis in kidneys, one of the major kidney functions. Glucagon was reported by some not to exert any significant effects on renal glucose synthesis.[23–25] Others concluded that glucagon stimulates glucose production by the kidney.[26,27] While glucagon can increase renal glucose transporter (GLUT)-mediated tubular glucose transport *in vitro*,[28] its role in tubular reabsorption of glucose from the glomerular filtrate by sodium-dependent glucose co-transporters (SGLTs) is unclear. Interestingly, inhibition of renal SGLT2 in humans and rodents causes hyperglucagonemia,[29,30] suggesting a potentially active feedback loop involving the kidney GCGR and SGLT2.

Human genetic studies reveal multiple associations of variants of the GCGR gene with a variety of clinical conditions or diseases. The G40S missense variant of the *GCGR* is linked to diabetes, hypertension, and central adiposity in some subgroups of study participants.[31–33] Several inactivating *GCGR* genetic variations (e.g., P86S) in humans cause Mahvash disease (glucagon cell adenomatosis).[34] In relation to kidney and liver function, individuals carrying the G40S, D63N, or F320del mutations exhibit some abnormalities, including altered sodium, potassium, and calcium ion handling; reduced glucagon-stimulated glucose production; and hyperaminoacidemia.[35–39] Moreover, human genome-wide association studies identify an association of single-nucleotide polymorphisms at the *GCGR* locus with hemoglobin concentration and hematocrit,[40] a trait closely related to kidney-produced erythropoietin. However, in none of these cases is it clear which tissue drives the reported phenotypic changes.

In CKD, kidney GCGR expression, and presumably its signaling activity, is dysregulated, as judged by transcriptomics analysis. For example, in a cohort of individuals with CKD of diverse disease etiologies (including diabetic nephropathy, hypertensive nephropathy, and the nephrotic syndrome), the expression of the kidney *GCGR* gene is significantly reduced in both the tubulointerstitium and the glomerulus.[41] A similar pattern of decreased renal *GCGR* expression is seen in another cohort of individuals with progressive CKD.[42] Interestingly, in the kidneys of subjects with diabetic nephropathy, *GCGR* expression is positively correlated with the estimated glomerular filtration rate,[43] in line with the aforementioned action of glucagon on renal filtration. Kidney GCGR expression is also altered in various animal models of CKD, e.g., diabetic nephropathy,[44] polycystic kidney disease,[45] X-linked hereditary nephropathy,[46] and induced kidney injury.[47,48] In all of these cases, kidney GCGR expression in diseased animals is significantly downregulated as the nephropathy progresses. These observations in human and animal studies therefore suggest a possible connection between reduced renal GCGR expression and CKD. However, whether such an impairment of kidney GCGR regulation directly contributes to the development of CKD is unknown.

Here, to elucidate the role of kidney GCGR in normal renal function and in disease development, we generated two new lines of mutant mice lacking the GCGR in kidney nephrons. The first kidney-specific knockout (KO) (designated as kidney KO) mouse line was generated by crossing the *Six2-Cre* mouse (*Six2* is expressed in metanephric mesenchymal stem cells during kidney development) and the *Gcgr*^{flox} mouse.[49,50] We studied the mice harboring heterozygous *Six2-Cre* and homozygous floxed (Flox) *Gcgr* alleles. During kidney organogenesis, the *Six2* promoter-driven *Cre* recombinase in nephron progenitor cells removes a loxP-flanked *Gcgr* coding sequence by recombination, thereby inactivating GCGR function in the *Six2* lineage cells of the kidney. The second KO (designated as inducible KO) mouse line carried the *Ksp*-reverse tetracycline controlled transactivator (*rtTA*), tetracycline-responsive element (*TRE*)-*Cre*, and Flox *Gcgr* alleles. In this mutant line, the targeted *Gcgr* coding segment in adult kidneys can be ablated by kidney tubule-specific, doxycycline (Dox)-inducible expression of *Cre* enzyme. For comparative analysis, we also specifically deleted the *Gcgr* gene in the mouse liver (designated as liver KO) by breeding the albumin-*Cre* mouse and the *Gcgr*^{flox} mouse, similar to the KO mice previously reported.[50] Our results demonstrate that presence of the kidney GCGR is required for the maintenance of systemic metabolic parameters, water, electrolyte, blood pressure, and redox and immune homeostasis. Mice with kidney-specific *Gcgr* inactivation exhibit several significant pathophysiological features of CKD. Hence, our findings support an important causative role of renal *GCGR* downregulation in CKD development, findings with translational implications.

RESULTS

Kidney-specific *Gcgr*-null mice show enhanced glucose tolerance and systemic insulin sensitivity

We first examined the expression of *Gcgr* mRNA in the kidneys of kidney KO and homozygous Flox control mice by quantitative

Please cite this article in press as: Wang et al., Downregulation of the kidney glucagon receptor, essential for renal function and systemic homeostasis, contributes to chronic kidney disease, Cell Metabolism (2023), https://doi.org/10.1016/j.cmet.2023.12.024

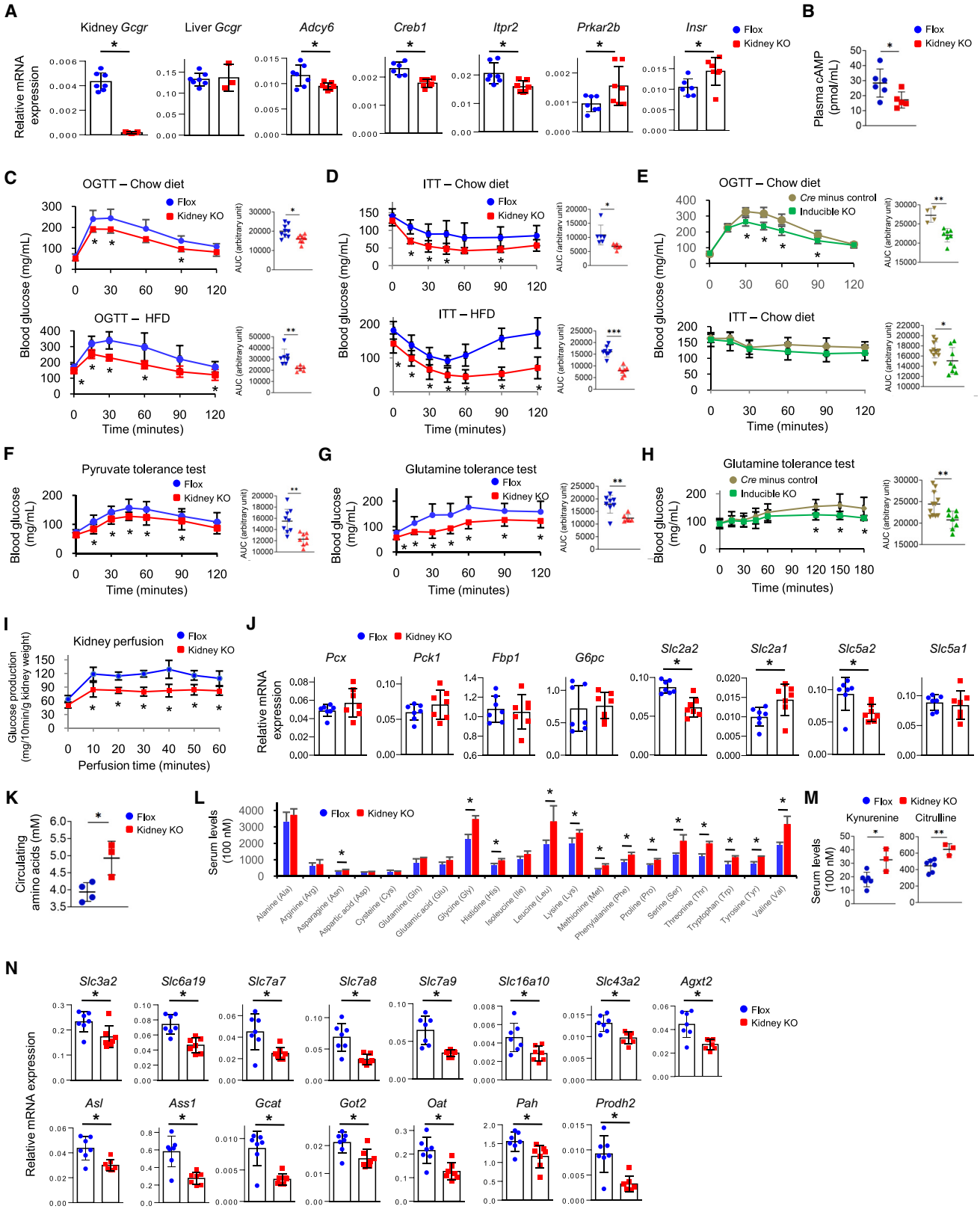

(legend on next page)

Please cite this article in press as: Wang et al., Downregulation of the kidney glucagon receptor, essential for renal function and systemic homeostasis, contributes to chronic kidney disease, Cell Metabolism (2023), https://doi.org/10.1016/j.cmet.2023.12.024

PCR (qPCR). Renal *Gcgr* transcripts were markedly reduced by 95% in the kidney KO mice, compared with controls (Figure 1A). In the control mice, the majority of *Gcgr*-positive renal cells showed co-expression with the tubular cell markers like *Slc12a1*, as revealed by RNAscope analysis (Figure S1A). In the KO mice, fluorescent signals for the remaining kidney *Gcgr* mRNA were mainly detected in the *Pecam1*-expressing endothelial cells (Figure S1A) that are known to derive from *Six2*-independent lineages.[49,51] Importantly, the expression of *Gcgr* mRNA in liver, stomach, small intestine, skeletal muscle, lung, brain, and facial bone from the KO mice was not changed (Figures 1A and S1B), with scatter in some tissues due to very low expression levels to start with. In the Dox-administered inducible KO mice, renal *Gcgr* expression levels were greatly decreased (Figure S1C), compared with those in similarly treated controls lacking the *TRE-Cre* allele (designated as *Cre* minus controls). These inducible KO mice also had normal *Gcgr* expression in non-renal tissues, including liver (Figure S1C).

We noticed that the mRNA levels of downstream effectors of the GCGR, such as adenylate cyclase (ADCY6), cyclic adenosine 3′, 5′-monophosphate (cAMP)-responsive element-binding protein 1 (CREB1), and inositol 1,4,5-triphosphate receptor (ITPR2), were slightly but significantly decreased in the kidneys from kidney KO mice (Figure 1A). In contrast, the transcript levels of insulin receptor (INSR) and the protein kinase A (inhibitory) regulatory subunit 2 beta (PRKAR2B) in the KO kidneys were significantly increased. Therefore, our results suggest a coordinated transcriptional response to the loss of GCGR signaling in the GCGR-deficient kidneys. Additional downstream mediators of GCGR signaling were also affected, even to the point that changes were apparent systemically: Levels of plasma cAMP (increased by glucagon stimulation of cells and extruded from cells via specific ATP-binding cassette transporters)[52,53] were significantly lower in kidney KO mice than in controls (Figure 1B).

Given the critical role that the GCGR exerts in metabolic homeostasis, we investigated the impact of renal *Gcgr* gene deletion on glucose metabolism. Kidney KO mice, both on a regular chow diet and on a high-fat diet (HFD), exhibited normal body weight, blood glucose, plasma insulin, and plasma glucagon at baseline (Figure S1D). The weights of both kidneys combined ("two-kidney weights") in kidney KO mice were comparable to controls, whereas those in liver KO and global KO mice were significantly higher (Figure S1E). To evaluate the disposal of a glucose load in renal GCGR-deficient mice, we conducted oral glucose tolerance tests (OGTTs). Kidney KO mice fed an HFD exhibited lower blood glucose excursions during the OGTTs than control mice, an effect which was apparent even when mice were fed a chow diet (Figure 1C).

Similarly, at temperatures considered to be within thermoneutrality (30°C) for mice, chow diet-fed kidney KO mice were more glucose-tolerant, while their body weights and food intake were normal (Figure S1F). These suggest enhanced insulin secretion and/or increased insulin action in kidney-specific KOs. Hepatic *Gcgr* KO mice (on an HFD), compared with controls, also displayed an improved response to the OGTT (Figure S1G), in line with earlier reports.[50] Our results from these tissue-specific GCGR-deficient mice indicate that the increased glucose disposal seen in global *Gcgr* KO[54,55] can be attributed to receptor deficiency not just in the liver but also in the kidney. To further characterize systemic insulin action in these mutant mice, we performed insulin tolerance tests. Blood glucose clearance in kidney KO mice following an insulin bolus was accelerated, compared with control mice (Figure 1D), consistent with increased whole-body insulin sensitivity. Remarkably, this

Figure 1. Kidney-specific *Gcgr*-null mice exhibit enhanced glucose tolerance, reduced renal glucose output, and hyperaminoacidemia

(A) qPCR analysis of kidney *Gcgr*, *Adcy6*, *Creb1*, *Itpr2*, *Prkar2b*, *Insr*, and liver *Gcgr* mRNA expression in kidney-specific *Gcgr* knockout (kidney KO) and floxed control (Flox) mice. Housekeeping gene 36b4 was used for normalization of gene transcript levels. *Gcgr*, glucagon receptor; *Adcy6*, adenylate cyclase type 6; *Creb1*, cAMP-responsive element-binding protein 1; *Itpr2*, inositol 1,4,5-triphosphate receptor type 2; *Prkar2b*, protein kinase A (inhibitory) regulatory subunit 2 beta; *Insr*, insulin receptor. Results are represented as mean ± SD; n = 7 mice per group; *p < 0.05 by Student's t test.

(B) Plasma cAMP levels of kidney KO and Flox mice. n = 5–6 mice per group; *p < 0.05.

(C and D) Blood glucose levels during oral glucose tolerance tests (OGTTs) (C) or insulin tolerance tests (ITTs) (D) performed in chow diet- or high-fat diet (HFD)-fed kidney KO and Flox mice. AUC, area under the curve. n = 5–7 mice per group; *p < 0.05, **p < 0.01, ***p < 0.001.

(E) Blood glucose levels during OGTTs or ITTs in inducible *Gcgr* KO and *Cre* minus control mice. AUC, area under the curve. n = 4–9 mice per group; *p < 0.05, **p < 0.01.

(F and G) Blood glucose levels during pyruvate tolerance tests (F) or glutamine tolerance tests (G) performed in chow diet-fed kidney KO and Flox mice. AUC, area under the curve. n = 8–10 mice per group; *p < 0.05, **p < 0.01.

(H) Blood glucose levels during glutamine tolerance tests performed in inducible *Gcgr* KO and *Cre*-minus control mice. AUC, area under the curve. n = 8–11 mice per group; *p < 0.05, **p < 0.01.

(I) Time course of glucose release into the perfusate solution by perfused kidneys from kidney KO and Flox mice. Gluconeogenic substrate mixture (pyruvate, glutamine, and lactate) was present at time zero. The perfusate was subsequently sampled at 10-min intervals for glucose analysis. n = 3–5 kidneys per group; *p < 0.05.

(J) qPCR analysis of renal gluconeogenic and glucose transport gene expression in kidney KO and Flox mice. *Pcx*, pyruvate carboxylase; *Pck1*, phosphoenol pyruvate carboxykinase; *Fbp1*, fructose-1,6-biphosphatase; *G6pc*, glucose-6-phosphatase catalytic subunit 1; *Slc2a2*, glucose transporter GLUT2; *Slc2a1*, glucose transporter GLUT1; *Slc5a2*, sodium-glucose co-transporter SGLT2; *Slc5a1*, sodium-glucose co-transporter SGLT1. n = 7 mice per group; *p < 0.05.

(K) Serum levels of total amino acids, exclusive of glycine, in kidney KO and Flox mice. n = 3–4 mice per group; *p < 0.05.

(L) Serum amino acid profiles in kidney KO and Flox mice. n = 3–6 mice per group; *p < 0.05.

(M) Serum levels of kynurenine, a tryptophan metabolite, and citrulline, a urea cycle intermediate, in kidney KO and Flox mice. n = 3–6 mice per group; *p < 0.05, **p < 0.01.

(N) qPCR analysis of kidney amino acid transport and degradation gene expression in kidney KO and Flox mice. *Slc3a2*, solute carrier family 3 member 2; *Slc6a19*, solute carrier family 6 member 19; *Slc7a7*, solute carrier family 7 member 7; *Slc7a8*, solute carrier family 7 member 8; *Slc7a9*, solute carrier family 7 member 9; *Slc16a10*, solute carrier family 16 member 10; *Slc43a2*, solute carrier family 43 member 2; *Agxt2*, alanine-glyoxylate aminotransferase 2; *Asl*, argininosuccinate lyase; *Ass1*, argininosuccinate synthase; *Gcat*, 2-amino-3-ketobutyrate coenzyme A ligase; *Got2*, aspartate aminotransferase; *Oat*, ornithine aminotransferase; *Pah*, phenylalanine-4-hydroxylase; *Prodh2*, hydroxyproline dehydrogenase. n = 6–7 mice per group; *p < 0.05.

Please cite this article in press as: Wang et al., Downregulation of the kidney glucagon receptor, essential for renal function and systemic homeostasis, contributes to chronic kidney disease, Cell Metabolism (2023), https://doi.org/10.1016/j.cmet.2023.12.024

finding was observed even in renal GCGR KO mice on a regular chow diet. In inducible KO mice fed the chow diet, we observed similar increases in insulin sensitivity, as illustrated by the OGTT and insulin tolerance test, with no change in body weight (Figures 1E and S1H).

Kidney-specific *Gcgr*-null mice exhibit reduced renal glucose output due to a limited amino acid substrate pool

Endogenous glucose synthesis via gluconeogenesis is one of the major kidney functions.[56] In the post-absorptive state, renal proximal tubules are involved in glucose production and glucose release into the blood circulation. To determine the impact of renal GCGR deficiency on glucose synthesis and release, we carried out metabolic tolerance tests using various renal gluconeogenic precursors, such as pyruvate and glutamine. Intraperitoneal injection of a pyruvate load caused a typical increase in blood glucose in control mice (Figure 1F), indicating the release of newly formed glucose driven by pyruvate. However, this increase in glucose levels was significantly reduced in kidney KO mice (Figure 1F). In kidney KO versus control mice subjected to a glutamine bolus, the blood glucose excursions were also less pronounced (Figure 1G). Moreover, inducible KO mice exhibited similar decreases in glucose production driven by glutamine (Figure 1H). Like liver KO and global KO mice, kidney KO and inducible KO mice displayed relatively low blood glucose levels in response to the administration of a long-acting glucagon analog IUB288 (Figure S2A). Consistent with these *in vivo* results, *ex vivo* perfused kidneys from kidney KO mice, when provided with a gluconeogenic substrate mixture (pyruvate, glutamine, and lactate), released significantly less glucose into the perfusate solution (Figure 1I). Collectively, these findings reflect impaired glucose output by the GCGR-null kidneys.

To gain further insights into the reduction of renal glucose output, we analyzed mRNA expression of key genes involved in renal gluconeogenesis and glucose transport by qPCR. The expression levels of the gluconeogenic genes pyruvate carboxylase (*Pcx*), phosphoenol pyruvate carboxykinase (*Pck1*), fructose-1,6-biphosphatase (*Fbp1*), and glucose 6-phosphatase (*G6pc*) were comparable in kidneys from kidney KO and control mice (Figure 1J). However, the transcripts for the facilitative glucose transporter GLUT2 (SLC2A2) and sodium-glucose cotransporter SGLT2 (SLC5A2) were significantly reduced in *Gcgr*-deficient kidneys (Figure 1J). The expression levels of genes for other transporters, such as Glut1 (*Slc2a1*; low abundance compared with *Slc2a2*) and Sglt1 (*Slc5a1*), were either increased or normal, respectively (Figure 1J). The expression and activity of most of the proteins encoded by these mRNAs is restricted to the proximal tubules.[7,57] Therefore, our analysis suggests that diminished glucose transporter expression in the proximal tubules can contribute to the decrease of glucose output from the kidneys lacking GCGR.

Previous studies suggested a role for glucagon in the stimulation of renal gluconeogenesis during fasting.[26] To determine whether kidney GCGR is required for this induction, we measured renal mRNA levels of gluconeogenic genes in the fed and fasted states. Our results show that upon 24 h fasting, the induction of renal *Pcx*, *Pck1*, and *G6pc* mRNA expression remained comparable in kidney KO versus Flox control mice (Figure S2B). As expected, fasting had no effect on the levels of *Gcgr* transcripts in control and KO kidneys (Figure S2B). Our findings suggest that fasting-induced increases in kidney gluconeogenic gene expression are independent of the presence of the renal GCGR. However, we demonstrate an association of renal adiponectin with gluconeogenic gene expression during fasting.[58] Thus, it is possible that renal adiponectin, but not the renal GCGR, mediates the adaptive response of kidney gluconeogenesis to fasting in mice.

Amino acids, except for leucine and lysine, are important sources of carbon skeletons for gluconeogenesis through their degradation into pyruvate or citric acid cycle intermediates.[59] Amino acid homeostasis is significantly impaired in global *Gcgr* KO mice.[60,61] To evaluate whether amino acid metabolism in *Gcgr*-deficient kidneys plays a role in the decrease of renal glucose output, we observed that, as previously reported for the global KO mice, both kidney KO and liver KO mice displayed increased amino acid levels in serum (hyperaminoacidemia) (Figures 1K and S2C). However, they had distinct patterns of serum amino acid profiles (Figures 1L and S2D). For example, serum amino acids phenylalanine and tryptophan (Trp) were increased in kidney KOs but not in liver KO mice, whereas alanine, isoleucine, glutamic acid, glutamine, and arginine were increased in liver KOs but not in kidney KO mice. Moreover, the Trp metabolite kynurenine and urea cycle intermediate citrulline in serum, two early CKD biomarkers that are higher in patients with CKD than in CKD-free subjects,[62] were also elevated in kidney KO mice (Figure 1M). Given the normal expression of hepatic *Gcgr* mRNA in kidney KO mice (Figure 1A), the observation of hyperaminoacidemia in these mutant mice suggests defective amino acid transport and catabolism in *Gcgr*-null kidneys. Our qPCR analysis indicate that the mRNA levels of genes involved in renal amino acid transport (*Slc3a2*, *Slc6a19*, *Slc7a7*, *Slc7a8*, *Slc7a9*, *Slc16a10*, and *Slc43a2*) and degradation (*Agxt2*, *Asl*, *Ass1*, *Gcat*, *Got2*, *Oat*, *Pah*, and *Prodh2*) were decreased in kidney KO mice (Figure 1N). Therefore, these results suggest that in kidney KO mice, the coordinated transcriptional repression of the genes for kidney amino acid catabolism and transport contributes to the attenuation of renal glucose output by reducing the availability of amino acid-derived gluconeogenic substrates in the mutant tissue.

Kidney-specific *Gcgr*-null mice display a dysregulation of body nitrogen and water balance

Excretion of excess nitrogenous compounds, such as protein-derived urea and muscle creatine-derived creatinine, is another major function of the kidney. Given the impairment of amino acid metabolism in kidney KO mice described above, we examined metabolic nitrogen balance in our mutant mice by measuring blood urea nitrogen (BUN) and serum creatinine levels. Chow diet-fed kidney KO mice at 5 months of age displayed azotemia with significantly elevated BUN but normal serum creatinine concentrations, whereas those aged 24 months had increased levels of both BUN and creatinine (Figure 2A), indicating dysfunctional urinary nitrogen excretion in the context of a renal GCGR loss. qPCR analysis showed that *Gcgr*-null kidneys of kidney KO mice had higher expression levels of urea transporters (UTA1, UTA2, UTA3, and UTB) than the Flox controls (Figure 2B), suggesting enhanced

Please cite this article in press as: Wang et al., Downregulation of the kidney glucagon receptor, essential for renal function and systemic homeostasis, contributes to chronic kidney disease, Cell Metabolism (2023), https://doi.org/10.1016/j.cmet.2023.12.024

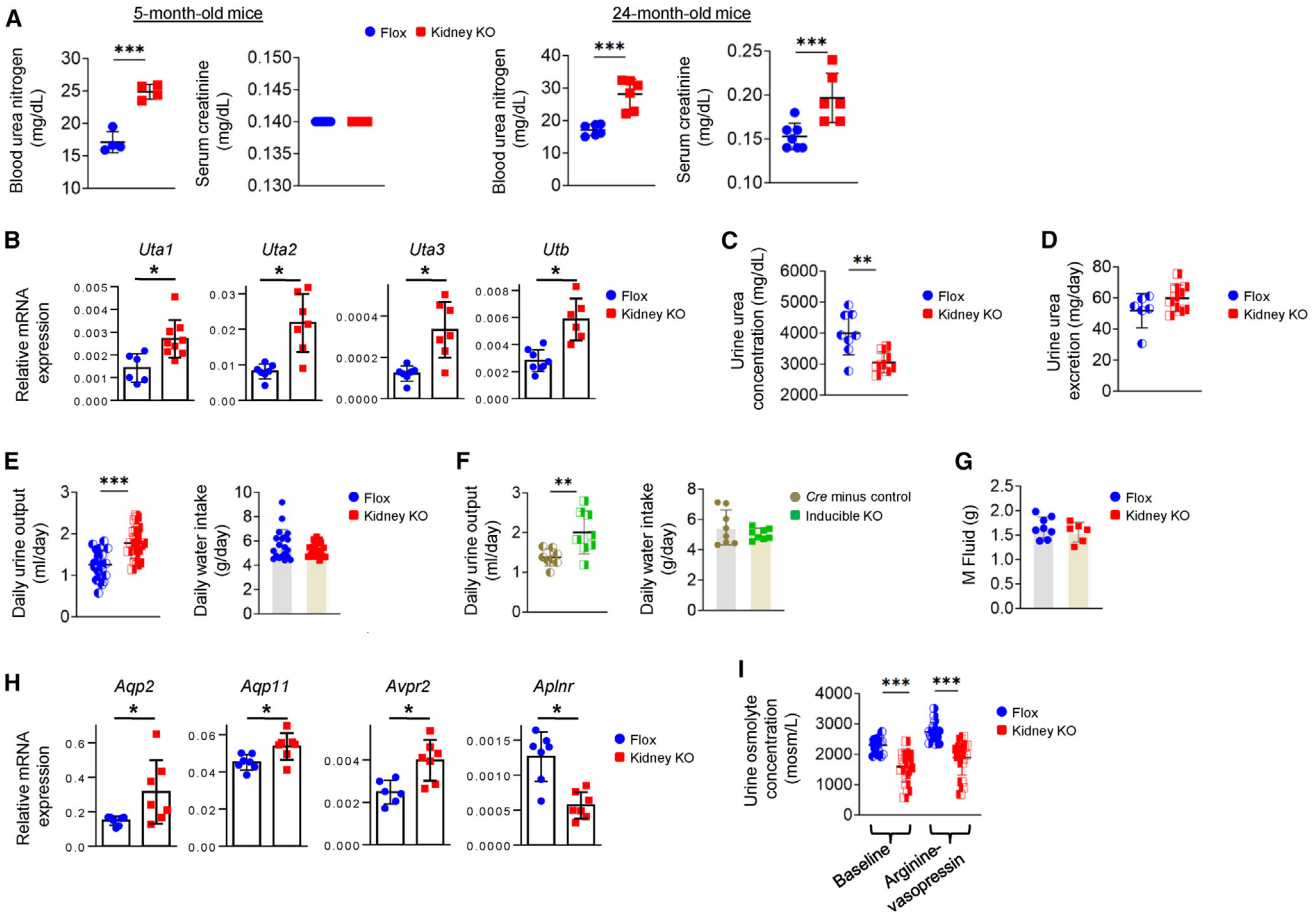

Figure 2. Kidney-specific *Gcgr*-null mice display nitrogen and water imbalance

(A) Serum levels of blood urea nitrogen and creatinine in kidney-specific *Gcgr* knockout (kidney KO) and floxed control (Flox) mice at 5 or 24 months of age. n = 4–6 mice per group; ***p < 0.001.

(B) qPCR analysis of kidney urea transporter (UTA1, UTA2, UTA3, and UTB) gene expression in kidney KO and Flox mice. n = 5–7 mice per group; *p < 0.05.

(C) Concentrations of urinary urea in kidney KO and Flox mice. n = 6–8 mice per group; **p < 0.01.

(D) Total daily urinary urea excretion in kidney KO and Flox mice. n = 6–10 mice per group.

(E) Total daily urine output and water intake in kidney KO and Flox mice. n = 10 mice per group; ***p < 0.001.

(F) Total daily urine output and water intake in inducible *Gcgr* KO and *Cre* minus control mice. n = 8 mice per group; **p < 0.01.

(G) Whole-body fluid content in kidney KO and Flox mice. M Fluid (g) is Free Body Fluid Mass in grams. n = 5–7 mice per group.

(H) qPCR analysis of kidney water channel (*Aqp2* and *Aqp11*), vasopressin-V2 receptor (*Avpr2*), and apelin receptor (*Aplnr*) gene expression in kidney KO and Flox mice. n = 6–7 mice per group; *p < 0.05.

(I) Urinary osmolyte concentrations in kidney KO and Flox mice in response to 4-h arginine-vasopressin treatment. n = 15–16 mice per group; ***p < 0.001.

reabsorption of filtered urea along the mutant nephron. Compared with the kidney-specific KO mice, the liver KO mice at young ages exhibited a distinct pattern of excess nitrogen in the blood. Their serum creatinine levels were increased with no changes in BUN (Figure S3A), similar to the parameters measured in global *Gcgr* KO mice (Figure S3B). In addition to the possible changes in urea reabsorption, the increase in BUN in the kidney KO mice could also be associated with excessive urine production (see below) in these mice. However, global KO mice with similar body water imbalance showed normal BUN levels, suggesting differential effects in our KOs. Overall, our data highlight that the kidney GCGR is required for the maintenance of a systemic nitrogen balance, consistent with previously established links between glucagon and nitrogen metabolism, as well as urea disposal.[10]

Our examination of urinary urea revealed that the concentrations of urine urea in kidney KO and global KO mice were significantly reduced (Figures 2C and S3C), suggesting an impaired ability for concentrating urea in urine. Nevertheless, the daily excretion of urea in the urine in these mice remained normal (Figures 2D and S3D). We observed that kidney KO mice had increased daily urine volume; however, our water intake measurements failed to reveal significant differences within the accuracy of our fluid intake measurements (Figure 2E). At thermoneutrality (30°C), these mutant mice also excreted a larger volume of urine per day (Figure S3E). Similarly, inducible KO mice showed excess urine output, but we were unable to observe a concomitant increase in water intake within the accuracy of our measurements (Figure 2F). Moreover, levels of whole-body fluid content were not different in kidney KO mice compared with Flox

Please cite this article in press as: Wang et al., Downregulation of the kidney glucagon receptor, essential for renal function and systemic homeostasis, contributes to chronic kidney disease, Cell Metabolism (2023), https://doi.org/10.1016/j.cmet.2023.12.024

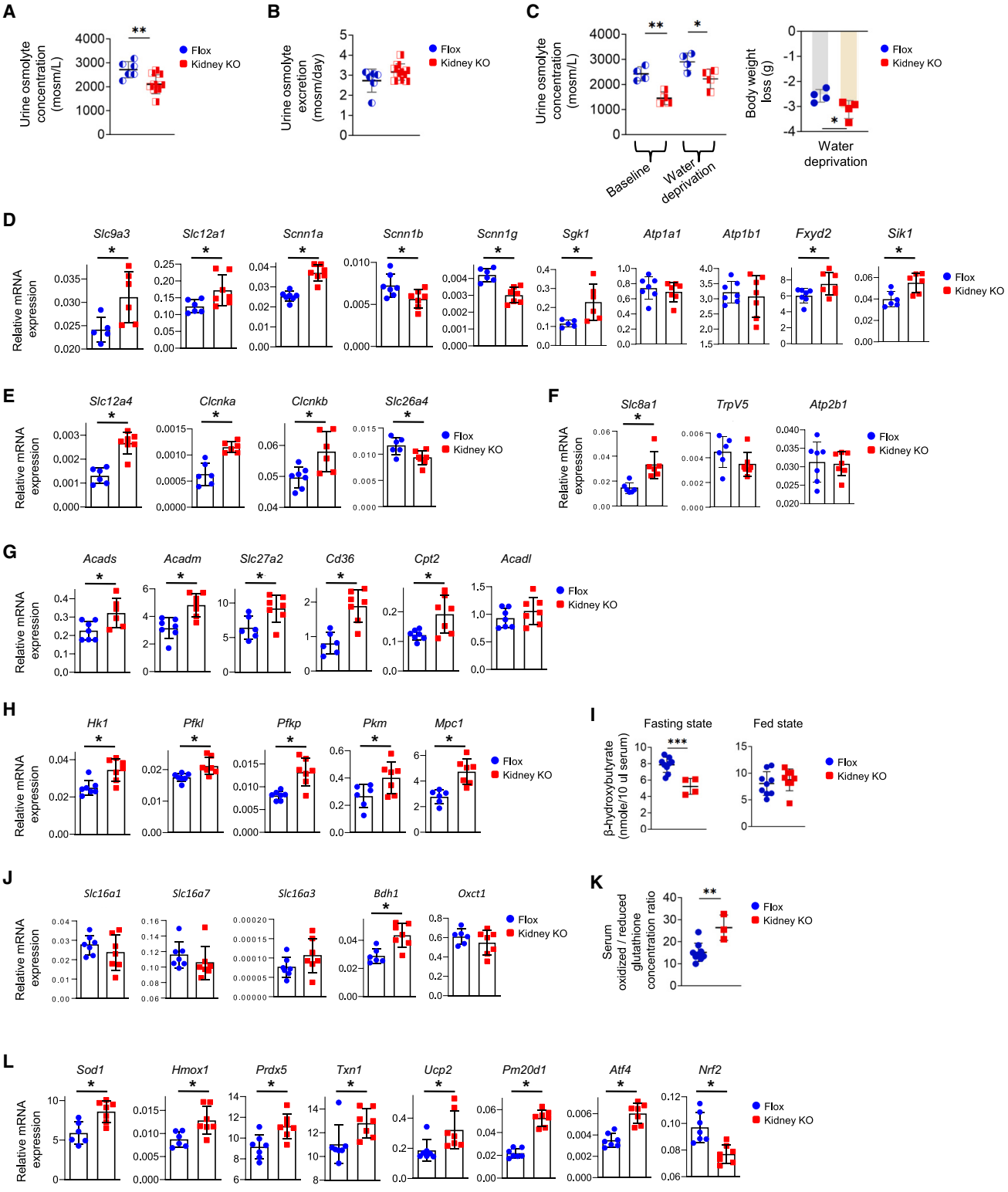

Figure 3. Kidney-specific *Gcgr*-null mice show electrolyte imbalance and have chronic oxidative stress

(A) Concentrations of urinary osmolytes in kidney-specific *Gcgr* knockout (kidney KO) and floxed control (Flox) mice. n = 6–9 mice per group; $^{**}p < 0.01$.

(B) Total daily urinary osmolyte excretion in kidney KO and Flox mice. n = 6–9 mice per group.

(C) Urinary osmolyte concentrations and body weight loss in kidney KO and Flox mice in response to 24-h water deprivation. n = 4 mice per group; $^{*}p < 0.05$, $^{**}p < 0.01$.

(legend continued on next page)

Please cite this article in press as: Wang et al., Downregulation of the kidney glucagon receptor, essential for renal function and systemic homeostasis, contributes to chronic kidney disease, Cell Metabolism (2023), https://doi.org/10.1016/j.cmet.2023.12.024

controls (Figure 2G). Consistent with these observations, kidney-specific and global *Gcgr* KO mice had normal levels of plasma renin activity (Figure S3F), indicative of no significant changes in renin-mediated extracellular fluid retention. By comparison, liver KO mice exhibited normal urine urea concentrations and excretion and had no change in body fluid homeostasis (Figures S3G and S3H). Therefore, these results suggest an increase of urinary water excretion specifically in *Gcgr*-null kidneys. The pathway(s) mediating a necessary compensatory water loss, e.g., through the footpads, respiratory tract, skin, etc.,[63,64] to make up for these differences in our kidney KO mice remains to be determined.

To gain insights into the molecular basis for the increased urine output in mutant kidneys, we measured the mRNA expression of genes encoding renal water channels (aquaporins [AQPs]). In kidney KO mice, renal *Aqp1*, *Aqp3*, *Aqp6*, and *Aqp7* expression levels were normal and *Aqp4* levels were decreased (Figure S3I). However, *Aqp2* and *Aqp11* transcripts, as well as AQP2 protein, were increased (Figures 2H and S3J). Arginine vasopressin V2 receptor (AVPR2) and the somewhat more controversial counteracting apelin-apelin receptor (APLNR) pathways may play a key role in the regulation of body fluid balance.[65,66] Renal *Avpr2* mRNA expression in the mutant mice was elevated, while *Aplnr* transcript levels were reduced (Figure 2H). Upon a stimulus of antidiuretic hormone AVP, the concentrations of urine osmolytes in administered kidney KO mice, compared with similarly treated Flox controls, remained low (Figure 2I).

Unlike control mice showing significant increases (with $p = 0.000085$), kidney KO mice had comparable urinary osmolyte concentrations (with $p = 0.13$) upon vasopressin treatment, compared with baseline (Figure 2I), reflecting a reduced response to the stimulation. Hence, our analysis suggests that kidney KO mice displayed adaptive responses to the excess loss of water via altered *Aqp2*, *Avpr2*, and *Aplnr* expression. However, these feedback responses were ineffective or blunted, probably due to post-receptor regulatory defects of water transport in the *Gcgr*-deficient nephrons.

Similar to the kidney KO mice described above, previous reports argued that female global glucagon (*Gcg*)-deficient mice exhibit polyuria.[67] Here, we provide further evidence that global *Gcgr* KO mice also displayed polyuria (Figure S3K). Notably, their daily urine output excess was much higher than that of kidney KO mice. Unlike kidney KO mice, global KO mice showed significantly attenuated expression of renal *Aqp1* through *Aqp4*, *Aqp6*, and *Aqp7* (Figure S3L), suggesting an extensive loss of fluids due to reduced reabsorption by all major AQPs. In addition, we noticed that these global KO mice indeed had increased water intake (Figure S3M), a change not seen in the kidney KO mice (Figure 2E). These findings highlight both an intrarenal and an extrarenal dysregulation of body fluid homeostasis in global *Gcgr* KO mice. Therefore, our data indicates that the kidney GCGR is at least partially responsible for the maintenance of whole-body water balance, and its deficiency triggers significant changes in many of the fluid parameters.

Kidney-specific *Gcgr*-null mice show derangements of electrolyte balance

We assessed the handling of various electrolytes, an important renal function, to see whether this aspect of kidney physiology is affected as well in the *Gcgr*-null kidneys. The concentrations of urine osmolytes in kidney KO and global KO mice were significantly decreased (Figures 2I, 3A, and S4A), probably associated with the excessive urine production (Figures 2E and S3K). The daily urine osmolyte excretion either showed a trend toward an increase in the kidney KOs or was significantly increased in the global KOs (Figures 3B and S4B). By contrast, liver KO mice had normal levels of these urine parameters (Figures S4C and S4D).

Water deprivation studies show that urinary osmolality was lower in dehydrated kidney KO mice than in water-deprived

(D) qPCR analysis of kidney mRNA expression of genes involved in handling sodium transport and homeostasis in kidney KO and Flox mice. *Slc9a3*, sodium-hydrogen exchanger Nhe3; *Slc12a1*, sodium-potassium-chloride co-transporter Nkcc2; *Scnn1a*, amiloride-sensitive sodium channel subunit alpha; *Scnn1b*, amiloride-sensitive sodium channel subunit beta; *Scnn1g*, amiloride-sensitive sodium channel subunit gamma; *Sgk1*, serine/threonine-protein kinase Sgk1; *Atp1a1*, sodium/potassium-ATPase subunit alpha-1; *Atp1b1*, sodium/potassium-ATPase subunit beta-1; *Fxyd2*, sodium/potassium-ATPase subunit gamma; *Sik1*, serine/threonine-protein kinase Sik1. n = 5–7 mice per group; *$p < 0.05$.

(E) qPCR analysis of kidney mRNA expression of genes involved in handling chloride transport in kidney KO and Flox mice. *Slc12a4*, potassium-chloride co-transporter Kcc1; *Clcnka*, chloride channel ClC-Ka; *Clcnkb*, chloride channel ClC-Kb; *Slc26a4*, solute carrier family 26 member 4 (pendrin). n = 5–7 mice per group; *$p < 0.05$.

(F) qPCR analysis of kidney mRNA expression of genes involved in handling calcium transport in kidney KO and Flox mice. *Slc8a1*, sodium-calcium exchanger Ncx1; *TrpV5*, transient receptor potential cation channel subfamily V member 5; *Atp2b1*, plasma membrane calcium-transporting ATPase. n = 5–7 mice per group; *$p < 0.05$.

(G) qPCR analysis of kidney fatty acid oxidation and lipid transport gene expression in kidney-specific *Gcgr* knockout (kidney KO) and floxed control (Flox) mice. Housekeeping gene 36b4 was used for normalization of gene transcript levels. *Acads*, short-chain-specific acyl-CoA dehydrogenase; *Acadm*, medium-chain-specific acyl-CoA dehydrogenase; *Slc27a2*, fatty acid transport protein 2; *Cd36*, platelet glycoprotein 4; *Cpt2*, carnitine O-palmitoyltransferase 2; *Acadl*, long-chain-specific acyl-CoA dehydrogenase. n = 6–7 mice per group; *$p < 0.05$.

(H) qPCR analysis of renal glycolytic and mitochondrial pyruvate transport gene expression in kidney KO and Flox mice. *Hk1*, hexokinase-1; *Pfkl*, ATP-dependent 6-phosphofructokinase, liver type; *Pfkp*, ATP-dependent 6-phosphofructokinase, platelet type; *Pkm*, pyruvate kinase Pkm; *Mpc1*, mitochondrial pyruvate carrier 1. n = 6–7 mice per group; *$p < 0.05$.

(I) Levels of circulating ketone β-hydroxybutyrate in kidney KO and Flox mice in the fasting and fed states. n = 4–9 mice per group; ***$p < 0.001$.

(J) qPCR analysis of renal ketone metabolism gene expression in kidney KO and Flox mice. *Slc16a1*, monocarboxylate transporter Mct1; *Slc16a7*, monocarboxylate transporter Mct2; *Slc16a3*, monocarboxylate transporter Mct4; *Bdh1*, D-β-hydroxybutyrate dehydrogenase; *Oxct1*, succinyl-CoA:3-ketoacid coenzyme A transferase 1. n = 7 mice per group; *$p < 0.05$.

(K) Ratio of serum oxidized over reduced glutathione concentrations in kidney KO and Flox mice. n = 3–8 mice per group; **$p < 0.01$.

(L) qPCR analysis of renal antioxidant and redox-sensitive gene expression in kidney KO and Flox mice. *Sod1*, superoxide dismutase; *Hmox1*, heme oxygenase 1; *Prdx5*, peroxiredoxin 5; *Txn1*, thioredoxin 1; *Ucp2*, uncoupling protein 2; *Pm20d1*, peptidase M20 domain-containing 1; *Atf4*, cAMP-dependent transcription factor Atf-4; *Nrf2*, nuclear factor erythroid-derived 2-related factor 2. n = 6–7 mice per group; *$p < 0.05$.

Please cite this article in press as: Wang et al., Downregulation of the kidney glucagon receptor, essential for renal function and systemic homeostasis, contributes to chronic kidney disease, Cell Metabolism (2023), https://doi.org/10.1016/j.cmet.2023.12.024

Table 1. Serum and urine electrolyte parameters in kidney-specific *Gcgr* knockout and floxed control mice

	Floxed control	Kidney knockout
Electrolyte concentration[a]		
Serum sodium (mM)	147.0 ± 1.4	150.5 ± 2.6[b]
Serum potassium (mM)	7.0 ± 1.2	7.3 ± 1.4
Serum calcium (mg/dL)	10.1 ± 0.3	10.6 ± 0.3[b]
Serum chloride (mM)	110.8 ± 1.3	114.8 ± 3.2[b]
Serum phosphate (mg/dL)	10.5 ± 1.8	10.5 ± 1.4
Urine sodium (mM)	188.9 ± 23.6	146.4 ± 16.3[b]
Urine potassium (mM)	298.9 ± 35.8	225.7 ± 41.7[b]
Urine calcium (mg/dL)	7.9 ± 0.5	5.6 ± 1.9[b]
Urine chloride (mM)	279.0 ± 20.5	223.0 ± 36.8[b]
Urine phosphate (mg/dL)	168.9 ± 47.1	127.7 ± 53.8
Daily electrolyte excretion[a]		
Urine sodium (mmol/day)	0.19 ± 0.05	0.23 ± 0.06
Urine potassium (mmol/day)	0.30 ± 0.06	0.34 ± 0.05
Urine calcium (mg/day)	0.08 ± 0.02	0.09 ± 0.04
Urine chloride (mmol/day)	0.28 ± 0.06	0.34 ± 0.06
Urine phosphate (mg/day)	1.70 ± 0.59	1.85 ± 0.50

[a]Values are expressed as mean ± SD; n = 6–9 mice per group.
[b]$p < 0.05$ versus floxed control.

Flox control mice, although the urine osmolyte concentrations, compared with the respective levels at baseline, were increased in each strain of mice following 24-h water deprivation (Figure 3C). Additionally, kidney KO mice exhibited a greater body weight loss in response to dehydration. These findings suggest impaired urinary concentrating capacity in kidney KO mice relative to the controls.

The kidney KO and the global KO mice showed overall somewhat distinct alterations in urine and serum electrolyte profiles, although they both were polyuric. In kidney KO mice, urinary sodium, potassium, calcium, chloride, and phosphate concentrations were reduced or trended lower, while their overall daily excretion was normal (Table 1). In global *Gcgr* KO mice, urine ion concentrations were decreased (sodium, potassium, and chloride) or normal (calcium and phosphate), but their daily excretion was increased across the board (Table S1). Moreover, in kidney KO mice, the levels of serum sodium, calcium, and chloride were elevated, whereas potassium and phosphate concentrations were normal (Table 1). In global KO mice, serum potassium and calcium were increased, while sodium, chloride, and phosphate remained normal (Table S1). Both urine and serum pH values were normal in kidney KO and global KO mice, compared with their respective controls (Figures S4E and S4F). Hence, our results indicate a significant imbalance of multiple electrolytes in the mice with renal *Gcgr* deficiency, consistent with a suggested possible role of glucagon in renal handling of ionic solutes previously reported.[10]

To explore the possible molecular basis of this electrolyte imbalance, we examined the mRNA expression of renal proteins involved in handling ion transport and homeostasis in kidney KO versus Flox control mice by qPCR. Sodium reabsorption via transcellular mechanism by the renal nephrons involves the apical sodium (Na)-hydrogen exchanger NHE3 (SLC9A3), the sodium (Na)-potassium (K)-chloride co-transporter NKCC2 (SLC12A1), the sodium (Na)-chloride co-transporter NCC (SLC12A3), and the epithelial sodium (Na) channel ENaC (SCNN1), as well as the basolateral sodium-potassium-ATPase and sodium (Na)-bicarbonate co-transporter NBC1 (SLC4A4).

The expression levels of the apical transporter genes *Slc9a3*, *Slc12a1*, and *Scnn1a* were elevated in *Gcgr*-null kidneys (Figure 3D). Whole-kidney SLC9A3 (NHE3) protein abundance in the KO was also increased (Figure S4G). *Scnn1b* and *Scnn1g* genes, encoding β and γ regulatory subunits of ENaC, were downregulated, while the gene for protein kinase *Sgk1* was upregulated (Figure 3D), suggesting an increase of ENaC activity. Another apical transporter gene, *Slc12a3*, had lower expression (Figure S4H). The abundance of basolateral sodium-potassium-ATPase was nearly normal with no changes in α (ATP1A1) and β (ATP1B1) subunits and a modest increase in γ (FXYD2) regulatory subunit. Salt-inducible kinase 1 (*Sik1*) gene expression was induced (Figure 3D), suggesting an elevation of sodium-potassium-ATPase activity. The transcript level of another basolateral transporter, *Slc4a4*, was similar in KO versus control kidneys (Figure S4H). Furthermore, kidney KO mice had increased expression levels of renal claudin-8 (*Cldn8*) (Figure S4H), suggesting a reduced backflow via paracellular mechanisms of reabsorbed sodium to the tubular lumen.[68] Thus, while the analysis of our current study focused mainly on mRNA expression, these results support the idea of enhanced sodium reabsorption through induction of several major sodium transporters (NHE3, NKCC2, and ENaC) and regulators (SGK1 and SIK1). More studies are needed to directly assess whether sodium resorption by the *Gcgr*-deficient nephron is increased, thereby contributing to the observed increase in serum sodium (Table 1).

Renal chloride reabsorption via transcellular mechanism involves, in addition to NKCC2 and NCC described above, the apical chloride-formate exchanger CFEX (SLC26A6), pendrin (SLC26A4) plus basolateral potassium-chloride co-transporter KCC1 (SLC12A4), and chloride channels ClC-K1 (CLCNKA) and ClC-K2 (CLCNKB). *Gcgr*-deficient kidneys of kidney KO mice had higher mRNA expression of *Slc12a4*, *Clcnka*, and *Clcnkb* genes, but lower transcript levels of *Slc26a4* (Figure 3E). *Slc26a6* expression was normal (Figure S4H).

Kidney transport proteins involved in calcium reabsorption via transcellular mechanism include the apical transient receptor potential cation channel TRPV5 and the basolateral sodium-calcium exchanger NCX1 (SLC8A1) and the plasma membrane calcium-transporting ATPase PMCA1 (ATP2B1).[69] *Slc8a1* mRNA expression was induced in *Gcgr*-deficient kidneys (Figure 3F), whereas the levels of *TrpV5* and *Atp2b1* were normal. Whether the hypercalcemia seen in kidney KO mice (Table 1) is a consequence of the increase in NCX1 abundance remains to be evaluated.

Multiple hormones, including angiotensin II, aldosterone, AVP, atrial natriuretic peptides, cholecystokinin, and parathyroid hormone, are involved in the regulation of electrolyte homeostasis.[69–73] We monitored the transcript expression of key signal transducer genes for these pathways. In the kidneys of kidney KO mice relative to Flox controls, the alterations in expression levels of angiotensin II receptor (AGTR1A), arginine vasopressin receptor 1A (AVPR1A), renal natriuretic peptide receptor 2 (NPR2), and cholecystokinin A receptor (CCKAR) (Figure S4I)

suggest diminished NaCl reabsorption or enhanced salt excretion along the mutant nephron. Similarly, the changes in parathyroid hormone-regulated vitamin D receptor (VDR), CYP24A1, and calcium-sensing receptor (CaSR) (Figure S4I) reflect attenuated calcium resorption by the *Gcgr*-null kidneys. Therefore, these alterations in expression of key signaling genes reveal the activation of multiple counter-regulatory transcriptional responses to the changes in ionic electrolyte levels. However, given the persistent electrolyte imbalance in kidney KO mice (Table 1), these responses to restore homeostasis by the KO kidneys were ineffective or at least blunted. Overall, our extensive analysis supports that renal GCGR action is crucial to maintain whole-body electrolyte homeostasis.

Kidney-specific *Gcgr*-null mice exhibit increased expression of key energy production genes and undergo chronic oxidative stress

In view of increased tubular reabsorption of filtered electrolytes described above, we further investigated whether energy metabolism in *Gcgr*-deficient kidneys is altered to meet the extra energy demand. The kidney utilizes both fatty acids and glucose as major metabolic fuels. In the renal cortex (especially in the proximal tubule, the site of renal gluconeogenesis), fatty acid β-oxidation acts as a main energy source. In *Gcgr*-null kidneys of kidney KO mice, the mRNA expression of several important fatty acid oxidation genes (mitochondrial short-chain- and medium-chain-specific acyl-coenzyme A [CoA] dehydrogenase [*Acads* and *Acadm*]) and lipid transport genes (fatty acid transport protein 2 [*Slc27a2*], *Cd36*, and mitochondrial carnitine O-palmitoyltransferase 2 [*Cpt2*]) was significantly increased, while long-chain-specific acyl-CoA dehydrogenase (*Acadl*) levels trended higher (Figure 3G). The expression of other oxidative and regulatory genes (carnitine O-palmitoyl transferase 1a [*Cpt1a*], acyl-CoA oxidase 1 [*Acox1*], carnitine/acylcarnitine carrier protein [*Slc25a20*], *Ppara*, and *Ppargc1a*) remained normal (Figure S4J). All five proteins ACADS, ACADM, SLC27A2, CD36, and CPT2, whose genes were significantly induced in the KOs at the mRNA level, are also highly expressed in the proximal tubules relative to other nephron segments, as indicated by quantitative proteomic analysis.[7] Thus, these results suggest that, in the proximal nephron of KO kidneys, fatty acid β-oxidation is moderately increased and can support the needs for extra energy-consuming solute transport activity. Moreover, we find that renal adiponectin expression is upregulated in global *Gcgr* KO mice,[58] as well as in kidney-specific KOs (Figure S4K). It is possible that in kidney KO mice, enhanced fatty acid β-oxidation is mediated by elevated adiponectin, and it can serve to partially replenish the pool of gluconeogenic precursors and intermediates, beyond ATP generation.

The distal nephron primarily uses glucose as a carbon fuel for glycolysis, with or without mitochondrial oxidative phosphorylation (depending on local oxygen availability), to meet its energy requirements. In kidney KO mice, renal transcript levels of genes encoding key glycolytic enzymes, such as hexokinase (*Hk1*), phosphofructokinase (*Pfk*l, *Pfkp*), and pyruvate kinase (*Pkm*), were elevated (Figure 3H). HK1, PFKP, and PKM proteins and their enzymatic activities are mostly localized to the distal nephron.[7,57] In addition, the expression of the mitochondrial pyruvate carrier 1 (MPC1), a membrane protein responsible for the transport of cytoplasmic pyruvate into the mitochondrial matrix, was upregulated in KO kidneys (Figure 3H). Hence our data suggest enhanced glucose oxidation in the distal nephron in the context of loss of renal *Gcgr* expression. This incremental ATP production is likely to reflect the increased energy demand of distal nephron segments in light of the elevated tubular transport requirements for filtered solutes, such as electrolytes.

Hepatogenic ketone bodies reflect another source of fuel substrates for the kidney. We observed that the levels of the ketone β-hydroxybutyrate in circulation were lower during the fasting state, but not in the fed state, in both kidney-specific and global *Gcgr* KO mice (Figures 3I and S4L). This is consistent with an increased use of ketone bodies by *Gcgr*-deficient kidneys. Monocarboxylate transporter genes Mct1 (*Slc16a1*), Mct2 (*Slc16a7*), and Mct4 (*Slc16a3*), involved in the renal uptake of ketone bodies, were normally expressed (Figure 3J). However, the mRNA expression in the kidney of the mitochondrial enzyme D-β-hydroxybutyrate dehydrogenase (BDH1) gene, involved in the conversion of β-hydroxybutyrate into acetoacetate, was significantly elevated in kidney KO mice (Figure 3J). Even though the transcript levels of mitochondrial succinyl-CoA:3-ketoacid CoA transferase 1 (OXCT1) gene for the activation of acetoacetate to acetoacetyl-CoA were not changed (Figure 3J), these results suggest that under fasting conditions, renal *Gcgr*-null kidneys took up larger quantities of circulating ketone bodies to synthesize more respiratory substrates for mitochondrial ATP production.

Given the apparent increase in renal oxidative metabolism described above, we examined whether redox homeostasis in kidney KO versus Flox control mice is altered. In chow diet-fed kidney KO mice, the ratio of oxidized over reduced glutathione concentrations in serum, as an index of whole-body redox status, was significantly increased (Figure 3K). Consistent with this relative oxidant excess, we found that the mRNA expression of endogenous kidney antioxidant genes, such as superoxide dismutase (*Sod1*; mainly expressed in the proximal tubules), heme oxygenase 1 (*Hmox1*), peroxiredoxin 5 (*Prdx5*), and thioredoxin 1 (*Txn1*), was induced (Figure 3L), suggesting sustained oxidative stress under baseline conditions in the mutant mice. The transcript levels of a few redox-sensitive genes, such as uncoupling protein 2 (*Ucp2*; mainly expressed in the distal nephron), peptidase M20 domain-containing 1 (*Pm20d1*; mainly expressed in the proximal tubules), and cAMP-dependent transcription factor ATF-4 (*Atf4*), were also elevated in *Gcgr*-null kidneys (Figure 3L). Intriguingly, the expression of nuclear factor erythroid-derived 2-related factor 2 gene (*Nrf2*), involved in redox homeostasis, was repressed in kidney KO mice (Figure 3L). However, the regulation of this key transcription factor is at the posttranscriptional and posttranslational levels.[74] Overall, our results support the view that kidney KO mice exhibited metabolically reprogrammed activities of fatty acid and glucose oxidation in the proximal and distal nephrons, respectively, to meet the metabolic demands for ATP production and gluconeogenesis. Consequently, these KO mice displayed heightened oxidative stress.

Kidney-specific *Gcgr*-null mice display hypertension and kidney injury at baseline

Considering the excessive fluid excretion and salt retention by the *Gcgr*-deficient kidneys (Figure 2E; Table 1), we were curious whether these changes have an impact on blood pressure. Not

Please cite this article in press as: Wang et al., Downregulation of the kidney glucagon receptor, essential for renal function and systemic homeostasis, contributes to chronic kidney disease, Cell Metabolism (2023), https://doi.org/10.1016/j.cmet.2023.12.024

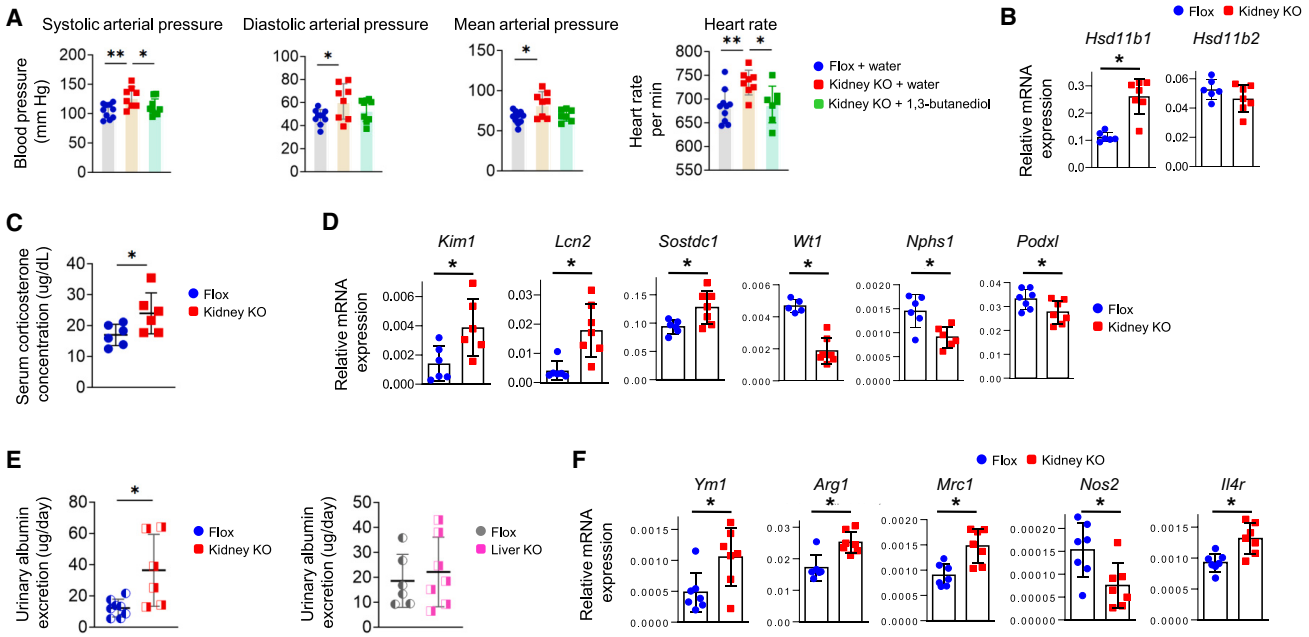

Figure 4. Kidney-specific *Gcgr*-null mice display hypertension and renal injury

(A) Arterial blood pressure and resting heart rate of kidney-specific *Gcgr* knockout (kidney KO) and floxed control (Flox) mice. KO mice received either drinking water containing 1,3-butanediol for 4 weeks or regular water without 1,3-butanediol for the same duration prior to blood pressure measurement. n = 8–10 mice per group; *p < 0.05, **p < 0.01.

(B) qPCR analysis of kidney corticosteroid 11-beta-dehydrogenase *Hsd11b1* and *Hsd11b2* gene expression in kidney KO and Flox mice. n = 6–7 mice per group; *p < 0.05.

(C) Serum levels of corticosterone in kidney KO and Flox mice. n = 6 mice per group; *p < 0.05.

(D) qPCR analysis of renal injury biomarker gene expression in kidney KO and Flox mice. *Kim1*, kidney injury molecule-1; *Lcn2*, lipocalin-2; *Sostdc1*, sclerostin domain-containing protein 1; *Wt1*, Wilm's tumor protein homolog; *Nphs1*, nephrin; *Podxl*, podocalyxin. n = 5–7 mice per group; *p < 0.05.

(E) Daily urinary albumin excretion in kidney-specific *Gcgr* KO, liver-specific *Gcgr* KO, and their respective control mice. n = 6–8 mice per group; *p < 0.05.

(F) qPCR analysis of kidney M1/M2 macrophage marker and regulator gene expression in kidney KO and Flox mice. *Ym1*, chitinase-like protein 3; *Arg1*, arginase-1; *Mrc1*, macrophage mannose receptor 1; *Nos2*, inducible nitricoxide synthase; *Il4r*, interleukin-4 receptor subunit alpha. n = 7 mice per group; *p < 0.05.

surprisingly, kidney KO mice fed even a normal salt diet exhibited arterial hypertension, with significantly elevated systolic, diastolic, and mean arterial blood pressure (Figure 4A). Their resting heart rate was higher than in Flox control mice. Similarly, the global *Gcgr* KO mice were hypertensive (Figure S5A). However, in contrast to the kidney KO mice, the global KO mice show a reduction in resting heart rate (Figure S5A). Our results indicate an impairment of blood pressure and heart rate control in mice with kidney-specific *Gcgr* ablation, with some possible compensation in the global *Gcgr* KO mice with respect to heart rate. These findings are in agreement with the observations that some subpopulations of human subjects carrying a GCGR G40S mutation have high blood pressure.[32]

We subsequently examined hypertension-related cardiac manifestations in kidney KO mice. These mutant mice displayed increases in the heart-to-body weight ratio and in heart as well as in cardiomyocyte size (Figure S5B). Thus, several structural features of cardiac hypertrophy developed in the hypertensive kidney KO mice.

Given the lower serum levels of β-hydroxybutyrate in kidney KO mice (Figure 3I), it is of interest that chronic administration of 1,3-butanediol (1,3-BD), an exogenous precursor of β-hydroxybutyrate, increases circulating β-hydroxybutyrate and decreases blood pressure in rodent models of hypertension.[75] We examined whether, in our KO mice, 1,3-BD treatment exerts similar anti-hypertensive effects. In the fasting state, serum β-hydroxybutyrate became higher in 1,3-BD-administered kidney KO mice than in similarly treated Flox controls (Figure S5C). In KO mice, 1,3-BD significantly attenuated systolic arterial pressure and resting heart rate and tended to reduce diastolic and mean arterial pressure (Figure 4A), thereby showing some improvements in hypertension through ketone supplementation.

To explore potential underlying mechanisms for the alterations in blood pressure, we monitored the renal expression of a few genes known to participate in blood pressure regulation. As described above, many specific signaling genes in *Gcgr*-null kidneys that we examined (Figure S4I) were significantly altered in a comprehensive transcriptional regulatory loop. The expression of several hormone receptors likely underwent negative feedback regulation. However, alterations in the levels of these receptors do not seem to be the primary mechanism of developing high blood pressure in kidney KO mice. Beyond that, the activity of plasma renin, a major regulator of blood pressure, was unchanged in both the kidney-specific and global *Gcgr* KO mice (Figure S3F).

Excessive levels of glucocorticoids have also long been recognized to induce hypertension in humans and animal models.[76] In the kidney, glucocorticoid availability is controlled

Please cite this article in press as: Wang et al., Downregulation of the kidney glucagon receptor, essential for renal function and systemic homeostasis, contributes to chronic kidney disease, Cell Metabolism (2023), https://doi.org/10.1016/j.cmet.2023.12.024

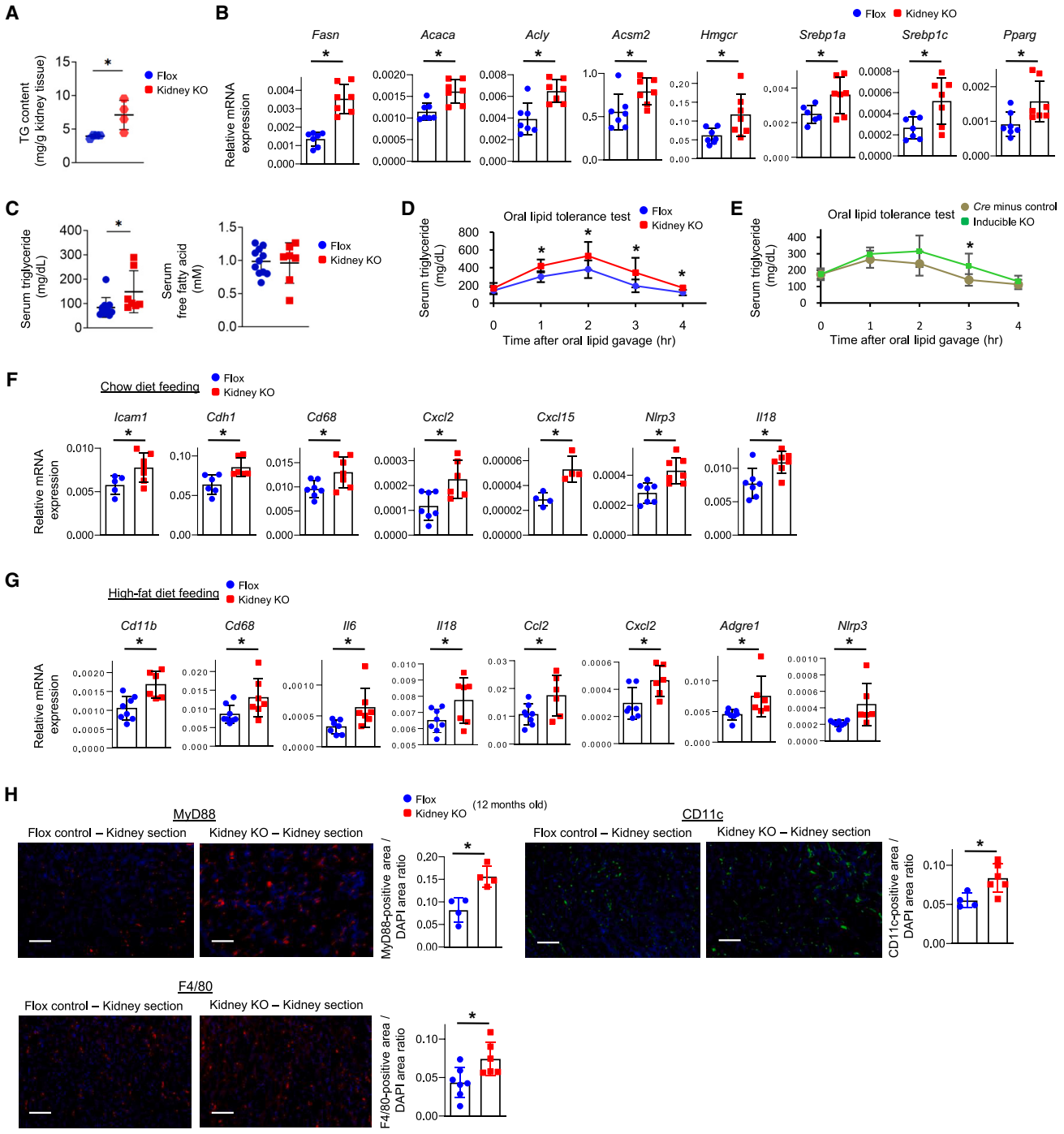

Figure 5. Kidney-specific *Gcgr*-null mice show excessive renal lipid deposition and lipid-related maladaptive responses

(A) Intrarenal triglyceride (TG) content in kidney-specific *Gcgr* knockout (kidney KO) and floxed control (Flox) mice. n = 4 mice per group; *p < 0.05.

(B) qPCR analysis of kidney lipogenesis and transcription factor gene expression in kidney KO and Flox mice. *Fasn*, fatty acid synthase; *Acaca*, acetyl-CoA carboxylase 1; *Acly*, ATP-citrate synthase; *Acsm2*, acyl-CoA synthetase medium-chain family member 2; *Hmgcr*, 3-hydroxy-3-methylglutaryl-CoA reductase; *Srebp1a*, sterol regulatory element-binding protein 1a; *Srebp1c*, sterol regulatory element-binding protein 1c; *Pparg*, peroxisome proliferator-activated receptor gamma. n = 7 mice per group; *p < 0.05.

(C) Serum levels of triglycerides and free fatty acids in kidney KO and Flox mice after 16-h fasting and 24-h refeeding. n = 7–11 mice per group; *p < 0.05.

(D) Serum triglyceride levels during oral lipid tolerance tests in kidney KO and Flox mice. n = 5–7 mice per group; *p < 0.05.

(E) Serum triglyceride levels during oral lipid tolerance tests in inducible *Gcgr* KO and *Cre*-minus control mice. n = 3–7 mice per group; *p < 0.05.

(legend continued on next page)

by corticosteroid 11-β-dehydrogenase enzymes HSD11B1 and HSD11B2. HSD11B1 produces the active glucocorticoid cortisol from the inactive form cortisone, whereas HSD11B2 catalyzes the reverse reaction. Previous studies have shown that the upregulation of kidney HSD11B1 or downregulation of HSD11B2 provokes blood pressure increases.[77] Our qPCR analysis indicates that in kidney KO mice, renal *Hsd11b1* gene expression was elevated, while *Hsd11b2* mRNA levels tended to be lower (Figure 4B), suggesting a role of renal HSD11B1 hyperactivity in the development of hypertension. Consistent with these observations, in the hypertensive kidney KO and global KO mice, serum corticosterone levels were increased (Figures 4C and S5D). On the whole, our data support that renal GCGR is essential for the control of systemic arterial blood pressure.

Given the broad renal dysfunctions described above, we evaluated whether renal *Gcgr*-null kidneys show any signs of low-grade injury under baseline conditions by measuring the expression of various pre-clinical biomarkers for kidney injury.[78] In chow diet-fed kidney KO mice, injury biomarkers, such as kidney injury molecule-1 (*Kim1* or *Havcr1*; mainly expressed in the proximal tubules), lipocalin-2 (*Lcn2* or Ngal; mainly in the distal nephron), and sclerostin domain-containing protein 1 (*Sostdc1* or Usag1; mainly in the distal nephron), were significantly upregulated (Figure 4D). These results suggest that even at baseline, kidney-specific *Gcgr*-null mice exhibited signs of tubular injury in different parts of kidney nephrons. Moreover, the mRNA levels of several podocyte marker genes, such as Wilm's tumor protein homolog (*Wt1*), nephrin (*Nphs1*), and podocalyxin (*Podxl*), were attenuated in *Gcgr*-deficient kidneys (Figure 4D), suggesting podocyte-related glomerular damage.[79] Consistent with these injury markers, kidney KO mice, in contrast to liver KO mice, displayed albuminuria with significantly elevated daily urinary albumin excretion (Figure 4E). Their levels of serum cystatin C, a marker of kidney function, were also increased (Figure S5E), possibly reflecting a decline in the renal glomerular filtration.

Histological analysis of kidneys revealed that at 8 weeks and 5 months of age, kidney KO mice and Flox controls had similar histological structures of kidney cortex and medulla (Figure S5F). Some (but not all) of the renal glomerular regions from kidney KO mice aged 5 months displayed larger intense trichrome stains (Figure S5G), suggesting increased glomerular extracellular matrix deposition. However, no significant tubulointerstitial staining was observed in the trichrome-stained kidney sections from 5-month-old mutant mice (Figure S5H).

With kidney injury, the reparative processes to restore tissue homeostasis usually involve macrophages. We characterized the presence of these immune cells in the kidney in relation to M1/M2 polarization. Renal macrophage populations in chow diet-fed kidney KO versus Flox control mice showed a shift toward enhanced M2-like phenotypes, as the mRNA expression of M2 markers (*Ym1*, *Arg1*, and *Mrc1*) was increased, while M1 markers (*Nos2*) were decreased, a phenotypic switch likely related to the elevated expression of interleukin-4 (IL-4) receptor subunit alpha (*Il4r*) (Figure 4F). These results suggest that the M2-like subsets of macrophages were increased in the course of damage within *Gcgr*-null kidneys. Taken together, our findings support that renal GCGR is required to protect against kidney injury and to support tissue homeostasis across a wide range of kidney functional parameters.

Kidney-specific *Gcgr*-null mice show excess lipid deposition, inflammasome activation, and substantial extracellular matrix accumulation in the kidney

Kidney injury is frequently accompanied by renal lipid accumulation.[80] GCGR is known to regulate hepatic lipid metabolism.[81–83] To elucidate the role of renal GCGR in the regulation of lipid homeostasis, we investigated the consequences of the inactivation of the *Gcgr* gene in the kidney for systemic and renal lipid metabolism. Kidney KO mice fed a chow diet or HFD displayed normal serum triglyceride levels (Figure S6A). The concentrations of cholesterol were similar in chow diet-fed KO and Flox control animals, whereas they were slightly but significantly increased in HFD-fed KOs (Figure S6A). Unlike what is observed for the global *Gcgr* KO mice,[54] the total fat and lean body mass at the whole-animal level was similar in the kidney-specific *Gcgr* KO versus control mice on a chow diet (Figure S6B). In HFD-fed kidney KO mice, while the fat body mass was normal, the lean mass showed a small but significant increase, compared with the controls (Figure S6B).

At the tissue level, we observed that the injured kidneys from kidney KO mice, even on a chow diet, exhibited increased triglyceride accumulation (Figure 5A). qPCR analysis indicated that in *Gcgr*-deficient kidneys, the expression of a number of key lipid synthesis genes was increased. This included fatty acid synthase (*Fasn*), acetyl-CoA carboxylase 1 (*Acaca*), ATP-citrate synthase (*Acly*), acyl-CoA synthetase medium-chain family member 2 (*Acsm2*), 3-hydroxy-3-methylglutaryl-CoA reductase (*Hmgcr*), sterol regulatory element-binding protein 1a and 1c (*Srebp1a* and *Srebp1c*), and peroxisome proliferator-activated receptor gamma (*Pparg*) (Figure 5B). The induction of these key genes was consistent with the elevation of lipid content in the KO kidney. Among the proteins for lipid synthesis, *Acaca*—the rate-limiting enzyme for lipogenesis—is expressed mainly in the distal nephron, whereas 3-hydroxy-3-methylglutaryl-CoA reductase—the rate-limiting enzyme for sterol synthesis—is expressed primarily in the proximal nephron,[6,7] suggesting a regional heterogeneity of accumulated triglycerides versus sterols along the *Gcgr*-deficient nephron. The transcript levels of other important genes, such as stearoyl-CoA desaturase 1 (*Scd1*), fatty acid

(F) qPCR analysis of kidney adhesion-, immune-, and inflammatory-related gene expression in chow diet-fed kidney KO and Flox mice. *Icam1*, intercellular adhesion molecule 1; *Cdh1*, cadherin-1; *Cd68*, macrosialin; *Cxcl2*, C-X-C motif chemokine 2; *Cxcl15*, C-X-C motif chemokine 15; *Nlrp3*, NACHT, LRR, and PYD domain-containing protein 3; *Il18*, interleukin-18. n = 5–7 mice per group; *p < 0.05.
(G) qPCR analysis of renal immune- and inflammatory-related gene expression in high-fat diet-fed kidney KO and Flox mice. *Cd11b*, integrin alpha-M; *Cd68*, macrosialin; *Il6*, interleukin-6; *Il18*, interleukin-18; *Ccl2*, C-C motif chemokine; *Cxcl12*, C-X-C motif chemokine 12; *Adgre1*, cell surface glycoprotein F4/80; *Nlrp3*, NACHT, LRR, and PYD domains-containing protein 3. n = 5–7 mice per group; *p < 0.05.
(H) Representative microphotographs of immunofluorescent staining with anti-MyD88 (in red), CD11c (in green), or F4/80 (in red) antibodies of kidney sections from 12-month-old kidney KO and Flox mice fed a chow diet. Nuclei were stained with DAPI (in blue). Scale bars, 100 μm. *p < 0.05.

Please cite this article in press as: Wang et al., Downregulation of the kidney glucagon receptor, essential for renal function and systemic homeostasis, contributes to chronic kidney disease, Cell Metabolism (2023), https://doi.org/10.1016/j.cmet.2023.12.024

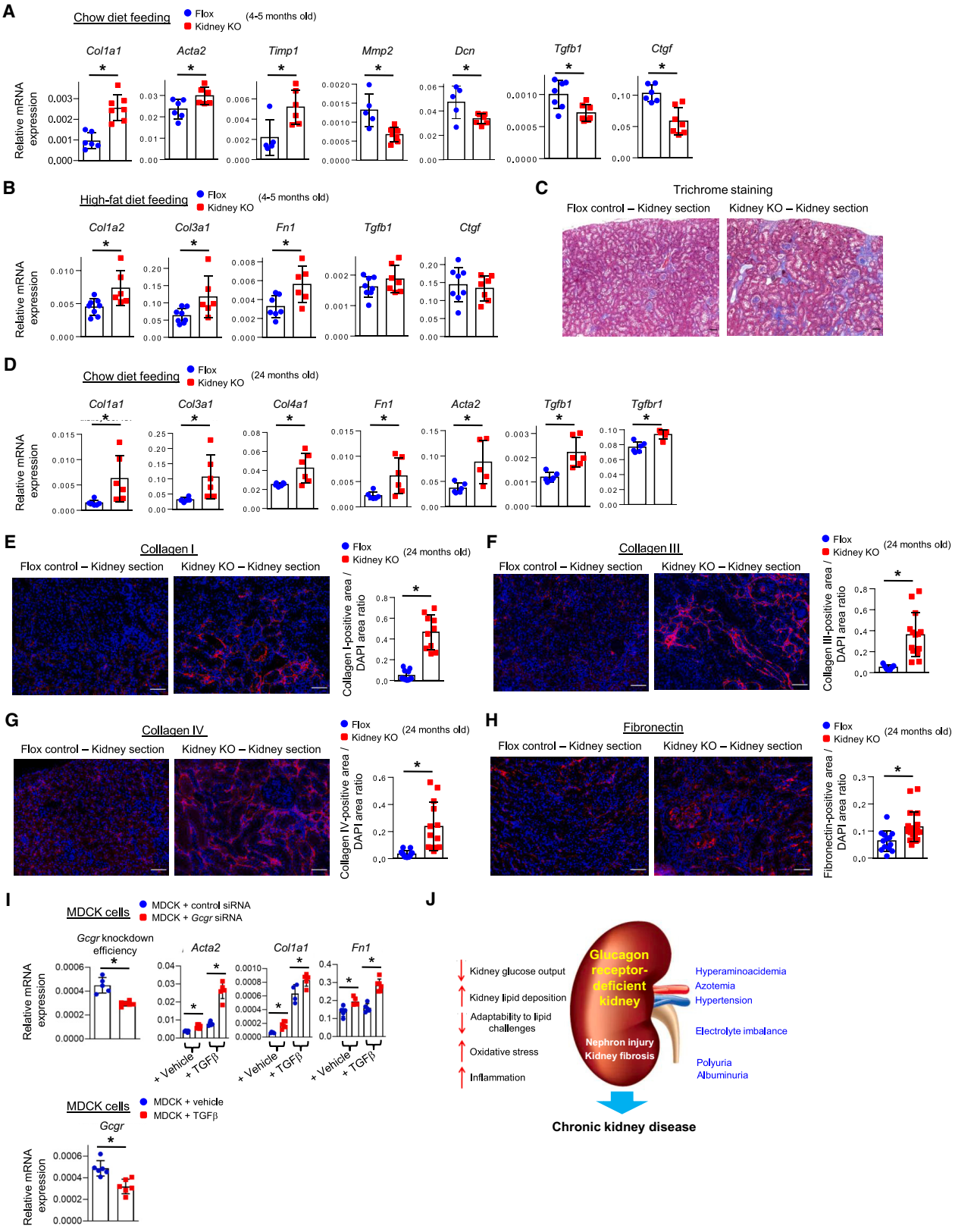

(legend on next page)

Please cite this article in press as: Wang et al., Downregulation of the kidney glucagon receptor, essential for renal function and systemic homeostasis, contributes to chronic kidney disease, Cell Metabolism (2023), https://doi.org/10.1016/j.cmet.2023.12.024

desaturase 1 (*Fads1*), cytoplasmic glycerol-3-phosphate dehydrogenase (*Gpd1*), diacylglycerol O-acyltransferase 1 (*Dgat1*), cytoplasmic hydroxymethylglutaryl-CoA synthase (*Hmgcs1*), and carbohydrate-responsive element-binding protein (*Mlxipl*), remained normal (Figure S6C). Therefore, under baseline conditions, the loss of renal GCGR signaling promotes excess lipid deposition in the injured kidney.

This excess renal lipid accumulation in kidney KO mice raises questions regarding the adaptive responses to a variety of metabolic challenges with respect to lipid metabolism. Fasting-refeeding dietary regimens show that in overnight fasted and refed kidney KO mice, serum triglycerides were significantly elevated in comparison with Flox control mice, while free fatty acid levels were normal (Figure 5C). Similarly, following a lipid load via oral gavage, *Gcgr* mutant mice exhibited significantly higher serum triglyceride concentrations at all times, except at baseline (Figure 5D). When these mice were housed at thermoneutrality (30°C), they displayed similar differences in lipid clearance after oral lipid gavage (Figure S6D). Moreover, inducible *Gcgr* KO mice were also lipid intolerant upon a lipid challenge (Figure 5E). These results suggest that the post-prandial response to an acute excess lipid load is impaired in mice missing the renal GCGR.

To determine whether the elevation of serum triglycerides during metabolic challenges in kidney KO mice is caused by a reduction in triglyceride clearance from the circulation, we performed lipid tolerance tests with ^{3}H-labeled triolein as a tracer. As expected, mouse liver, kidney, brown adipose tissue, and heart accumulated more radioactive tracer than other tissues (Figure S6E). White and brown adipose tissues in kidney KO mice showed an increase in tracer uptake relative to the Flox control mice, whereas the hearts showed a significant decrease (Figure S6E). Overall, this amounts to a nearly normal lipid clearance during lipid tolerance tests. Moreover, similar tracer counts were remaining in the small intestine of kidney KO versus control mice (Figure S6E), indicating no alterations in intestinal absorption of administered labeled lipids. Hence, our data suggest that the increased serum triglycerides observed in kidney KO mice may be due to enhanced chylomicron triglyceride (TG) secretion or increased hepatic very low-density lipoprotein TG secretion into the circulation.

Given the observed alterations in lipid metabolism described above, we evaluated proinflammatory and profibrotic responses in the kidneys of *Gcgr* KO mice. In chow-fed kidney KO mice, the mRNA levels in the kidneys of intercellular adhesion molecule 1 (*Icam1*), cadherin-1 (*Cdh1*), the immune cell marker CD68, C-X-C motif chemokine 2 (Cxcl2 or Mip2) and 15 (*Cxcl15*), the inflammasome component NACHT, LRR and PYD domain-containing protein 3 (NLRP3), and the proinflammatory cytokine IL-18 (*Il18*) were significantly increased (Figure 5F), while the abundance of immune cell markers F4/80 (*Adgre1*) and CD11c (*Itgax*), proinflammatory cytokines IL-1 beta (*Il1b*), IL-6 (*Il6*), tumor necrosis factor (*Tnf*), C-C motif chemokine 2 (*Ccl2* or Mcp1), and C-X-C motif chemokine 10 (*Cxcl10*) were relatively low (Figure S6F). These results highlight that the renal NLRP3 inflammasome was upregulated and activated in chow diet-fed kidney KO mice. On an HFD, the mutant mice showed a further maladaptive response. Their kidneys had significantly elevated mRNA levels of *Cd11b*, *Cd68*, *Il6*, *Il18*, *Ccl2*, *Cxcl2*, *Adgre1*, and *Nlrp3* genes (Figure 5G), while those of *Cxcl10*, *Tnf*, and *Il1b* trended higher but were not significantly changed (Figure S6G), suggesting excessive renal immune infiltration and persistent kidney inflammation in kidney KO mice upon chronic lipid overload. Furthermore, immunofluorescence analysis reveals that in 12-month-old kidney KO mice fed a chow diet, intrarenal MyD88, CD11c, and F4/80 protein expression levels were relatively high (Figure 5H), suggesting accumulation of inflammatory immune cells (e.g., dendritic cells and macrophages) in *Gcgr*-deficient versus control kidneys.

With respect to renal fibrosis, in chow diet-fed kidney KO mice at 4–5 months of age, the expression levels of profibrogenic genes, such as collagen type I alpha 1 (*Col1a1*), smooth muscle

Figure 6. Kidney-specific *Gcgr*-null mice exhibit substantial renal accumulation of key profibrotic markers

(A) qPCR analysis of kidney fibrotic-related gene expression in 4- to 5-month-old kidney-specific *Gcgr* knockout (kidney KO) and floxed control (Flox) mice fed a chow diet. *Col1a1*, collagen type I alpha 1; *Acta2*, smooth muscle actin; *Timp1*, metalloproteinase inhibitor 1; *Mmp2*, matrix metalloproteinase-2; *Dcn*, proteoglycan decorin; *Tgfb1*, transforming growth factor beta 1; *Ctgf*, connective tissue growth factor. n = 5–7 mice per group; *p < 0.05.

(B) qPCR analysis of kidney fibrotic-related gene expression in 4- to 5-month-old kidney KO and Flox mice fed a high-fat diet. *Col1a2*, collagen type I alpha 2; *Col3a1*, collagen type III alpha 1; *Fn1*, fibronectin 1; *Tgfb1*, transforming growth factor beta 1; *Ctgf*, connective tissue growth factor. n = 5–7 mice per group; *p < 0.05.

(C) Representative microphotographs of trichrome-stained kidney sections from 12-month-old kidney KO and Flox mice fed a chow diet. Scale bars, 70 μm.

(D) qPCR analysis of kidney profibrotic gene expression in 24-month-old kidney KO and Flox mice fed a chow diet. *Col1a1*, collagen type I alpha 1; *Col3a1*, collagen type III alpha 1; *Col4a1*, collagen type IV alpha 1; *Fn1*, fibronectin 1; *Acta2*, smooth muscle actin; *Tgfb1*, transforming growth factor beta 1; *Tgfbr1*, TGF beta receptor type 1. n = 5–6 mice per group; *p < 0.05.

(E) Representative microphotographs of immunofluorescent staining (in red) with anti-collagen I antibody of kidney sections from 24-month-old kidney KO and Flox mice fed a chow diet. Nuclei were stained with DAPI (in blue). Scale bars, 70 μm. *p < 0.05.

(F) Representative microphotographs of immunofluorescent staining (in red) with anti-collagen III antibody of kidney sections from 24-month-old kidney KO and Flox mice fed a chow diet. Nuclei were stained with DAPI (in blue). Scale bars, 70 μm. *p < 0.05.

(G) Representative microphotographs of immunofluorescent staining (in red) with anti-collagen IV antibody of kidney sections from 24-month-old kidney KO and Flox mice fed a chow diet. Nuclei were stained with DAPI (in blue). Scale bars, 70 μm. *p < 0.05.

(H) Representative microphotographs of immunofluorescent staining (in red) with anti-fibronectin antibody of kidney sections from 24-month-old kidney KO and Flox mice fed a chow diet. Nuclei were stained with DAPI (in blue). Scale bars, 70 μm. *p < 0.05.

(I) qPCR analysis of gene expression in MDCK cells in response to *Gcgr* knockdown and TGF-β treatment. Housekeeping gene for canine beta-2-microglobulin was used for normalization of gene transcript levels. *Gcgr*, glucagon receptor; *Acta2*, smooth muscle actin; *Col1a1*, collagen type I alpha 1; *Fn1*, fibronectin 1. *p < 0.05.

(J) Schematic diagram illustrating the effect of kidney-specific *Gcgr* ablation on renal metabolism and function in mice. Kidney KO mice exhibit metabolically reprogrammed activities and impaired kidney functions. For example, they show hyperaminoacidemia, associated with reduced kidney glucose output. These mutant mice display azotemia, polyuria, and electrolyte imbalance. The deficiency of renal GCGR expression or activity can contribute to the development of chronic kidney disease.

Please cite this article in press as: Wang et al., Downregulation of the kidney glucagon receptor, essential for renal function and systemic homeostasis, contributes to chronic kidney disease, Cell Metabolism (2023), https://doi.org/10.1016/j.cmet.2023.12.024

actin (*Acta2*, a marker of renal interstitial myofibroblasts), and metalloproteinase inhibitor 1 (*Timp1*), were increased in the kidney (Figure 6A). In contrast, the levels of matrix metalloproteinase-2 (*Mmp2*), the proteoglycan decorin (*Dcn*), transforming growth factor β1 (*Tgfb1*), and connective tissue growth factor (*Ctgf*) were decreased (Figure 6A). Collagen type I alpha 2 (*Col1a2*) and type III alpha 1 (*Col3a1*), as well as fibronectin 1 (*Fn1*), were not different (Figure S6H). In age-matched HFD-fed kidney KO mice, the transcript levels of renal *Col1a2*, *Col3a1*, and *Fn1* were significantly higher (Figure 6B), suggesting increased production of extracellular matrix proteins. *Tgfb1* and *Ctgf* abundance was similar in KO and control kidneys. Thus, these results support that the lack of renal GCGR exacerbates lipid-induced immune activation, chronic inflammation, and profibrotic responses in the kidney, indicative of maladaptive changes upon metabolic challenges.

To study the long-term effect of renal *Gcgr* deficiency on the development of kidney fibrosis, we used chow-fed kidney KO and Flox control mice aged 12 months or older to evaluate the deposition of extracellular matrix proteins in the kidney by Masson's trichrome and immunofluorescent staining methods. While control kidneys showed little or no evidence of interstitial fibrosis on trichrome-stained sections, *Gcgr* KO kidneys had extensive tubulointerstitial staining (shown in blue) in the renal cortex of collagenous materials (Figure 6C), suggesting severe fibrosis. qPCR analysis revealed that in aged mice on a chow diet, the mRNA expression of renal *Col1a1*, *Col3a1*, *Col4a1*, and *Fn1* was significantly elevated in kidney KO mice (Figure 6D). Moreover, myofibroblast marker (*Acta2*) and profibrotic mediator (*Tgfb1* and TGF-β receptor type 1 [*Tgfbr1*]) genes were induced in the kidneys of aged mutant mice (Figure 6D). In agreement with these findings, the immunofluorescence-stained areas (shown in red) of collagen type I, III, and IV, as well as fibronectin, were significantly larger in sections from *Gcgr*-null kidneys (Figures 6E–6H), indicating excess accumulation of various extracellular matrix proteins in the KO kidneys. Therefore, our observations on kidney-specific *Gcgr* KO mice strongly support a causal connection between kidney *Gcgr* loss of function and induction of renal fibrogenesis in chow diet-fed mice.

To probe for the anti-fibrotic actions of the *Gcgr* more directly, we evaluated whether a siRNA-mediated *Gcgr* knockdown (KD) in Madin-Darby canine kidney (MDCK) cells, a distal tubular cell line, affects the cellular responses to profibrotic induction by TGF-β. In the *Gcgr* KD cells, *Acta2*, *Col1a1*, and *Fn1* mRNA expression was significantly upregulated in the basal unstimulated state and further induced upon TGF-β treatment (Figure 6I). Of interest, TGF-β exposure in normal MDCK cells transcriptionally repressed the expression of the *Gcgr* gene (Figure 6I). These results indicate that *Gcgr*-deficient MDCK cells exhibited increased susceptibility to TGF-β-mediated profibrotic activation *ex vivo*, consistent with our *in vivo* findings.

DISCUSSION

In the present study, we aimed to elucidate with a comprehensive approach the role of the kidney GCGR in normal renal function and in CKD development. Our results indicate that adult mice with either a constitutive (congenital) or conditional (in the adult animal) genetic inactivation of renal *Gcgr* display multiple functional defects in their kidneys, including dysfunctions in the control of key metabolic components, nitrogen, water, electrolytes, blood pressure, redox, and immune homeostasis (Figure 6J). While glucagon action has previously been implicated as a possible regulator for some of these renal functions, our observations here establish the direct relevance of the renal GCGR in multiple aspects of kidney physiology. Our findings show that the kidney GCGR is essential for the regulation of normal renal function and systemic homeostasis. Furthermore, our mouse study provides novel insights into the possible causative links between human renal *GCGR* downregulation and CKD development. The breadth and the magnitude of the effects observed came as a surprise to us.

Kidney-specific *Gcgr* KO mice show CKD-associated metabolic anomalies and profibrotic activation

Mice selectively lacking the *Gcgr* in kidneys recapitulated some important pathophysiological and clinical features of human CKD. Specifically, the mice exhibit CKD-associated metabolic anomalies. For example, accumulation of excess lipids in the kidney is a well-recognized hallmark of CKD.[80,84,85] The underlying mechanisms may involve dysregulation of renal lipogenesis,[86] lipid uptake,[87] and/or fatty acid oxidation.[88] We show that in kidney-specific *Gcgr* KO mice, renal triglyceride content is significantly elevated, accompanied by an induction of important genes involved in kidney fatty acid and cholesterol synthesis, lipid transport, and activation of additional transcriptional programs. Likewise, humans or animals with CKD exhibit a renal upregulation of genes encoding proteins involved in lipid synthesis (e.g., *Fasn*, *Acly*, *Acaca*, and *Hmgcr*), lipid transport (e.g., *Cd36*), and transcription factors (e.g., *Srebf1* and *Pparg*).[86,89–92] Hence, in human CKD, kidney GCGR reduction may contribute to abnormal renal lipid disposition.

Increased oxidative stress, inflammation, and fibrosis in the kidney are often regarded as prominent pathogenic conditions involved in the development of CKD.[93–95] Our results indicate that kidney-specific *Gcgr*-null mice display chronic redox imbalance and inflammasome-related inflammation under baseline conditions and present enhanced proinflammatory and profibrotic responses upon lipid overload. Consumption of lipid-rich diets is a known risk factor for the development of CKD.[96] As observed in our kidney KO mice, people or animal models with CKD manifest an elevated ratio of serum oxidized over reduced glutathione, along with a reduction of the key antioxidant regulator NRF2 in affected kidneys.[97–100] Humans and animals with CKD, as well as our kidney KO mice, all have higher levels of the inflammasome component NLRP3, increased numbers of CD68- or CD11-positive immune cells, and elevated levels of cytokines and chemokines, such as IL-6, IL-18, CCL2 (MCP-1), CXCL2 (MIP2), and CXCL10 (IP-10).[101–106] Both the diseased[107,108] and *Gcgr*-deficient kidneys show increased expression of the profibrotic cytokine TGF-β1 and its type 1 receptor. Importantly, they exhibit similar profibrotic activation, as judged by the upregulation and accumulation of extracellular matrix proteins, such as collagen types I, III, and IV, as well as fibronectin.[109,110] Overall, in the context of human CKD, an impaired GCGR regulation in the kidney is a likely contributor to chronic oxidative stress, inflammation, and tubulointerstitial fibrosis.

Please cite this article in press as: Wang et al., Downregulation of the kidney glucagon receptor, essential for renal function and systemic homeostasis, contributes to chronic kidney disease, Cell Metabolism (2023), https://doi.org/10.1016/j.cmet.2023.12.024

Human subjects with CKD are susceptible to developing hypoglycemia.[111] Decreased renal gluconeogenesis is considered to be one of the factors responsible for these hypoglycemic events.[112] We provide evidence that in kidney-specific *Gcgr* KO mice, the reduction in renal glucose output is related to a diminished pool of gluconeogenic precursors, due to impaired handling of amino acids by the mutant kidneys. Similar to kidney KO mice, human subjects or animal models of CKD exhibit decreases in the expression of genes for renal amino acid transporters (e.g., *Slc7a7*, *Slc7a8*, *Slc7a9*, *Slc16a10*, and *Slc43a2*) and amino acid catabolism (e.g., *Agxt2*, *Asl*, *Ass1*, *Gcat*, and *Prodh2*),[43,45] suggesting a limited supply of carbon skeletons for glucose production in the diseased kidneys. Human individuals with CKD also have low transcript levels of genes involved in the renal citric acid cycle,[113] thereby contributing to the reduction in gluconeogenic substrate availability. Another factor pertinent to the blood glucose levels is renal glucose reabsorption via SGLTs. This activity is diminished in individuals with nephrotic syndrome, a form of CKD.[114] Renal glycosuria, reflecting overt tubular glucose reabsorption defects, occurs in some of the patients with non-diabetic CKD.[115] Just like *Gcgr*-deficient kidneys, non-diabetic CKD kidneys display decreased expression of Sglt2 (*Slc5a2*) gene.[116]

We have observed that renal adiponectin stimulates gluconeogenesis via increased fatty acid β-oxidation.[58] We note that the upregulation of this protein in global *Gcgr* KO mice refers to the local induction of the adiponectin gene, not to adipose tissue adiponectin expression. Thus, in kidney-specific *Gcgr* KO mice, elevated adiponectin expression may exert a compensatory role to replenish the renal gluconeogenic substrate pool. A similar induction of the kidney adiponectin gene, with concurrent attenuation of GCGR expression, can be found in several settings of CKD,[43,46] suggestive of an inverse relationship in disease states between kidney adiponectin and GCGR. Importantly, in individuals with CKD, increased adiponectin levels and reduced kidney *GCGR* expression are both associated with lower glomerular filtration rate.[43,117] In light of these observations, we propose that the increase of circulating adiponectin observed in CKD, by extension, may actually represent a greater decline of renal GCGR activities and of overall kidney function. Our mouse work provides a possible mechanistic link between kidney GCGR diminution, renal dysfunction, and CKD development, presumably with increased vulnerability to serious adverse outcomes and even mortality. In people with CKD, elevated adiponectin, as a proxy for the diminished GCGR action and renal function discussed above, is shown to be associated with increased risks for all-cause and cardiovascular mortality.[118] Therefore, these results support the pathophysiological relevance of renal GCGR downregulation to human kidney dysfunction and CKD and its relationship to adiponectin levels.

Kidney-specific *Gcgr* KO mice exhibit CKD-associated renal homeostatic dysfunction

Additionally, our kidney *Gcgr*-null mice display renal homeostatic dysfunction characteristic for humans with CKD. For instance, hypertension is strongly associated with human CKD along with adverse cardiovascular complications.[119] Hypertension occurs through renal or systemic mechanisms, such as impaired kidney tubular sodium handling and altered angiotensin II-mediated regulatory activity.[120] In humans and rodents, chronic high dietary sodium intake represses kidney GCGR mRNA expression and increases systolic and diastolic blood pressure,[121,122] suggesting an inverse association between sodium levels and *Gcgr* expression. Our data reveal that kidney-specific *Gcgr*-null mice even on a normal salt diet have arterial hypertension, similar to human subjects carrying GCGR G40S missense variant (with reduced signaling activity).[32] Excess sodium retention via enhanced tubular sodium reabsorption is thought to contribute to the pathogenesis of hypertension. This view is supported by the human studies on monogenic forms of hypertension. For example, in patients with Liddle's syndrome, constitutive hyperactivity of ENaC, a sodium channel involved in renal sodium reabsorption, leads to hypertension.[123] We show that in hypernatremic kidney KO mice, the expression of several genes encoding key sodium transport proteins (ENaC, NKCC2, and NHE3) in the kidney are upregulated, suggesting a rise in renal sodium retention and, consequently, in blood pressure. Moreover, our data suggest that the HSD11B-mediated cortisol excess and the BDH1-mediated β-hydroxybutyrate deficit in *Gcgr*-deficient kidneys can play a role in the pathogenesis of hypertension as well.[75,77] We provide evidence that administration of a β-hydroxybutyrate precursor to the hypertensive kidney KO mice significantly decreased systolic arterial pressure. On the whole, our results support that, in human subjects, renal GCGR attenuation promotes the development of hypertension and CKD.

Chronic BUN elevation is a marker of kidney dysfunction in patients and animal models with CKD.[124,125] We observed that kidney KO mice fed a regular chow diet have increased BUN levels at baseline, indicating a functional impairment of GCGR KO kidneys. Mechanistically, this blood urea excess may involve enhanced renal tubular reabsorption of urea mediated by the induction of urea transporters along the *Gcgr*-deficient nephron. Similarly, human subjects with persistent azotemia have higher tubular urea reabsorption than controls.[126] In animal models of CKD, the expression of kidney urea transporters is dysregulated, and the direction of changes depends on primary disease etiologies. For example, animals with type 1 diabetes or hypertension have an elevated abundance of renal urea transporters (UTA1 and UTA3),[127,128] while those with nephrotic syndrome or chronic renal failure show attenuated transporter expression,[129,130] a divergent response perhaps related to the variable interstitial tonicity in diseased kidneys.[131]

Human individuals with CKD display an impaired ability to concentrate urine with low urine osmolarity.[132] This clinical manifestation is linked to excess excretion of filtered water or extra retention of filtered solutes (e.g., sodium and urea) by the diseased kidneys. We show that kidney KO mice have reduced urinary concentrating capacity in response to vasopressin and water deprivation. Moreover, these mutant mice under baseline conditions exhibit a decrease in urine osmolarity with increased urine output and elevated serum electrolytes and urea. In CKD, the alterations in the abundance of major kidney water and sodium transport proteins often parallel the changes in urea transporter expression,[127,133] suggesting a dysfunctional linkage. The regulation of water, sodium, and urea transporters involves several hormones, including vasopressin, angiotensin II, and glucocorticoids.[134–136] In kidney KO mice, the mechanisms underlying the dysregulation of renal transporter genes in relation to

these hormones remain to be determined. Collectively, however, our findings support a causative connection between renal GCGR downregulation and chronic imbalance of body nitrogen, fluid, and electrolytes in human CKD.

GCGR mediates its normal regulatory actions via intracellular cAMP production and calcium mobilization. Kidney cAMP signals are known to participate in the regulation of blood pressure and of tubular water, urea, and electrolyte transport.[137] Hence, the various functional anomalies in kidney-specific *Gcgr* KO mice discussed above likely stem from the dysregulated responses to the impairment of renal signaling through cAMP and/or calcium. In human CKD with associated kidney GCGR reduction (see introduction), therapeutic approaches selectively targeting renal cAMP- and calcium-related pathways (e.g., glucagon-like peptide 1 receptor-based therapy)[138–140] can potentially be beneficial for kidney function. In summary, our study highlights the essential role of kidney GCGR in normal renal function and the potential contribution of its downregulation to human CKD development.

Limitations of the study

There are several limitations of our study. The first limitation involves the role of kidney endothelial GCGR in renal function. In kidney KO mice, the *Gcgr* gene in the endothelial cells is not inactivated by the *Six2* promoter-driven *Cre* recombinase, because endothelial cells are not derived from the *Six2* lineage.[51] The *Gcgr* gene is expressed in the endothelial cells of the kidney vasculature,[141] and glucagon infusions can have renal vasodilatory effects (see introduction). Functionally, kidney *Gcgr* expression is positively associated with glomerular filtration. In the renal glomerulus of patients with CKD, *GCGR* mRNA levels are significantly reduced.[41] Hence, future studies are warranted to elucidate the regulatory role of endothelial GCGR in normal kidneys. In the context of CKD, it remains to be evaluated whether kidney *Gcgr* downregulation contributes to glomerular dysfunction and peritubular microvascular damage, two prominent pathophysiological features of CKD. The second limitation is about sexual dimorphisms in renal physiology and disease, such as water, electrolyte, and blood pressure homeostasis, as well as CKD.[67,142–145] In our study, we used male mice only to examine the response to renal *Gcgr* deficiency. Whether female kidney KO mice show distinct phenotypes needs further study. The third limitation concerns the mechanisms of action for the diminished expression of kidney GCGR in CKD. Dietary factors are likely to play a role, since renal *Gcgr* gene expression is sensitive to the composition of the diet. For example, rodent model studies show that chronic high dietary sodium or phosphorus intake represses *Gcgr* mRNA expression in the kidneys.[121,146] Thus, a long-term salt- or phosphorus-rich dietary pattern may increase the risk of developing CKD in humans through the downregulation of renal GCGR expression.

STAR★METHODS

Detailed methods are provided in the online version of this paper and include the following:

SUPPLEMENTAL INFORMATION

Supplemental information can be found online at https://doi.org/10.1016/j.cmet.2023.12.024.

ACKNOWLEDGMENTS

We thank the UTSW Animal Resource Center, Histology Core, Metabolic Phenotyping Core, and O'Brien Kidney Research Core Center for their excellent assistance with experiments performed here. We also thank Susan Legan for her help with blood pressure measurement and Shimadzu Scientific Instruments and Shimadzu Corporation for the collaborative efforts in mass spectrometry technology resources. This study was supported by US NIH grants RC2-DK118620, R01-DK55758, R01-DK099110, R01-DK127274, and R01-DK131537 to P.E.S., NIH grant R00-AG068239 and Voelcker Fund Young Investigator Pilot grant to S.Z., AHA Career Development Award 855170 to Q.Z., and CIHR grant 154321 to D.J.D. D.J.D. is supported by a Banting and Best Diabetes Centre-Novo Nordisk Chair in Incretin Biology and a Sinai Health Novo Nordisk Foundation Fund in Regulatory Peptides.

AUTHOR CONTRIBUTIONS

M.-Y.W. conceptualized the study. M.-Y.W. and P.E.S. designed experiments. M.-Y.W. conducted experiments with technical assistance and expertise provided by Z.Z., S.Z., T.O., X.-N.S., Q.Z., C.L., N.L., S.C., M.P., L.G., and R.G. D.J.D., M.J.C., Z.Z., and S.Z. provided mice. M.-Y.W. and P.E.S. analyzed and interpreted experimental data. M.-Y.W. drafted and P.E.S. and D.J.D. edited the manuscript with significant feedback from D.K.M. and Z.Z.

DECLARATION OF INTERESTS

The authors declare no competing interests.

Received: September 22, 2022
Revised: September 10, 2023
Accepted: December 19, 2023
Published: January 17, 2024

REFERENCES

1. Webster, A.C., Nagler, E.V., Morton, R.L., and Masson, P. (2017). Chronic kidney disease. Lancet *389*, 1238–1252.
2. GBD; Chronic; Kidney; Disease Collaboration (2020). Global, regional, and national burden of chronic kidney disease, 1990–2017: a systematic analysis for the Global Burden of Disease Study 2017. Lancet *395*, 709–733.
3. Bowe, B., Xie, Y., Xu, E., and Al-Aly, Z. (2021). Kidney outcomes in long COVID. J. Am. Soc. Nephrol. *32*, 2851–2862.
4. Gansevoort, R.T., Correa-Rotter, R., Hemmelgarn, B.R., Jafar, T.H., Heerspink, H.J.L., Mann, J.F., Matsushita, K., and Wen, C.P. (2013). Chronic kidney disease and cardiovascular risk: epidemiology, mechanisms, and prevention. Lancet *382*, 339–352.
5. Park, J., Shrestha, R., Qiu, C., Kondo, A., Huang, S., Werth, M., Li, M., Barasch, J., and Suszták, K. (2018). Single-cell transcriptomics of the mouse kidney reveals potential cellular targets of kidney disease. Science *360*, 758–763.
6. Poll, B.G., Chen, L., Chou, C.L., Raghuram, V., and Knepper, M.A. (2021). Landscape of GPCR expression along the mouse nephron. Am. J. Physiol. Ren. Physiol. *321*, F50–F68.
7. Limbutara, K., Chou, C.L., and Knepper, M.A. (2020). Quantitative proteomics of all 14 renal tubule segments in rat. J. Am. Soc. Nephrol. *31*, 1255–1266.
8. Butlen, D., and Morel, F. (1985). Glucagon receptors along the nephron: [125I]glucagon binding in rat tubules. Pflugers Arch. *404*, 348–353.
9. Li, X.C., Carretero, O.A., Shao, Y., and Zhuo, J.L. (2006). Glucagon receptor- mediated extracellular signal-regulated kinase 1/2 phosphorylation in rat mesangial cells: role of protein kinase A and phospholipase C. Hypertension *47*, 580–585.
10. Bankir, L., Bouby, N., Blondeau, B., and Crambert, G. (2016). Glucagonactionson the kidney revisited: possible role in potassium homeostasis. Am. J. Physiol. Ren. Physiol. *311*, F469–F486.
11. Parving, H.H., Noer, J., Kehlet, H., Mogensen, C.E., Svendsen, P.A., and Heding, L. (1977). The effect of short-term glucagon infusion on kidney function in normal man. Diabetologia *13*, 323–325.
12. Johannesen, J., Lie, M., and Kiil, F. (1977). Effect of glycine and glucagon on glomerular filtration and renal metabolic rates. Am. J. Physiol. *233*, F61–F66.
13. Takeda, Y., Fujita, Y., Bessho, R., Sato, M., Abe, T., Yanagimachi, T., Sakagami, H., Abiko, A., Takiyama, Y., Ota, T., and Haneda, M. (2019). Increment of plasma glucose by exogenous glucagon is associated with present and future renal function in type 2 diabetes: a retrospective study from glucagon stimulation test. BMC Endocr. Disord. *19*, 99.
14. de Rouffignac, C., Elalouf, J.M., and Roinel, N. (1991). Glucagon inhibits water and NaCl transports in the proximal convoluted tubule of the rat kidney. Pflugers Arch. *419*, 472–477.
15. Ahloulay, M., Déchaux, M., Laborde, K., and Bankir, L. (1995). Influence of glucagon on GFR and on urea and electrolyte excretion: direct and indirect effects. Am. J. Physiol. *269*, F225–F235.
16. Elalouf, J.M., Sari, D.C., and de Rouffignac, C. (1986). Additive effects of glucagon and vasopressin on renal Mg reabsorption and urine concentrating ability in the rat. Pflugers Arch. *407*, S66–S71.
17. Mercier, O., Bichara, M., Delahousse, M., Prigent, A., Leviel, F., and Paillard, M. (1989). Effects of glucagon on H(+)-HCO3-transport in Henle's loop, distal tubule, and collecting ducts in the rat. Am. J. Physiol. *257*, F1003–F1014.
18. Good, D.W. (1990). Inhibition of bicarbonate absorption by peptide hormones and cyclic adenosine monophosphate in rat medullary thick ascending limb. J. Clin. Invest. *85*, 1006–1013.
19. Miller, R.A., and Birnbaum, M.J. (2016). Glucagon: acute actions on hepatic metabolism. Diabetologia *59*, 1376–1381.
20. Galsgaard, K.D., Pedersen, J., Knop, F.K., Holst, J.J., and Wewer Albrechtsen, N.J. (2019). Glucagon receptor signaling and lipid metabolism. Front. Physiol. *10*, 413.
21. Cheng, X., Kim, S.Y., Okamoto, H., Xin, Y., Yancopoulos, G.D., Murphy, A.J., and Gromada, J. (2018). Glucagon contributes to liver zonation. Proc. Natl. Acad. Sci. USA *115*, E4111–E4119.
22. Kusminski, C.M., and Scherer, P.E. (2018). New zoning laws enforced by glucagon. Proc. Natl. Acad. Sci. USA *115*, 4308–4310.
23. Stumvoll, M., Meyer, C., Kreider, M., Perriello, G., and Gerich, J. (1998). Effects of glucagon on renal and hepatic glutamine gluconeogenesis in normal postabsorptive humans. Metabolism *47*, 1227–1232.
24. Gustavson, S.M., Chu, C.A., Nishizawa, M., Neal, D., Farmer, B., Yang, Y., Donahue, E.P., Flakoll, P., and Cherrington, A.D. (2004). Effects of hyperglycemia, glucagon, and epinephrine on renal glucose release in the conscious dog. Metabolism *53*, 933–941.
25. Bowman, R.H. (1970). Gluconeogenesis in the isolated perfused rat kidney. J. Biol. Chem. *245*, 1604–1612.
26. Mutel, E., Gautier-Stein, A., Abdul-Wahed, A., Amigó-Correig, M., Zitoun, C., Stefanutti, A., Houberdon, I., Tourette, J.-A., Mithieux, G., and Rajas, F. (2011). Control of blood glucose in the absence of hepatic glucose production during prolonged fasting in mice: induction of renal and intestinal gluconeogenesis by glucagon. Diabetes *60*, 3121–3131.
27. Roobol, A., and Alleyne, G.A. (1973). Regulation of renal gluconeogenesis by calciumions, hormones and adenosine 3′:5′-cyclicmonophosphate. Biochem. J. *134*, 157–165.
28. Marks, J., Debnam, E.S., Dashwood, M.R., Srai, S.K., and Unwin, R.J. (2003). Detection of glucagon receptor mRNA in the rat proximal tubule: potential role for glucagon in the control of renal glucose transport. Clin. Sci. (Lond.) *104*, 253–258.
29. Merovci, A., Solis-Herrera, C., Daniele, G., Eldor, R., Fiorentino, T.V., Tripathy, D., Xiong, J., Perez, Z., Norton, L., Abdul-Ghani, M.A., and DeFronzo, R.A. (2014). Dapagliflozin improves muscle insulin sensitivity but enhances endogenous glucose production. J. Clin. Invest. *124*, 509–514.
30. Bonner, C., Kerr-Conte, J., Gmyr, V., Queniat, G., Moerman, E., Thévenet, J., Beaucamps, C., Delalleau, N., Popescu, I., Malaisse, W.J., et al. (2015). Inhibition of the glucose transporter SGLT2 with dapagliflozin in pancreatic alpha cells triggers glucagon secretion. Nat. Med. *21*, 512–517.
31. Hager, J., Hansen, L., Vaisse, C., Vionnet, N., Philippi, A., Poller, W., Velho, G., Carcassi, C., Contu, L., and Julier, C. (1995). A missense mutation in the glucagon receptor gene is associated with non-insulin-dependent diabetes mellitus. Nat. Genet. *9*, 299–304.
32. Morris, B.J., and Chambers, S.M. (1996). Hypothesis: glucagon receptor glycine to serine missense mutation contributes to one in 20 cases of essential hypertension. Clin. Exp. Pharmacol. Physiol. *23*, 1035–1037.
33. Siani, A., Iacone, R., Russo, O., Barba, G., Russo, P., Cappuccio, F.P., Galletti, F., and Strazzullo, P. (2001). Gly40Ser polymorphism of the glucagon receptor gene is associated with central adiposity in men. Obes. Res. *9*, 722–726.
34. Yu, R. (2018). Mahvash Disease: 10 years after discovery. Pancreas *47*, 511–515.
35. Strazzullo, P., Iacone, R., Siani, A., Barba, G., Russo, O., Russo, P., Barbato, A., D'Elia, L., Farinaro, E., and Cappuccio, F.P. (2001). Altered renal sodium handling and hypertension in men carrying the glucagon receptor gene (Gly40Ser) variant. J. Mol. Med. *79*, 574–580.
36. Bankir, L., Barbato, A., Russo, O., Crambert, G., Iacone, R., Bouby, N., Perna, L.P., and Strazzullo, P. (2018). Renal potassium handling in carriers of the Gly40Ser mutation of the glucagon receptor suggests a role for glucagon in potassium homeostasis. Physiol. Rep. *6*, e13661.
37. Gild, M.L., Tsang, V., Samra, J., Clifton-Bligh, R.J., Tacon, L., and Gill, A.J. (2018). Hypercalcemia in glucagon cell hyperplasia and neoplasia (Mahvash Syndrome): A new association. J. Clin. Endocrinol. Metab. *103*, 3119–3123.

38. Tonolo, G., Melis, M.G., Ciccarese, M., Secchi, G., Atzeni, M.M., Maioli, M., Pala, G., Massidda, A., Manai, M., Pilosu, R.M., et al. (1997). Physiological and genetic characterization of the Gly40Ser mutation in the glucagon receptor gene in the Sardinian population. The Sardinian diabetes genetic study group. Diabetologia *40*, 89–94.

39. Li, H., Zhao, L., Singh, R., Ham, J.N., Fadoju, D.O., Bean, L.J.H., Zhang, Y., Xu, Y., Xu, H.E., and Gambello, M.J. (2018). The first pediatric case of glucagon receptor defect due to biallelic mutations in GCGR is identified by newborn screening of elevated arginine. Mol. Genet. Metab. Rep. *17*, 46–52.

40. Chen, M.H., Raffield, L.M., Mousas, A., Sakaue, S., Huffman, J.E., Moscati, A., Trivedi, B., Jiang, T., Akbari, P., Vuckovic, D., et al. (2020). Trans-ethnic and ancestry-specific blood-cell genetics in 746,667 individuals from 5 global populations. Cell *182*, 1198–1213.e14.

41. Grayson, P.C., Eddy, S., Taroni, J.N., Lightfoot, Y.L., Mariani, L., Parikh, H., Lindenmeyer, M.T., Ju, W., Greene, C.S., Godfrey, B., et al. (2018). Metabolic pathways and immunometabolism in rare kidney diseases. Ann. Rheum. Dis. *77*, 1226–1233.

42. Perco, P., Ju, W., Kerschbaum, J., Leierer, J., Menon, R., Zhu, C., Kretzler, M., Mayer, G., and Rudnicki, M.; Nephrotic Syndrome Study Network (NEPTUNE) (2019). Identification of dicarbonyl and L-xylulosereductase as a therapeutic target in human chronic kidney disease. JCI Insight *4*, e128120.

43. Fan, Y., Yi, Z., D'Agati, V.D., Sun, Z., Zhong, F., Zhang, W., Wen, J., Zhou, T., Li, Z., He, L., et al. (2019). Comparison of kidney transcriptomic profiles of early and advanced diabetic nephropathy reveals potential new mechanisms for disease progression. Diabetes *68*, 2301–2314.

44. Kelly, K.J., Liu, Y., Zhang, J., Goswami, C., Lin, H., and Dominguez, J.H. (2013). Comprehensive genomic profiling in diabetic nephropathy reveals the predominance of proinflammatory pathways. Physiol. Genomics *45*, 710–719.

45. Malas, T.B., Formica, C., Leonhard, W.N., Rao, P., Granchi, Z., Roos, M., Peters, D.J.M., and 't Hoen, P.A. (2017). Meta-analysis of polycystic kidney disease expression profiles defines strong involvement of injury repair processes. Am. J. Physiol. Ren. Physiol. *312*, F806–F817.

46. Chu, C.P., Hokamp, J.A., Cianciolo, R.E., Dabney, A.R., Brinkmeyer-Langford, C., Lees, G.E., and Nabity, M.B. (2017). RNA-seq of serial kidney biopsies obtained during progression of chronic kidney disease from dogs with X-linked hereditary nephropathy. Sci. Rep. *7*, 16776.

47. Arvaniti, E., Moulos, P., Vakrakou, A., Chatziantoniou, C., Chadjichristos, C., Kavvadas, P., Charonis, A., and Politis, P.K. (2016). Whole-transcriptome analysis of UUO mouse model of renal fibrosis reveals new molecular players in kidney diseases. Sci. Rep. *6*, 26235.

48. Liu, J., Kumar, S., Dolzhenko, E., Alvarado, G.F., Guo, J., Lu, C., Chen, Y., Li, M., Dessing, M.C., Parvez, R.K., et al. (2017). Molecular characterization of the transition from acute to chronic kidney injury following ischemia/reperfusion. JCI Insight *2*, e94716.

49. Wang, S.S., Gu, Y.F., Wolff, N., Stefanius, K., Christie, A., Dey, A., Hammer, R.E., Xie, X.J., Rakheja, D., Pedrosa, I., et al. (2014). Bap1 is essential for kidney function and cooperates with Vhl in renal tumorigenesis. Proc. Natl. Acad. Sci. USA *111*, 16538–16543.

50. Longuet, C., Robledo, A.M., Dean, E.D., Dai, C., Ali, S., McGuinness, I., de Chavez, V., Vuguin, P.M., Charron, M.J., Powers, A.C., et al. (2013). Liver- specific disruption of the murine glucagon receptor produces α-cell hyperplasia: evidence for a circulating α-cell growth factor. Diabetes *62*, 1196–1205.

51. Kobayashi, A., Valerius, M.T., Mugford, J.W., Carroll, T.J., Self, M., Oliver, G., and McMahon, A.P. (2008). Six2 defines and regulates a multipotent self-renewing nephron progenitor population throughout mammalian kidney development. Cell Stem Cell *3*, 169–181.

52. Broadus, A.E., Kaminsky, N.I., Northcutt, R.C., Hardman, J.G., Sutherland, E.W., and Liddle, G.W. (1970). Effects of glucagon on adenosine 3′,5′-monophosphate and guanosine 3′,5′-monophosphate in human plasma and urine. J. Clin. Invest. *49*, 2237–2245.

53. Godinho, R.O., Duarte, T., and Pacini, E.S. (2015). New perspectives in signaling mediated by receptors coupled to stimulatory G protein: the emerging significance of cAMP efflux and extracellular cAMP-adenosine pathway. Front. Pharmacol. *6*, 58.

54. Gelling, R.W., Du, X.Q., Dichmann, D.S., Rømer, J., Huang, H., Cui, L., Obici, S., Tang, B., Holst, J.J., Fledelius, C., et al. (2003). Lower blood glucose, hyperglucagonemia, and pancreatic α cell hyperplasia in glucagon receptor knockout mice. Proc. Natl. Acad. Sci. USA *100*, 1438–1443.

55. Conarello, S.L., Jiang, G., Mu, J., Li, Z., Woods, J., Zycband, E., Ronan, J., Liu, F., Roy, R.S., Zhu, L., et al. (2007). Glucagon receptor knockout mice are resistant to diet-induced obesity and streptozotocin-mediated beta cell loss and hyperglycaemia. Diabetologia *50*, 142–150.

56. Legouis, D., Faivre, A., Cippà, P.E., and de Seigneux, S. (2022). Renal gluconeogenesis: an underestimated role of the kidney in systemic glucose metabolism. Nephrol. Dial. Transplant. *37*, 1417–1425.

57. Guder, W.G., and Ross, B.D. (1984). Enzyme distribution along the nephron. Kidney Int. *26*, 101–111.

58. Onodera, T., Wang, M.-Y., Rutkowski, J.M., Deja, S., Chen, S., Balzer, M.S., Kim, D.-S., Sun, X., An, Y.A., Field, B.C., et al. (2023). Endogenous renal adiponectin drives gluconeogenesis through enhancing pyruvate and fatty acid utilization. Nat. Commun. *14*, 6531.

59. Li, X., Zheng, S., and Wu, G. (2020). Amino acid metabolism in the kidneys: nutritional and physiological significance. Adv. Exp. Med. Biol. *1265*, 71–95.

60. Kim, J., Okamoto, H., Huang, Z., Anguiano, G., Chen, S., Liu, Q., Cavino, K., Xin, Y., Na, E., Hamid, R., et al. (2017). Amino acid transporter Slc38a5 controls glucagon receptor inhibition-induced pancreatic α cell hyperplasia in mice. Cell Metab. *25*, 1348–1361.e8.

61. Dean, E.D., Li, M., Prasad, N., Wisniewski, S.N., Von Deylen, A., Spaeth, J., Maddison, L., Botros, A., Sedgeman, L.R., Bozadjieva, N., et al. (2017). Interrupted glucagon signaling reveals hepatic alpha cell axis and role for L-glutamine in alpha cell proliferation. Cell Metab. *25*, 1362–1373.e5.

62. Rhee, E.P., Clish, C.B., Ghorbani, A., Larson, M.G., Elmariah, S., McCabe, E., Yang, Q., Cheng, S., Pierce, K., Deik, A., et al. (2013). A combined epidemiologic and metabolomic approach improves CKD prediction. J. Am. Soc. Nephrol. *24*, 1330–1338.

63. Nicolaus, M.L., Bergdall, V.K., Davis, I.C., and Hickman-Davis, J.M. (2016). Effect of ventilated caging on water intake and loss in 4 strains of laboratory mice. J. Am. Assoc. Lab. Anim. Sci. *55*, 525–533.

64. Kasza, I., Adler, D., Nelson, D.W., Eric Yen, C.L., Dumas, S., Ntambi, J.M., MacDougald, O.A., Hernando, D., Porter, W.P., Best, F.A., et al. (2019). Evaporative cooling provides a major metabolic energy sink. Mol. Metab. *27*, 47–61.

65. Salhadar, K., Matthews, A., Raghuram, V., Limbutara, K., Yang, C.R., Datta, A., Chou, C.L., and Knepper, M.A. (2021). Phosphoproteomic identification of vasopressin/cAMP/protein kinase A-dependent signaling in kidney. Mol. Pharmacol. *99*, 358–369.

66. Janssens, P., Decuypere, J.P., Bammens, B., Llorens-Cortes, C., Vennekens, R., and Mekahli, D. (2022). The emerging role of the apelinergic system in kidney physiology and disease. Nephrol. Dial. Transplant. *37*, 2314–2326.

67. Hayashi, Y., Yamamoto, M., Mizoguchi, H., Watanabe, C., Ito, R., Yamamoto, S., Sun, X.Y., and Murata, Y. (2009). Mice deficient for glucagon gene-derived peptides display normoglycemia and hyperplasia of islet alpha-cells but not of intestinal L-cells. Mol. Endocrinol. *23*, 1990–1999.

68. Sassi, A., Wang, Y., Chassot, A., Komarynets, O., Roth, I., Olivier, V., Crambert, G., Dizin, E., Boscardin, E., Hummler, E., and Feraille, E. (2020). Interaction between epithelial sodium channel γ-subunit and claudin-8 modulates paracellular sodium permeability in renal collecting duct. J. Am. Soc. Nephrol. *31*, 1009–1023.

69. Moor, M.B., and Bonny, O. (2016). Ways of calcium reabsorption in the kidney. Am. J. Physiol. Ren. Physiol. *310*, F1337–F1350.

70. Oliverio, M.I., Best, C.F., Smithies, O., and Coffman, T.M. (2000). Regulation of sodium balance and blood pressure by the AT(1A) receptor for angiotensin II. Hypertension *35*, 550–554.

71. Kortenoeven, M.L.A., Pedersen, N.B., Rosenbaek, L.L., and Fenton, R.A. (2015). Vasopressin regulation of sodium transport in the distal nephron and collecting duct. Am. J. Physiol. Ren. Physiol. *309*, F280–F299.

72. Melo, L.G., Steinhelper, M.E., Pang, S.C., Tse, Y., and Ackermann, U. (2000). ANP in regulation of arterial pressure and fluid-electrolyte balance: lessons from genetic mouse models. Physiol. Genomics *3*, 45–58.

73. Duggan, K.A., Hams, G., and MacDonald, G.J. (1988). Modification of renal and tissue cation transport by cholecystokin in octapeptide in the rabbit. J. Physiol. *397*, 527–538.

74. Dodson, M., de la Vega, M.R., Cholanians, A.B., Schmidlin, C.J., Chapman, E., and Zhang, D.D. (2019). Modulating NRF2 in disease: timing is everything. Annu. Rev. Pharmacol. Toxicol. *59*, 555–575.

75. Chakraborty, S., Galla, S., Cheng, X., Yeo, J.-Y., Mell, B., Singh, V., Yeoh, B., Saha, P., Mathew, A.V., Vijay-Kumar, M., and Joe, B. (2018). Salt-responsive metabolite, β- hydroxybutyrate, attenuates hypertension. Cell Rep. *25*, 677–689.e4.

76. Whitworth, J.A. (1987). Mechanisms of glucocorticoid-induced hypertension. Kidney Int. *31*, 1213–1224.

77. Bailey, M.A. (2017). 11β-Hydroxysteroid dehydrogenases and hypertension in the metabolic syndrome. Curr. Hypertens. Rep. *19*, 100.

78. Zhang, W.R., and Parikh, C.R. (2019). Biomarkers of acute and chronic kidney disease. Annu. Rev. Physiol. *81*, 309–333.

79. Gebeshuber, C.A., Kornauth, C., Dong, L., Sierig, R., Seibler, J., Reiss, M., Tauber, S., Bilban, M., Wang, S., Kain, R., et al. (2013). Focal segmental glomerulosclerosis is induced by microRNA-193a and its downregulation of WT1. Nat. Med. *19*, 481–487.

80. Bobulescu, I.A. (2010). Renal lipid metabolism and lipotoxicity. Curr. Opin. Nephrol. Hypertens. *19*, 393–402.

81. Longuet, C., Sinclair, E.M., Maida, A., Baggio, L.L., Maziarz, M., Charron, M.J., and Drucker, D.J. (2008). The glucagon receptor is required for the adaptive metabolic response to fasting. Cell Metab. *8*, 359–371.

82. Yang, J., MacDougall, M.L., McDowell, M.T., Xi, L., Wei, R., Zavadoski, W.J., Molloy, M.P., Baker, J.D., Kuhn, M., Cabrera, O., and Treadway, J.L. (2011). Polyomic profiling reveals significant hepatic metabolic alterations in glucagon-receptor (GCGR) knockout mice: implications on anti-glucagon therapies for diabetes. BMC Genomics *12*, 281.

83. Spolitu, S., Okamoto, H., Dai, W., Zadroga, J.A., Wittchen, E.S., Gromada, J., and Ozcan, L. (2019). Hepatic glucagon signaling regulates PCSK9 and low-density lipoprotein cholesterol. Circ. Res. *124*, 38–51.

84. Herman-Edelstein, M., Scherzer, P., Tobar, A., Levi, M., and Gafter, U. (2014). Altered renal lipid metabolism and renal lipid accumulation in human diabetic nephropathy. J. Lipid Res. *55*, 561–572.

85. Foster, M.C., Hwang, S.J., Porter, S.A., Massaro, J.M., Hoffmann, U., and Fox, C.S. (2011). Fatty kidney, hypertension, and chronic kidney disease: the Framingham Heart Study. Hypertension *58*, 784–790.

86. Afshinnia, F., Nair, V., Lin, J., Rajendiran, T.M., Soni, T., Byun, J., Sharma, K., Fort, P.E., Gardner, T.W., Looker, H.C., et al. (2019). Increased lipogenesis and impaired β-oxidation predict type 2 diabetic kidney disease progression in American Indians. JCI Insight *4*, e130317.

87. Yang, X., Okamura, D.M., Lu, X., Chen, Y., Moorhead, J., Varghese, Z., and Ruan, X.Z. (2017). CD36 in chronic kidney disease: novel insights and therapeutic opportunities. Nat. Rev. Nephrol. *13*, 769–781.

88. Kang, H.M., Ahn, S.H., Choi, P., Ko, Y.A., Han, S.H., Chinga, F., Park, A.S.D., Tao, J., Sharma, K., Pullman, J., et al. (2015). Defective fatty acid oxidation in renal tubular epithelial cells has a key role in kidney fibrosis development. Nat. Med. *21*, 37–46.

89. Chen, Y., Deb, D.K., Fu, X., Yi, B., Liang, Y., Du, J., He, L., and Li, Y.C. (2019). ATP-citrate lyase is an epigenetic regulator to promote obesity-related kidney injury. FASEB J. *33*, 9602–9615.

90. Baines, R.J., Chana, R.S., Hall, M., Febbraio, M., Kennedy, D., and Brunskill, N.J. (2012). CD36 mediates proximal tubular binding and uptake of albumin and is upregulated in protein uric nephropathies. Am. J. Physiol. Ren. Physiol. *303*, F1006–F1014.

91. Wang, Z., Jiang, T., Li, J., Proctor, G., McManaman, J.L., Lucia, S., Chua, S., and Levi, M. (2005). Regulation of renal lipid metabolism, lipid accumulation, and glomerulosclerosis in FVB db/db mice with type 2 diabetes. Diabetes *54*, 2328–2335.

92. Lepenies, J., Hewison, M., Stewart, P.M., and Quinkler, M. (2010). Renal PPARγ mRNA expression increases with impairment of renal function in patients with chronic kidney disease. Nephrology (Carlton) *15*, 683–691.

93. Daenen, K., Andries, A., Mekahli, D., Van Schepdael, A.V., Jouret, F., and Bammens, B. (2019). Oxidative stress in chronic kidney disease. Pediatr. Nephrol. *34*, 975–991.

94. Stenvinkel, P., Chertow, G.M., Devarajan, P., Levin, A., Andreoli, S.P., Bangalore, S., and Warady, B.A. (2021). Chronic inflammation in chronic kidney disease progression: role of Nrf2. Kidney Int. Rep. *6*, 1775–1787.

95. Liu, Y. (2011). Cellular and molecular mechanisms of renal fibrosis. Nat. Rev. Nephrol. *7*, 684–696.

96. Odermatt, A. (2011). The Western-style diet: a major risk factor for impaired kidney function and chronic kidney disease. Am. J. Physiol. Ren. Physiol. *301*, F919–F931.

97. Tomás-Simó, P., D'Marco, L., Romero-Parra, M., Tormos-Muñoz, M.C., Sáez, G., Torregrosa, I., Estañ-Capell, N., Miguel, A., Gorriz, J.L., and Puchades, M.J. (2021). Oxidative stress in non-dialysis-dependent chronic kidney disease patients. Int. J. Environ. Res. Public Health *18*, 7806.

98. Juul-Nielsen, C., Shen, J., Stenvinkel, P., and Scholze, A. (2022). Systematic review of the nuclear factor erythroid 2-related factor 2 (NRF2) system in human chronic kidney disease: alterations, interventions, and relation to morbidity. Nephrol. Dial. Transplant. *37*, 904–916.

99. Kim, H.J., and Vaziri, N.D. (2010). Contribution of impaired Nrf2-Keap1 pathway to oxidative stress and inflammation in chronic renal failure. Am. J. Physiol. Ren. Physiol. *298*, F662–F671.

100. Bolati, D., Shimizu, H., Yisireyili, M., Nishijima, F., and Niwa, T. (2013). Indoxyl sulfate, auremictoxin, downregulates renal expression of Nrf2 through activation of NF-κB. BMC Nephrol. *14*, 56.

101. Vilaysane, A., Chun, J., Seamone, M.E., Wang, W., Chin, R., Hirota, S., Li, Y., Clark, S.A., Tschopp, J., Trpkov, K., et al. (2010). The NLRP3 inflammasome promotes renal inflammation and contributes to CKD. J. Am. Soc. Nephrol. *21*, 1732–1744.

102. Segerer, S., Heller, F., Lindenmeyer, M.T., Schmid, H., Cohen, C.D., Draganovici, D., Mandelbaum, J., Nelson, P.J., Gröne, H.J., Gröne, E.F., et al. (2008). Compartment specific expression of dendritic cell markers in human glomerulonephritis. Kidney Int. *74*, 37–46.

103. Zhang, W., Wang, W., Yu, H., Zhang, Y., Dai, Y., Ning, C., Tao, L., Sun, H., Kellems, R.E., Blackburn, M.R., et al. (2012). Interleukin 6 underlies angiotensin II- induced hypertension and chronic renal damage. Hypertension *59*, 136–144.

104. Grandaliano, G., Gesualdo, L., Ranieri, E., Monno, R., Montinaro, V., Marra, F., and Schena, F.P. (1996). Monocyte chemotactic peptide-1 expression in acute and chronic human nephritides: a pathogenetic role in interstitial monocytes recruitment. J. Am. Soc. Nephrol. *7*, 906–913.

105. Ichii, O., Otsuka, S., Sasaki, N., Namiki, Y., Hashimoto, Y., and Kon, Y. (2012). Altered expression of microRNA miR-146a correlates with the development of chronic renal inflammation. Kidney Int. *81*, 280–292.

106. Romagnani, P., Lazzeri, E., Lasagni, L., Mavilia, C., Beltrame, C., Francalanci, M., Rotondi, M., Annunziato, F., Maurenzig, L., Cosmi, L., et al. (2002). IP-10 and Mig production by glomerular cells in human proliferative glomerulonephritis and regulation by nitric oxide. J. Am. Soc. Nephrol. *13*, 53–64.

107. Kassianos, A.J., Wang, X., Sampangi, S., Muczynski, K., Healy, H., and Wilkinson, R. (2013). Increased tubulointerstitial recruitment of human

CD141(hi) CLEC9A(+) and CD1c(+) myeloid dendritic cell subsets in renal fibrosis and chronic kidney disease. Am. J. Physiol. Ren. Physiol. *305*, F1391–F1401.

108. Wang, B., Jha, J.C., Hagiwara, S., McClelland, A.D., Jandeleit-Dahm, K., Thomas, M.C., Cooper, M.E., and Kantharidis, P. (2014). Transforming growth factor-β1- mediated renal fibrosis is dependent on the regulation of transforming growth factor receptor 1 expression by let-7b. Kidney Int. *85*, 352–361.

109. Rastaldi, M.P., Ferrario, F., Giardino, L., Dell'Antonio, G., Grillo, C., Grillo, P., Strutz, F., Müller, G.A., Colasanti, G., and D'Amico, G. (2002). Epithelial-mesenchymal transition of tubular epithelial cells in human renal biopsies. Kidney Int. *62*, 137–146.

110. Van Vliet, A., Baelde, H.J., Vleming, L.J., de Heer, E., and Bruijn, J.A. (2001). Distribution of fibronectin isoforms in human renal disease. J. Pathol. *193*, 256–262.

111. Moen, M.F., Zhan, M., Hsu, V.D., Walker, L.D., Einhorn, L.M., Seliger, S.L., and Fink, J.C. (2009). Frequency of hypoglycemia and its significance in chronic kidney disease. Clin. J. Am. Soc. Nephrol. *4*, 1121–1127.

112. Hettige, T.S., and Cooper, M.E. (2017). Hypoglycaemia in patients with diabetes mellitus and renal impairment. Diab. Vasc. Dis. Res. *14*, 166–168.

113. Hallan, S., Afkarian, M., Zelnick, L.R., Kestenbaum, B., Sharma, S., Saito, R., Darshi, M., Barding, G., Raftery, D., Ju, W., et al. (2017). Metabolomics and gene expression analysis reveal down-regulation of the citric acid (TCA) cycle in non-diabetic CKD patients. EBiomedicine *26*, 68–77.

114. Usberti, M., Federico, S., Cianciaruso, B., Costanzo, R., Russo, D., and Andreucci, V.E. (1979). Relationship between serum albumin concentration and tubular reabsorption of glucose in renal disease. Kidney Int. *16*, 546–551.

115. Hung, C.C., Lin, H.Y.-H., Lee, J.J., Lim, L.M., Chiu, Y.W., Chiang, H.P., Hwang, S.J., and Chen, H.C. (2016). Glycosuria and renal outcomes in patients with nondiabetic advanced chronic kidney disease. Sci. Rep. *6*, 39372.

116. Nakamura, N., Masuda, S., Takahashi, K., Saito, H., Okuda, M., and Inui, K. (2004). Decreased expression of glucose and peptide transporters in rat remnant kidney. Drug Metab. Pharmacokinet. *19*, 41–47.

117. Guebre-Egziabher, F., Bernhard, J., Funahashi, T., Hadj-Aissa, A., and Fouque, D. (2005). Adiponectin in chronic kidney disease is related more to metabolic disturbances than to decline in renal function. Nephrol. Dial. Transplant. *20*, 129–134.

118. Menon, V., Li, L., Wang, X., Greene, T., Balakrishnan, V., Madero, M., Pereira, A.A., Beck, G.J., Kusek, J.W., Collins, A.J., et al. (2006). Adiponectin and mortality in patients with chronic kidney disease. J. Am. Soc. Nephrol. *17*, 2599–2606.

119. Ku, E., Lee, B.J., Wei, J., and Weir, M.R. (2019). Hypertension in CKD: Core curriculum 2019. Am. J. Kidney Dis. *74*, 120–131.

120. Wadei, H.M., and Textor, S.C. (2012). The role of the kidney in regulating arterial blood pressure. Nat. Rev. Nephrol. *8*, 602–609.

121. Alsheikh, A.J., Dasinger, J.H., Abais-Battad, J.M., Fehrenbach, D.J., Yang, C., Cowley, A.W., Jr., and Mattson, D.L. (2020). CCL2 mediates early renal leukocyte infiltration during salt-sensitive hypertension. Am. J. Physiol. Ren. Physiol. *318*, F982–F993.

122. Mente, A., O'Donnell, M.J., Rangarajan, S., McQueen, M.J., Poirier, P., Wielgosz, A., Morrison, H., Li, W., Wang, X., Di, C., et al. (2014). Association of urinary sodium and potassium excretion with blood pressure. N. Engl. J. Med. *371*, 601–611.

123. Hansson, J.H., Nelson-Williams, C., Suzuki, H., Schild, L., Shimkets, R., Lu, Y., Canessa, C., Iwasaki, T., Rossier, B., and Lifton, R.P. (1995). Hypertension caused by a truncated epithelial sodium channel gamma subunit: genetic heterogeneity of Liddle syndrome. Nat. Genet. *11*, 76–82.

124. Seki, M., Nakayama, M., Sakoh, T., Yoshitomi, R., Fukui, A., Katafuchi, E., Tsuda, S., Nakano, T., Tsuruya, K., and Kitazono, T. (2019). Blood urea nitrogen is independently associated with renal outcomes in Japanese patients with stage 3–5 chronic kidney disease: a prospective observational study. BMC Nephrol. *20*, 115.

125. Puri, T.S., Shakaib, M.I., Chang, A., Mathew, L., Olayinka, O., Minto, A.W.M., Sarav, M., Hack, B.K., and Quigg, R.J. (2010). Chronic kidney disease induced in mice by reversible unilateral ureteral obstruction is dependent on genetic background. Am. J. Physiol. Ren. Physiol. *298*, F1024–F1032.

126. Conte, G., Dal Canton, A., Terribile, M., Cianciaruso, B., Di Minno, G., Pannain, M., Russo, D., and Andreucci, V.E. (1987). Renal handling of urea in subjects with persistent azotemia and normal renal function. Kidney Int. *32*, 721–727.

127. Blount, M.A., Sands, J.M., Kent, K.J., Smith, T.D., Price, S.R., and Klein, J.D. (2008). Candesartan augments compensatory changes in medullary transport proteins in the diabetic rat kidney. Am. J. Physiol. Ren. Physiol. *294*, F1448–F1452.

128. Fenton, R.A., Chou, C.L., Ageloff, S., Brandt, W., Stokes, J.B., and Knepper, M.A. (2003). Increased collecting duct urea transporter expression in Dahl salt-sensitive rats. Am. J. Physiol. Ren. Physiol. *285*, F143–F151.

129. Fernández-Llama, P., Andrews, P., Nielsen, S., Ecelbarger, C.A., and Knepper, M.A. (1998). Impaired aquaporin and urea transporter expression in rats with Adriamycin-induced nephrotic syndrome. Kidney Int. *53*, 1244–1253.

130. Hu, M.C., Bankir, L., Michelet, S., Rousselet, G., and Trinh-Trang-Tan, M.M. (2000). Massive reduction of urea transporters in remnant kidney and brain of uremic rats. Kidney Int. *58*, 1202–1210.

131. Nakayama, Y., Peng, T., Sands, J.M., and Bagnasco, S.M. (2000). The TonE/TonEBP pathway mediates tonicity-responsive regulation of UT-Aurea transporter expression. J. Biol. Chem. *275*, 38275–38280.

132. Malmberg, M.H., Mose, F.H., Pedersen, E.B., and Bech, J.N. (2020). Urine concentration ability is reduced to the same degree in adult dominant polycystic kidney disease compared with other chronic kidney diseases in the same CKD-stage and lower than in healthy control subjects -a CASE control study. BMC Nephrol. *21*, 379.

133. Bickel, C.A., Knepper, M.A., Verbalis, J.G., and Ecelbarger, C.A. (2002). Dysregulation of renal salt and water transport proteins in diabetic Zucker rats. Kidney Int. *61*, 2099–2110.

134. Kim, D., Sands, J.M., and Klein, J.D. (2004). Role of vasopressin in diabetes mellitus-induced changes in medullary transport proteins involved in urine concentration in Brattleboro rats. Am. J. Physiol. Ren. Physiol. *286*, F760–F766.

135. Klein, J.D., Murrell, B.P., Tucker, S., Kim, Y.H., and Sands, J.M. (2006). Urea transporter UT-A1 and aquaporin-2 proteins decrease in response to angiotensin II or norepinephrine-induced acute hypertension. Am. J. Physiol. Ren. Physiol. *291*, F952–F959.

136. Chen, Y.C., Cadnapaphornchai, M.A., Summer, S.N., Falk, S., Li, C., Wang, W., and Schrier, R.W. (2005). Molecular mechanisms of impaired urinary concentrating ability in glucocorticoid-deficient rats. J. Am. Soc. Nephrol. *16*, 2864–2871.

137. Sholokh, A., and Klussmann, E. (2021). Local cyclic adenosine monophosphate signalling cascades-Roles and targets in chronic kidney disease. Acta Physiol. Oxf. *232*, e13641.

138. Mann, J.F.E., Ørsted, D.D., Brown-Frandsen, K., Marso, S.P., Poulter, N.R., Rasmussen, S., Tornøe, K., Zinman, B., and Buse, J.B.; LEADER Steering Committee and Investigators (2017). Liraglutide and renal outcomes in Type 2 diabetes. N. Engl. J. Med. *377*, 839–848.

139. Wang, C., Li, L., Liu, S., Liao, G., Li, L., Chen, Y., Cheng, J., Lu, Y., and Liu, J. (2018). GLP-1 receptor agonist ameliorates obesity-induced chronic kidney injury via restoring renal metabolism homeostasis. PLoS One *13*, e0193473.

140. Hviid, A.V.R., and Sørensen, C.M. (2020). Glucagon-like peptide-1 receptors in the kidney: impact on renal autoregulation. Am. J. Physiol. Ren. Physiol. *318*, F443–F454.

141. Barry, D.M., McMillan, E.A., Kunar, B., Lis, R., Zhang, T., Lu, T., Daniel, E., Yokoyama, M., Gomez-Salinero, J.M., Sureshbabu, A., et al. (2019). Molecular determinants of nephron vascular specialization in the kidney. Nat. Commun. *10*, 5705.

142. Nair, A.V., Yanhong, W., Paunescu, T.G., Bouley, R., and Brown, D. (2019). Sex- dependent differences in water homeostasis in wild-type and V-ATPase B1-subunit deficient mice. PLOS One *14*, e0219940.

143. Veiras, L.C., Girardi, A.C.C., Curry, J., Pei, L., Ralph, D.L., Tran, A., Castelo-Branco, R.C., Pastor-Soler, N., Arranz, C.T., Yu, A.S.L., and McDonough, A.A. (2017). Sexual dimorphic pattern of renal transporters and electrolyte homeostasis. J. Am. Soc. Nephrol. *28*, 3504–3517.

144. Drury, E.R., Wu, J., Gigliotti, J.C., and Le, T.H. (2024). Sex differences in blood pressure regulation and hypertension: renal, hemodynamic, and hormonal mechanisms. Physiol. Rev. *104*, 199–251.

145. Ricardo, A.C., Yang, W., Sha, D., Appel, L.J., Chen, J., Krousel-Wood, M., Manoharan, A., Steigerwalt, S., Wright, J., Rahman, M., et al. (2019). Sex-related disparities in CKD progression. J. Am. Soc. Nephrol. *30*, 137–146.

146. Suyama, T., Okada, S., Ishijima, T., Iida, K., Abe, K., and Nakai, Y. (2012). High phosphorus diet-induced changes in NaPi-IIb phosphate transporter expression in the rat kidney: DNA microarray analysis. PLoS One *7*, e29483.

147. An, Y.A., Chen, S., Deng, Y., Wang, Z.V., Funcke, J.B., Shah, M., Shan, B., Gordillo, R., Yoshino, J., Klein, S., et al. (2021). The mitochondrial dicarboxylate carrier prevents hepatic lipotoxicity by inhibiting white adipocyte lipolysis. J. Hepatol. *75*, 387–399.

148. Cannavino, J., Shao, M., An, Y.A., Bezprozvannaya, S., Chen, S., Kim, J., Xu, L., McAnally, J.R., Scherer, P.E., Liu, N., et al. (2021). Regulation of cold-induced thermogenesis by the RNA binding protein FAM195A. Proc. Natl. Acad. Sci. USA *118*, e2104650118.

Please cite this article in press as: Wang et al., Downregulation of the kidney glucagon receptor, essential for renal function and systemic homeostasis, contributes to chronic kidney disease, Cell Metabolism (2023), https://doi.org/10.1016/j.cmet.2023.12.024

STAR★METHODS

KEY RESOURCES TABLE

REAGENT or RESOURCE	SOURCE	IDENTIFIER
Antibodies		
Goat anti-MyD88 (F-19)	Santa Cruz Biotechnology	Cat#: sc-8197; RRID:AB_2146726
Hamster anti-mouse CD11c	AbD Serotec	Cat#: MCA1369; RRID:AB_324490
Mouse anti-beta Actin (AC-15)	Sigma-Aldrich	Cat#: A1978; RRID:AB_476692
Rabbit anti-Aquaporin 2	Thermo Fisher Scientific	Cat#: PA5-78809; RRID:AB_2745925
Rabbit anti-collagen I	Thermo Fisher Scientific	Cat#: PA5-95137; RRID:AB_2806942
Rabbit anti-collagen type III (N-terminal)	Proteintech	Cat#: 22734-1-AP; RRID:AB_2879158
Rabbit anti-collagen IV	Abcam	Cat#: Ab6588; RRID: AB_305585
Rabbit anti-fibronectin	Chemicon	Cat#: AB1943; RRID: AB_3076383
Rabbit anti-SLC9A3 (HNE3)	Proteintech	Cat#: 27190-1-AP; RRID:AB_2880793
Rat anti-mouse F4/80 (BM8), Alexa Fluor 647	Thermo Fisher Scientific	Cat#: MF48021; RRID:AB_10375289
Donkey anti-mouse IgG, IRDye 680RD	LI-COR Biosciences	Cat#: 926-68072; RRID: AB_10953628
Goat anti-rabbit IgG, IRDye 800CW	LI-COR Biosciences	Cat#: 925-32211; RRID: AB_2651127
Goat anti-Syrian hamster IgG, Alexa Fluor 488	Thermo Fisher Scientific	Cat#: A-21110; RRID:AB_2535759
Donkey anti-rabbit IgG, Alexa Flour 594	Thermo Fisher Scientific	Cat#: A-21207; RRID:AB_141637
Donkey anti-goat IgG, Alexa Flour 594	Thermo Fisher Scientific	Cat#: A-11058; RRID:AB_2534105
Chemicals, peptides, and recombinant proteins		
Alexa Fluor 594-conjugated WGA	Thermo Fisher	Cat#: W11262
Antifade mounting medium with DAPI	Vectashield	Cat#: H-1200
Aprotinin from bovine lung	Sigma-Aldrich	Cat#: A6279
BSA	Sigma-Aldrich	Cat#: A8806
(±)-1,3-Butanediol	Sigma-Aldrich	Cat#: B84785
Chloroform	Sigma-Aldrich	Cat#: C2432
DAPI (4′,6-Diamidino-2-phenylindole dihydrochloride)	Sigma-Aldrich	Cat#: D8417
DMEM with low glucose	Thermo Fisher	Cat#: 11885084
Fetal Bovine Serum	Sigma-Aldrich	Cat#: 12303C
Glucose	Gibco	Cat#: 15023021
L-Glutamine	Sigma-Aldrich	Cat#: G3126
HEPES	Gibco	Cat#: 15630080
Insulin	Eli Lilly	Product ID: A10008415
Intralipid	Sigma-Aldrich	Cat#: 6I141
Lipofectamine RNAiMAX Transfection Reagent	Thermo Fisher	Cat#: 13778075
Long-acting glucagon analogue IUB288	Kind gift from Eli Lilly	N/A
NuPAGE LDS Sample Buffer (4X)	Thermo Fisher	Cat#: NP0008
Opti- MEM I reduced serum medium	Gibco	Cat#: 31985062
Paraformaldehyde	Sigma-Aldrich	Cat#: P6148
Penicillin and streptomycin	Gibco	Cat#: 15140122
Pierce Phosphatase Inhibitor Mini Tablets	Thermo Fisher	Cat#: A32957
Pierce Protease Inhibitor Mini Tablets	Thermo Fisher	Cat#: A32953
Polysorbate 80	Thermo Fisher	Cat#: 278632500
Recombinant Human TGF-beta 1 Protein	R&D Systems Inc.	Cat#: 7754-BH-005
Sodium L-lactate	Sigma-Aldrich	Cat#: 71718
Sodium pyruvate	Sigma-Aldrich	Cat#: P2256
^{3}H-Triolein	PerkinElmer	Cat#: NEC075H050UC
Trizol	Invitrogen	Cat#: 12034977

(*Continued on next page*)

Please cite this article in press as: Wang et al., Downregulation of the kidney glucagon receptor, essential for renal function and systemic homeostasis, contributes to chronic kidney disease, Cell Metabolism (2023), https://doi.org/10.1016/j.cmet.2023.12.024

Continued

REAGENT or RESOURCE	SOURCE	IDENTIFIER
[Arg8]-Vasopressin acetate salt	Sigma-Aldrich	Cat#: V9879
Critical commercial assays		
L-Amino Acid Quantitation Kit	Sigma-Aldrich	Cat#: MAK002
cAMP complete ELISA kit	Enzo Life Sciences	Cat#: ADI-900-163
Beta-Hydroxybutyrate Assay Kit	Sigma-Aldrich	Cat#: MAK041
Corticosterone Competitive ELISA Kit	Thermo Fisher	Cat#: EIACORT
Cystatin C (CST3) Mouse ELISA Kit	Thermo Fisher	Cat#: EMCST3
HR Series NEFA-HR(2) Color Reagent A	Wako	Cat#: 999-34691
HR Series NEFA-HR(2) Color Reagent B	Wako	Cat#: 991-34891
HR Series NEFA-HR(2) Color Solvent A	Wako	Cat#: 995-34791
HR Series NEFA-HR(2) Color Solvent B	Wako	Cat#: 993-35191
Infinity Cholesterol Reagent	Thermo Fisher	Cat#: TR13421
Infinity Triglycerides Reagent	Thermo Fisher	Cat#: TR22421
iScript cDNA Synthesis Kit	BioRad	Cat#: 170-8891
Mouse albumin ELISA kit	Fisher Scientific	Cat#: NC9608467
Mouse Glucagon ELISA-10 uL Kit	Mercodia	Cat#: 10-1281-01
Mouse Ultra Sensitive Insulin ELISA Kit	Crystal Chem	Cat#: 90080
Pierce BCA Protein Assay kit	Thermo Fisher	Cat#: 23225
PGO Enzyme Preparation	Sigma-Aldrich	Cat#: P7119
RIPA buffer	Sigma-Aldrich	Cat#: R0278
SensoLyte 520 Mouse Renin Assay Kit (Fluorimetric)	AnaSpec.com	Cat#: AS-72161
Sybr Green Master Mix	Applied Biosystems	Cat#: A25778
Experimental models: Cell lines		
MDCK cells	Kind gift from Dr. Guosheng Liang, UTSW medical center	N/A
Experimental models: Organisms/strains		
Mouse: Albumin-Cre	The Jackson Laboratory	JAX003574; RRID:IMSR_JAX:003574
Mouse: Gcgr flox/flox	Longuet et al.[50]	N/A
Mouse: Global Gcgr knockout	Gelling et al.[54]	N/A
Mouse: KspCad-rtTA	UTSW O'Brien Kidney Research Core Center	N/A
Mouse: Six2-Cre	UTSW O'Brien Kidney Research Core Center	N/A
Mouse: TRE-Cre	The Jackson Laboratory	JAX006234; RRID: IMSR_JAX:006234
Oligonucleotides		
Primers for qPCR	Table S2	N/A
Software and algorithms		
BP-2000 Analysis	Visitech Systems	https://www.2biol.com/2biol_BP%20Blood%20Pressure%20Recorder.htm; RRID:SCR_022985
Excel	Microsoft	N/A
Image J (version 1.53c)	NIH	https://imagej.nih.gov/ij/; RRID: SCR_003070
Image Studio Lite	LI-COR Biosciences	http://www.licor.com/bio/products/software/image_studio_lite/; RRID:SCR_013715
NDP.view2 Plus (version 2.9.29)	Hamamatsu Photonics	N/A
PowerPoint	Microsoft	N/A
Prism (version 10.0)	GraphPad Software	GraphPad Software
Word	Microsoft	N/A

(*Continued on next page*)

Please cite this article in press as: Wang et al., Downregulation of the kidney glucagon receptor, essential for renal function and systemic homeostasis, contributes to chronic kidney disease, Cell Metabolism (2023), https://doi.org/10.1016/j.cmet.2023.12.024

Continued

REAGENT or RESOURCE	SOURCE	IDENTIFIER
Other		
60% HFD paste	Bio-serv	S1850
Automatic Temperature controller	Warner Instrument	Cat#: TC-324C
Beckman Coulter LS6500 multi-purpose scintillation counter	Beckman	N/A
Bruker Minispec mq10	Brucker	Cat#: TMTA2892161
Doxycycline chow diet (600 mg/kg diet)	Bio-serv	S4107
Glucometers	Bayer Health Care	N/A
Heparinized micro-Hematocrit capillary tubes	Fisher Scientific	Cat#: 22-362-566
In-line heater (Model: SH-27B)	Warner Instrument	Cat#: 64-0102
Keyence BZ-X710 Fluorescence Microscope	Keyence	N/A
Microvette CB 300Z	Sarstedt	Cat#: 16440100
Microvette CB 300 K2E	Sarstedt	Cat#: 16444100
Micro-Renathane tubing	Braintree Scientific	Cat#: MRE-033
MISSION siRNA Universal Negative Control #1	Sigma-Aldrich	Cat#: SIC001
NanoZoomer S60 digital slide scanner	Hamamatsu Photonics	N/A
Nexera X2 UHPLC-LCMS-8060	Shimadzu Scientific Instruments	N/A
Normal chow diet	TEKLAD	2916
Odyssey Infrared Imager	LI-COR Biosciences	N/A
Predesigned siRNA Gcgr NM 000160 Sequence Start 691	Sigma-Aldrich	Cat#: SASI_Hs01_00240226
Predesigned siRNA Gcgr NM 000160 Sequence Start 1413	Sigma-Aldrich	Cat#: SASI_Hs01_00240227
QuantStudio 6 flex real-time PCR system	Applied Biosystems	N/A
RNAscope probe Mm-Gcgr-O5-C1	Advanced Cell Diagnostics	Cat#: 1244271
RNAscope probe Mm-Slc12a1-C2	Advanced Cell Diagnostics	Cat#: 476841-C2
RNAscope probe Mm-Pecam1-C2	Advanced Cell Diagnostics	Cat#: 316721-C2
RNAscope probe Mm-Pdgfrb-C2	Advanced Cell Diagnostics	Cat#: 411381-C2
RNAscope probe Mm-Csf1r-C2	Advanced Cell Diagnostics	Cat#: 428191-C2
Rodent thermo-Chamber	Powers Scientific	N/A
Scintillation vial	RPI	SKU: 121000CA
Tail-cuff blood pressure system BP-2000 series II	Visitech Systems	N/A
Trans-blot Turbo Nitrocellulose Transfer pack	BioRad	Cat#: 1704158
Trans-blot Turbo PVDF Transfer pack	BioRad	Cat#: 1704156

RESOURCE AVAILABILITY

Lead contact

Further information and requests for resources and reagents should be directed to and will be fulfilled by the lead contact, Philipp E. Scherer (philipp.scherer@utsouthwestern.edu).

Materials availability

Mouse lines generated in this study are available upon request from the lead contact.

Data and code availability

- Data S1 - Source Data contains the data used to generate the main and supplemental figures in the paper.
- This paper does not report original code.
- Any additional information required to reanalyze the data reported in this paper is available from the lead contact upon request.

Please cite this article in press as: Wang et al., Downregulation of the kidney glucagon receptor, essential for renal function and systemic homeostasis, contributes to chronic kidney disease, Cell Metabolism (2023), https://doi.org/10.1016/j.cmet.2023.12.024

EXPERIMENTAL MODEL AND STUDY PARTICIPANT DETAILS

Mouse Models

Mouse experimental protocols were approved by the Institutional Animal Care and Use Committee of the University of Texas Southwestern (UTSW) Medical Center at Dallas, TX. Constitutive kidney-specific *Gcgr* knockout mice were generated by a cross between the *Six2-Cre* mouse (purchased from the O'Brien Kidney Research Core Center, UTSW Medical Center) and the $Gcgr^{flox}$ mouse.[50] For generation of conditional kidney tubule-specific *Gcgr* knockout mice, the $Gcgr^{flox}$ mouse was first bred with the *KspCad-rtTA* mouse (purchased from the O'Brien Kidney Research Core Center, UTSW Medical Center) or with the *TRE-Cre* mouse.[147] The offspring harboring hemizygous *KspCad-rtTA* and homozygous floxed *Gcgr* alleles were then crossed with those carrying hemizygous *TRE-Cre* and homozygous floxed *Gcgr* alleles to generate a transgenic mouse line, with hemizygosity for *KspCad-rtTA* and *TRE-Cre* alleles and homozygosity for the floxed *Gcgr* allele, for conditional *Gcgr* ablation in the kidneys. Liver-specific *Gcgr* knockout mice were obtained by breeding the Albumin-*Cre* mouse (Jackson Laboratory) and the $Gcgr^{flox}$ mouse, similar to the knockout mice previously reported.[50] All mice were bred in the C57BL/6 genetic background. Global *Gcgr* knockout mice[54] were provided by Dr. Maureen Charron (Albert Einstein College of Medicine). Mouse knockouts were identified and verified by specific PCR genotyping.

All mice were housed under pathogen-free conditions in a 12-hour light/12-hour dark cycle. They were fed either a standard chow diet (LabDiet) or a high-fat diet (60% kCal from fat; Research Diets) and water *ad libitum*. Male mice at 3-5 months of age were used in the studies, unless specified otherwise. To excise the loxP-flanked *Gcgr* coding region via *Cre*-mediated recombination specifically in adult mouse kidneys, 2-3-month-old conditional *Gcgr* knockout mice described above were fed a chow diet containing 600 mg/kg doxycycline (Bio-Serv) for 6 weeks to induce kidney tubule-specific expression of *Cre* recombinase.

For the study at mouse thermoneutrality, mice fed a chow diet were housed at 30°C for7 weeks in a chamber with a 12-h light/12-h dark cycle. In the fasting-refeeding study, mice were fasted for 16 hours and then refed with the chow diet for 24 hours. For the study of 1,3-butanediol treatment, mice were randomly divided into two groups to receive either drinking water containing 15% (v/v) 1,3-butanediol (Sigma) for 4 weeks or regular water without 1,3-butanediol over the same period.

METHOD DETAILS

In Vivo metabolic tolerance tests

Oral glucose tolerance tests were performed in mice following overnight fasting. Glucose (2 g/kg body weight) was administered into fasted mice by oral gavage. Blood glucose concentrations at the baseline and indicated intervals over a span of 2 hours after the glucose load were measured by a hand-held glucometer (Bayer HealthCare).

Insulin tolerance tests were conducted in mice after morning fasting (9 am to 2 pm). A bolus of Humulin R regular insulin (0.5 U/kg body weight for chow diet-fed groups and 0.75 U/kg body weight for high-fat diet-fed groups, Eli Lilly) was delivered via intraperitoneal injection. Blood glucose levels over time in mice receiving a dose of insulin were monitored by the glucometer as described above. The area under the glucose curve was calculated by the trapezoidal method using GraphPad Prism software (version 10.0).

Pyruvate and glutamine tolerance tests were carried out in mice without access to food overnight prior to the administration by intraperitoneal injection of 2 g sodium pyruvate (Sigma) or L-glutamine (Sigma) per kg body weight. Following the load, blood glucose and the area under the curve was determined as described above.

Oral lipid tolerance tests were performed in mice fasted for 16 hr. A load of Intralipid fat emulsion (15 μl/g body weight; Sigma) was administered via oral gavage. Blood samples were then taken every one hour through tail vein for the measurement of serum triglyceride levels by the Infinity triglycerides liquid stable reagent (ThermoFisher Scientific). For experiments involving ^{3}H-labeled triolein as a tracer, administration of Intralipid along with ^{3}H-labeled triolein (2 μCi/mouse, PerkinElmer) was through retro- orbital injection. Various tissues were harvested 15 min after the lipid load and were flash frozen immediately in liquid nitrogen. Tissue lipids were extracted with 2:1 chloroform-methanol mixture (v/v). The chloroform phase-associated ^{3}H radioactivity, as a marker of tissue lipid uptake from the blood circulation, was determined by a scintillation counter (Beckman).

Long-acting glucagon analog treatment

Following overnight fasting, *Gcgr*-deficient and control mice received intraperitoneally a long-acting glucagon analogue IUB288 (dosed at 10 nmol/kg body weight; a kind gift from Eli Lilly), dissolved at 2 pmol/μL in T8 buffer containing 40 mM Tris-HCl, pH 8.0, and 0.02% polysorbate 80 (Thermo Fisher Scientific). Blood glucose concentrations in IUB288-administered mice were measured at the indicated times by a hand-held glucometer (Bayer HealthCare). The area under the glucose curve was calculated as described above.

Mouse body composition analysis

Whole-body fat and lean mass, as well as fluid content, in control and knockout mice was analyzed using a NMR minispec device (Bruker Corporation) at the Metabolic Phenotyping Core of UTSW Medical Center.

Please cite this article in press as: Wang et al., Downregulation of the kidney glucagon receptor, essential for renal function and systemic homeostasis, contributes to chronic kidney disease, Cell Metabolism (2023), https://doi.org/10.1016/j.cmet.2023.12.024

Serum, plasma, and urine collection

Mouse serum and plasma were prepared from whole blood using Microvette CB 300Z serum, capillary blood collection (Sarstedt) and Microvette CB 300 K2 EDTA, capillary blood collection (Sarstedt), respectively. For plasma glucagon assays, 0.5 μl of a protinin saline solution (Sigma) was added to each collection tube.

For urine collection, the mice were individually placed in the metabolic cages (Techniplast). After a day of acclimatization, urine from each mouse was collected every 24 h for 5 days. The daily values of urine output and water intake were noted.

In water deprivation study, the mice were placed in the metabolic cages, and after acclimatization, urine samples were collected daily for 4 days. Mice were then deprived of drinking water for 24 h (with free access to food). Over this period of dehydration, body weights were monitored and urines were collected for osmolality measurements.

Exogenous arginine vasopressin treatment

Control and knockout mice were intraperitoneally injected with 5 ng of [8-D-arginine] vasopressin (MilliporeSigma) in 100 μl saline solution. Immediately before and 4 hours after injection, urines from these mice were collected for osmolality measurements.

Insulin, glucagon, cAMP, and corticosterone measurement

The concentrations of plasma insulin, glucagon, and cAMP, as well as serum corticosterone were determined using an ultrasensitive mouse insulin ELISA kit (Crystal Chem), glucagon ELISA - 10 μL kit (Mercodia), cAMP complete ELISA kit (Enzo Life Sciences), and corticosterone competitive ELISA kit (Invitrogen), respectively.

Albumin, cystatin C, and renin measurement

The levels of urinary albumin and serum cystatin C, as well as the activity of plasma renin were measured using an Immunology Consultants mouse albumin ELISA kit (Fisher Scientific), Invitrogen cystatin C mouse ELISA kit (ThermoFisher Scientific), and SensoLyte 520 mouse renin assay kit (AnaSpec), respectively.

Analysis of amino acids and metabolites in serum and urine

Serum or urinary levels of total L-amino acids, exclusive of glycine, in control and knockout mice were determined using an L-amino acid quantitation kit (Sigma). The profiling of individual amino acids, kynurenine, citrulline, and glutathione was performed by the Metabolic Phenotyping Core of UTSW Medical Center, using a Nexera X2 UHPLC-LCMS-8060 system coupled to an automatic sample preparation method CLAM-2030 (Shimadzu Scientific Instruments).[148] Creatinine in serum and urea in both serum and urine were assayed at the Metabolic Phenotyping Core of UTSW Medical Center, using a VITROS 350 chemistry system clinical analyzer (Ortho Clinical Diagnostics). Ketone β-hydroxybutyrate in serum collected from mice either fed *ad Libitum* or following a 4-h fast was measured with a β-hydroxybutyrate colorimetric assay kit (Sigma). Serum triglyceride, free fatty acids, and cholesterol were assayed using the Infinity triglycerides liquid stable reagent (Thermo Fisher Scientific), the Wako NEFA- HR(2) color reagent (FUJIFILM Medical Systems), and the Infinity cholesterol liquid stable reagent (Thermo Fisher Scientific), respectively.

Analysis of electrolytes and pH in serum and urine

The measurement of serum and urinary sodium, potassium, calcium, chloride, and phosphate ion concentrations was performed by the Metabolic Phenotyping Core of UTSW Medical Center, using a VITROS 350 chemistry system clinical analyzer. Urinary osmolyte levels and pH in serum and urine were assessed by the O'Brien Kidney Research Core Center of UTSW Medical Center.

Measurement of blood pressure and heart rate

Systolic blood pressure, diastolic blood pressure, mean arterial pressure, and resting heart rate in conscious control and knockout mice were monitored by a noninvasive automated tail-cuff blood pressure system (BP-2000 series II, Visitech Systems) in a quiet room at the O'Brien Kidney Research Core Center of UTSW Medical Center. The mice were given 3-4 days of training sessions to become accustomed to the restrainers and tail-cuff procedures. Subsequently, sessions of total 40-50 recorded measurements were carried out on two consecutive days for the determination of blood pressure and heart rate of each individual mouse.

Mouse kidney perfusion

Control and knockout mice were anesthetized with 2% isoflurane in 95% O_2/5% CO_2 gas. The mice were fixed in a supine position and the peritoneal cavity was opened with a midline incision. An opened ligature was placed around right renal vein close to the junction with vena cava to collect the perfusate. Two tied ligatures were placed around the celiac artery and mesenteric artery, and heparin (100 U per 25 g body weight) was injected via a 31G needle into lower abdominal vena cava. Another two opened ligatures were placed at the proximal end of aorta right below mesenteric artery junction and around the aorta right above celiac artery.

At the beginning of perfusion, the opened suture below the mesenteric artery junction was closed first and an 18G blunt end needle loaded with perfusion medium was installed, and the other opened suture located at the aorta right above the celiac artery was tightened. Micro-Renathane tubing (Braintree Scientific) was inserted and the opened suture around the right renal vein was closed. The perfusion medium contained 129mM NaCl, 4.8mM KCl, 10mM bicarbonate, 9.6mM $CaCl_2$, 1mM $MgSO_4$, 1mM KH_2PO_4, 0.65% BSA, 3.6% dextran, and 20mM HEPES. The medium temperature was adjusted around 37 °C by an in-line heater (Warner Instrument). The perfusion pressure was maintained below 80 mmHg at the rate of 0.8-1 ml/min. For assessment of glucose output by the perfused

kidneys, the perfusion medium was supplemented with 40mM pyruvate, 10 mM glutamine and 25 mM lactate as gluconeogenic substrates, following a 10-min equilibration period with the medium alone. Samples of perfusate collected at10-min intervals during the perfusion after substrate addition were used for analysis of glucose concentrations by a PGO enzyme method (Sigma).

Measurement of renal triglyceride content

Kidney tissue samples harvested from control and knockout mice were flash frozen immediately. Triglyceride content in the kidney was measured by the Metabolic Phenotyping Core of UTSW Medical Center. Briefly, total lipids in 100mg samples were extracted with 2:1 chloroform-methanol mixture (v/v), dried under nitrogen, and dissolved in ethanol containing 1% Triton X-100. The concentrations of triglyceride were determined using the Infinity triglycerides liquid stable reagent (Thermo Fisher Scientific).

Histological analysis

Mouse kidneys fixed in 10% neutral buffered formalin overnight were embedded in paraffin, sectioned, and stained with trichrome or with hematoxylin and eosin by the Histo Pathology Core of UTSW Medical Center. For immunofluorescence analysis, paraffin-embedded kidney sections were deparaffinized and heated in 10 mM sodium citrate (pH 6.0) along with 0.05% Tween-20 for epitope retrieval. For immunofluorescent staining of extracellular matrix proteins, the sections were blocked with Tris-buffered saline containing 20% AquaBlock (Abcam) and 0.1% Tween-20, and were then incubated overnight at 4 °C with the following primary antibodies: collagen I polyclonal antibody (1:500 dilution, Invitrogen), collagen type III (N-terminal) polyclonal antibody (1:500 dilution, Thermo Fisher Scientific), collagen IV polyclonal antibody (1:500 dilution, Abcam), or anti-fibronectin antibody (1:500 dilution, Chemicon). After washing in PBS with 0.05% Tween-20, the sections were incubated with AlexaFluor 594-conjugated anti-rabbit secondary antibody (1:500 dilution, Invitrogen), were counterstained with DAPI(4',6-diamidino-2-phenylindole), and were mounted with anti-fade mounting medium (Vectashield). Multiple visual fields of each immunostained section were examined using BZ-X710 all-in-one fluorescence microscope (Keyence). The captured digital images of 5-10 fields were used to quantify areas of matrix protein- and DAPI-positive fluorescent stains by NIH ImageJ software (version 1.53c).

For immunofluorescent staining of renal transporter proteins, kidney sections were prepared as described above, followed by the overnight incubation with primary antibodies to SLC9A3 (NHE3; 1:500 dilution, Proteintech) or AQP2 (1:500 dilution, Thermo Fisher Scientific). After washing, the sections were incubated with secondary antibodies conjugated to Alexa Fluor 594 and nuclei were labeled with DAPI. The fluorescent images of immunostained sections were taken with BZ-X710 all-in-one fluorescence microscope (Keyence). For immunofluorescent staining of immune markers, kidney sections were prepared as described above, followed by the incubation with primary antibodies to MyD88 (1:50 dilution, Santa Cruz Biotechnology), CD11c (1:50 dilution, AbD Antibodies Direct), or F4/80 (1:500 dilution, Invitrogen). After incubation with the secondary antibodies, the stained sections were observed under BZ-X710 all-in-one fluorescence microscope (Keyence). The fluorescent stain areas were quantified as described above.

Mouse hearts fixed in 10% neutral buffered formalin were embedded in paraffin, sectioned, and stained with hematoxylin and eosin (H&E) by the Histo Pathology Core of UTSW Medical Center. Microphotographs of H&E-stained heart sections were obtained with a NanoZoomer S60 digital slide scanner and NDP.view2 image viewing software (Hamamatsu Photonics). For wheat germ agglutinin (WGA) staining, heart sections were deparaffinized, hydrated, and incubated in Tris-buffered saline containing 20% AquaBlock (Abcam) and 0.1% Tween-20. Staining of cardiomyocyte membrane was performed overnight at 4°C with Alexa Fluor 594-conjugated WGA (10 μg/mL, Thermo Fisher Scientific), followed by three washing steps. The images of WGA-stained sections were captured using BZ-X710 all-in-one fluorescence microscope (Keyence).

Immunoblot analysis

Mouse kidneys were homogenized in RIPA buffer (50mM Tris-HCl, pH8.0, 150 mM NaCl, 1% Triton X-100, 0.5% sodium deoxycholate, 0.1% SDS) plus phosphatase and protease inhibitor cocktail (Thermo Fisher Scientific). Total protein extracts were resolved by SDS-PAGE using NuPAGE 4-20% Bis-Tris mini protein gels (Invitrogen), and transferred to a polyvinylidene difluoride membrane (BioRad). After blocking with 5% nonfat dry milk in Tris-buffered saline containing 0.1% Tween (TBST), the blotted membrane was incubated with a primary anti-NHE3 antibody (1:1000 dilution, Proteintech) or anti-AQP2 antibody (1:1000 dilution, Invitrogen) for overnight at 4°C.The membrane was then washed in TBST buffer and incubated with a secondary antibody IRDye 800CW goat anti-rabbit IgG (1:5000 dilution, LI-COR Biosciences). The signals on the immunoblot membrane were visualized using an Odyssey Infrared Imager. β-Actin protein was used as a loading control. The same membrane was stripped with a stripping buffer (LI-COR Biosciences) and re-probed with an anti-beta actin antibody (Sigma-Aldrich) and a secondary antibody IRDye680RD goat anti-mouse IgG (LI-COR Biosciences). Densitometric analysis of the corresponding bands was performed using NIH ImageJ software.

RNAscope *in situ* hybridization

RNAscope multiplex fluorescent assay was performed by the Metabolic Phenotyping Core of UTSW Medical Center to detect the transcripts for target genes of interest in fixed frozen sections of mouse kidneys. The section slides were pretreated by following the manufacturer's instructions (Advanced Cell Diagnostics (ACD)). After boiling slides in a Target Retrieval solution, they were rinsed in distilled water and dehydrated in100% ethanol. Sectioned tissue was enzymatically digested at 40 °C for 15 min. The *in situ* hybridization was performed with reagents from the RNAscope multiplex Detection Kit V2 (ACD) by following the recommended ACD procedure. The probes, including Mm-Gcgr-O5-C1, Mm-Slc12a1-C2, Mm-Pecam1-C2, Mm-Pdgfrb-C2, and Mm-Csf1r-C2, were applied at 40 °C for 2 h. Amplification steps were done following the manufacturer's instructions using Opal dyes 520 and 570. Slides

were counterstained with DAPI before applying mounting medium (ProLong Gold Antifade) and cover slips over the kidney sections. Fluorescence signals were observed and captured using BZ- X710 all-in-one fluorescence microscope (Keyence).

Gene expression analysis by RT-QPCR

Mouse tissue samples were homogenized in Trizol (Invitrogen) using the TissueLyser II (Qiagen) for total RNA extraction. Aliquots (1 μg) of purified RNA were reverse transcribed to cDNAs using aniScript cDNA Synthesis Kit (BioRad). The expression of specific genes was measured with SYBR Green PCR Master Mix (Applied Biosystems) by quantitative PCR using a QuantStudio 6 flex real-time PCR system (Applied Biosystems). Relative mRNA expression was calculated by the comparative Ct method using a housekeeping gene 36b4 (mouse tissue samples) or beta-2-microglobulin (MDCK cell samples) for normalization.

MDCK cell culture

Madin-Darby canine kidney (MDCK) cells (provided by Dr. Guosheng Liang, UTSW Medical Center) were cultured at 37°C in Dulbecco's Modified Eagle Medium (with glucose at 1 g/L) supplemented with 10% fetal bovine serum and with 100 units/mL penicillin and 100 μg/mL streptomycin in 5%CO_2/95% air. For *Gcgr* knockdown experiments, MDCK cells grown to 70% confluence were transfected for 72 hours with a mixture of either predesigned human *Gcgr* small interfering RNA (siRNA) or siRNA universal negative control (final concentration 20 pmol/ml; MilliporeSigma) and Lipofectamine RNAiMAX transfection reagent (Thermo Fisher Scientific) in an Opti-MEM I reduced serum medium (Gibco). For transforming growth factor β (TGFβ) treatment, normal or siRNA-transfected MDCK cells were incubated for 24 hours with recombinant human TGFβ1 (5 ng/mL; R&D Systems). The cells were then harvested for RNA isolation and RT-QPCR analysis.

QUANTIFICATION AND STATISTICAL ANALYSIS

Results are presented as mean ± SD and were evaluated by Student's t test using Excel (Microsoft) for comparison between two groups. Exact values of n can be found in the figure legends. P values of less than 0.05 were considered statistically significant.

Cell Metabolism, Volume *36*

Supplemental information

Downregulation of the kidney glucagon receptor, essential for renal function and systemic homeostasis, contributes to chronic kidney disease

May-Yun Wang, Zhuzhen Zhang, Shangang Zhao, Toshiharu Onodera, Xue-Nan Sun, Qingzhang Zhu, Chao Li, Na Li, Shiuhwei Chen, Megan Paredes, Laurent Gautron, Maureen J. Charron, Denise K. Marciano, Ruth Gordillo, Daniel J. Drucker, and Philipp E. Scherer

Figure S1

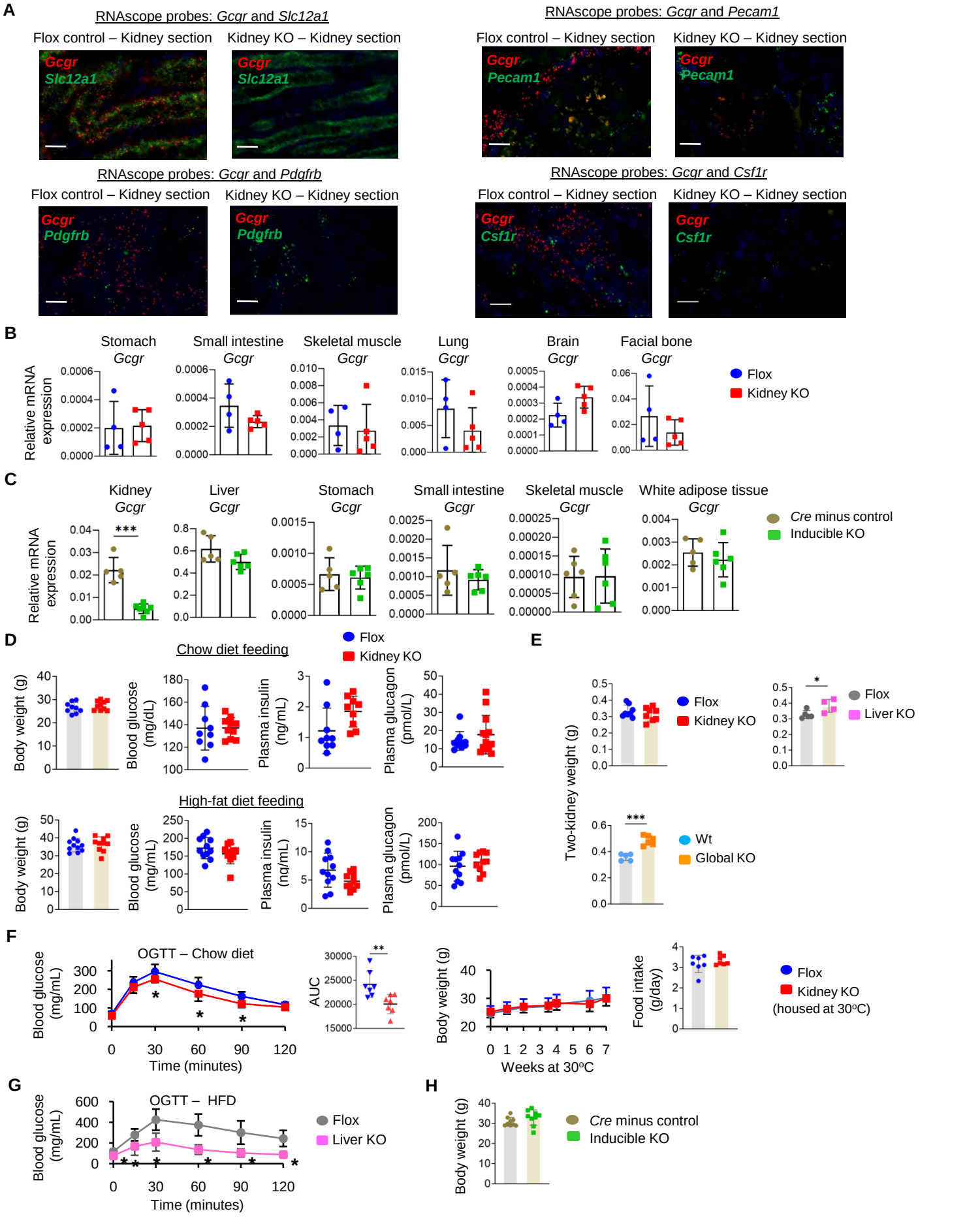
A
RNAscope probes: Gcgr and Slc12a1
Flox control – Kidney section
Kidney KO – Kidney section
Gcgr
Slc12a1
RNAscope probes: Gcgr and Pecam1
Gcgr
Pecam1
RNAscope probes: Gcgr and Pdgfrb
Gcgr
Pdgfrb
RNAscope probes: Gcgr and Csf1r
Gcgr
Csf1r
B
Stomach
Small intestine
Skeletal muscle
Lung
Brain
Facial bone
Gcgr
Relative mRNA expression
Flox
Kidney KO
C
Kidney
Liver
Stomach
Small intestine
Skeletal muscle
White adipose tissue
***
Cre minus control
Inducible KO
D
Chow diet feeding
High-fat diet feeding
Body weight (g)
Blood glucose (mg/dL)
Blood glucose (mg/mL)
Plasma insulin (ng/mL)
Plasma glucagon (pmol/L)
Flox
Kidney KO
E
Two-kidney weight (g)
Flox
Kidney KO
Flox
Liver KO
***
Wt
Global KO
F
OGTT – Chow diet
Blood glucose (mg/mL)
Time (minutes)
AUC
**
Body weight (g)
Weeks at 30°C
Food intake (g/day)
Flox
Kidney KO
(housed at 30°C)
G
OGTT – HFD
Blood glucose (mg/mL)
Time (minutes)
Flox
Liver KO
H
Body weight (g)
Cre minus control
Inducible KO

Figure S1. Characterization of kidney- and liver-specific *Gcgr* knockout mice. Related to Figure 1.
(A) Representative microphotographs of RNAscope *in situ* hybridization for mRNAs of *Gcgr* (in red) and various cell-type markers (*Slc12a1*, *Pecam1*, *Pdgfrb, Csf1r*; in green) on kidney sections from kidney-specific *Gcgr* knockout (kidney KO) and floxed control (Flox) mice. Nuclei were stained with DAPI (in blue). *Gcgr*, glucagon receptor; *Slc12a1*, solute carrier family 12 member 1; *Pecam1*, platelet endothelial cell adhesion molecule; *Pdgfrb*, platelet-derived growth factor receptor beta; *Csf1r*, macrophage colony-stimulating factor 1 receptor. Scale bar, 20 μm. **(B)** QPCR analysis of glucagon receptor (*Gcgr*) mRNA expression in different tissues from kidney KO and Flox mice. Housekeeping gene 36b4 was used for normalization of gene transcript levels. Results are represented as mean ± SD; n = 4-5 mice per group; *p < 0.05 by Student's t test. **(C)** QPCR analysis of glucagon receptor (*Gcgr*) mRNA expression in different tissues from doxycycline-treated inducible *Gcgr* KO and *Cre* minus control mice. n = 5-6 mice per group; ***p < 0.001. **(D)** Body weights and metabolic parameters (blood glucose, plasma insulin, and plasma glucagon) in kidney KO and Flox mice fed a chow diet or a high fat diet (for 5 weeks). n = 7-11mice per group. **(E)** Two-kidney weights in various *Gcgr*-deficient and respective control mice. Liver KO and Flox, liver-specific *Gcgr* knockout and floxed control mice; global KO and wt, global *Gcgr* knockout and wild-type control mice. n = 4-8 mice per group; *p < 0.05, ***p < 0.001. **(F)** Blood glucose levels during oral glucose tolerance tests (OGTTs), body weights and food intake in kidney KO and Flox mice housed at 30^{o}C. AUC, area under the curve. n = 7 mice per group; *p < 0.05, **p < 0.01. **(G)** Blood glucose levels during OGTTs performed in high fat diet (HFD)-fed liver KO and Flox mice. n = 5 mice per group; *p < 0.05. **(H)** Body weights in inducible KO and *Cre* minus control mice. n = 4-9 mice per group.

Figure S2

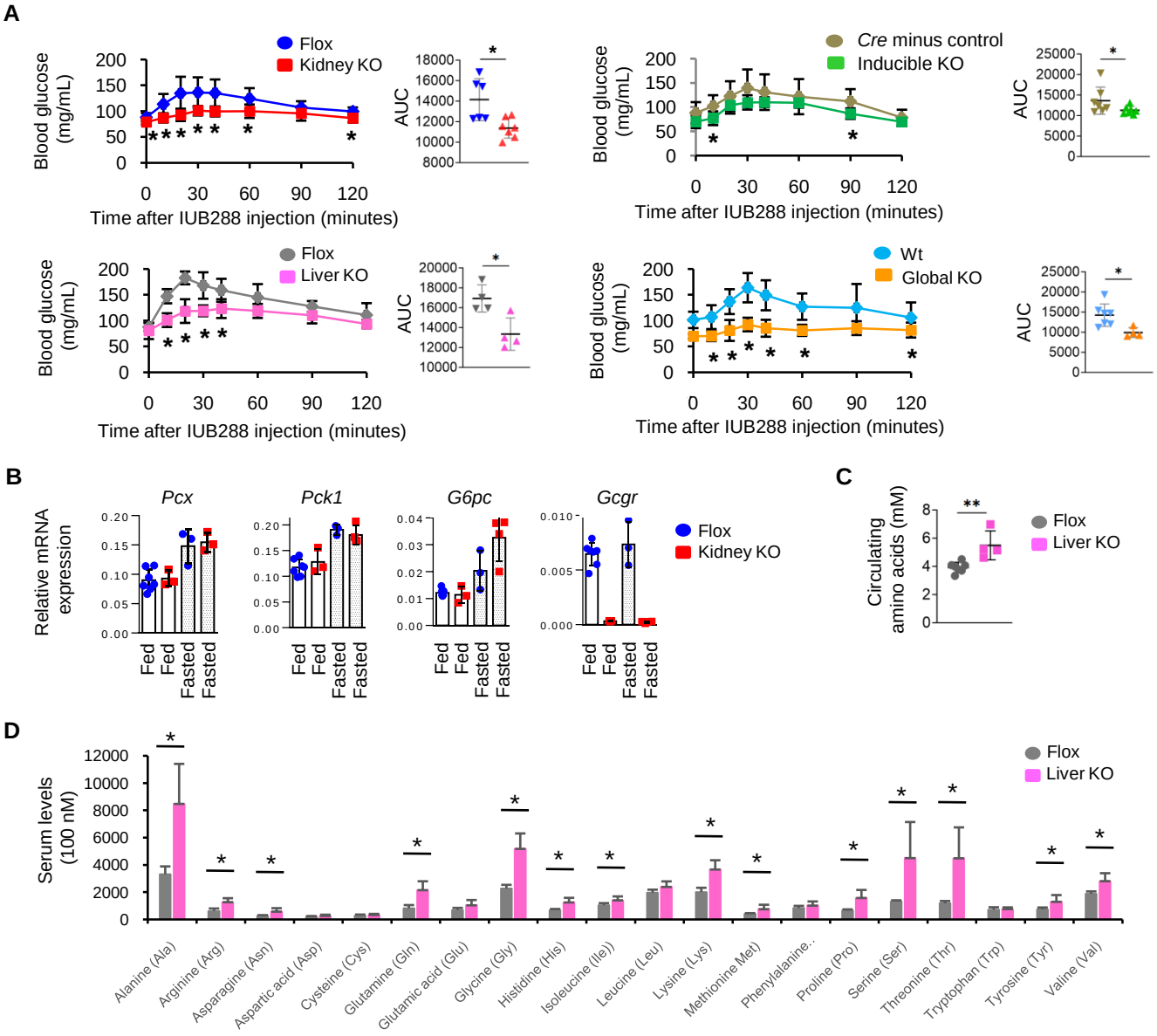
A
Flox
Kidney KO
Blood glucose (mg/mL)
Time after IUB288 injection (minutes)
AUC
Cre minus control
Inducible KO
Flox
Liver KO
Wt
Global KO
B
Pcx
Pck1
G6pc
Gcgr
Relative mRNA expression
Fed
Fasted
Flox
Kidney KO
C
Circulating amino acids (mM)
Flox
Liver KO
D
Serum levels (100 nM)
Flox
Liver KO
Alanine (Ala)
Arginine (Arg)
Asparagine (Asn)
Aspartic acid (Asp)
Cysteine (Cys)
Glutamine (Gln)
Glutamic acid (Glu)
Glycine (Gly)
Histidine (His)
Isoleucine (Ile))
Leucine (Leu)
Lysine (Lys)
Methionine Met)
Phenylalanine..
Proline (Pro)
Serine (Ser)
Threonine (Thr)
Tryptophan (Trp)
Tyrosine (Tyr)
Valine (Val)

Figure S2. Effect of *Gcgr* ablation on glucagon analogue-induced blood glucose changes and on circulating amino acid profiles in mice. Related to Figure 1.

(A) Blood glucose levels following a single dose of long-acting glucagon analogue IUB288 in various fasted *Gcgr*-deficient mice and their respective fasted controls. AUC, area under the curve. n = 4-7 mice per group; *p < 0.05. **(B)** QPCR analysis of kidney gluconeogenic and glucagon receptor (*Gcgr*) gene expression in kidney-specific *Gcgr* knockout (kidney KO) and floxed control (Flox) mice with or without 24 hr fasting. *Pcx*, pyruvate carboxylase; *Pck1*, phosphoenol pyruvate carboxykinase; *G6pc*, glucose-6-phosphatase catalytic subunit 1. n = 3-7 mice per group. **(C)** Serum levels of total amino acids, exclusive of glycine, in liver-specific *Gcgr* KO (liver KO) and floxed control (Flox) mice. n = 4-6 mice per group; **p < 0.01. **(D)** Serum amino acid profiles in liver KO and Flox mice. n = 3-6 mice per group; *p < 0.05.

Figure S3

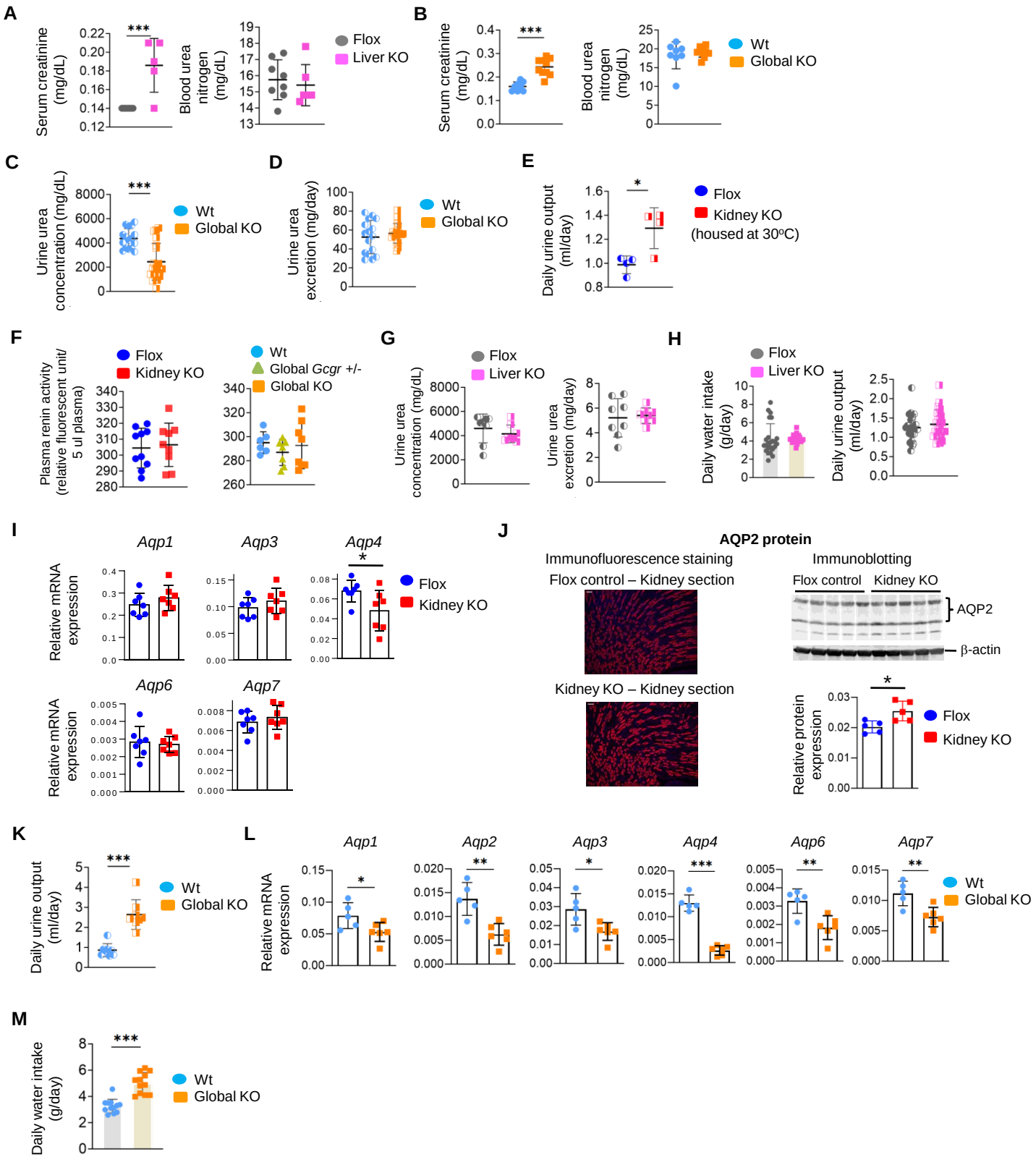
A
Serum creatinine (mg/dL)
Blood urea nitrogen (mg/dL)
Flox
Liver KO
B
Serum creatinine (mg/dL)
Blood urea nitrogen (mg/dL)
Wt
Global KO
C
Urine urea concentration (mg/dL)
Wt
Global KO
D
Urine urea excretion (mg/day)
Wt
Global KO
E
Daily urine output (ml/day)
Flox
Kidney KO
(housed at 30ºC)
F
Plasma renin activity (relative fluorescent unit/ 5 ul plasma)
Flox
Kidney KO
Wt
Global Gcgr +/-
Global KO
G
Urine urea concentration (mg/dL)
Urine urea excretion (mg/day)
Flox
Liver KO
H
Daily water intake (g/day)
Daily urine output (ml/day)
Flox
Liver KO
I
Aqp1
Aqp3
Aqp4
Aqp6
Aqp7
Relative mRNA expression
Flox
Kidney KO
J
AQP2 protein
Immunofluorescence staining
Flox control – Kidney section
Kidney KO – Kidney section
Immunoblotting
Flox control
Kidney KO
AQP2
β-actin
Relative protein expression
Flox
Kidney KO
K
Daily urine output (ml/day)
Wt
Global KO
L
Aqp1
Aqp2
Aqp3
Aqp4
Aqp6
Aqp7
Relative mRNA expression
Wt
Global KO
M
Daily water intake (g/day)
Wt
Global KO

Figure S3. Effect of *Gcgr* inactivation on systemic nitrogen and water balance in mice. Related to Figure 2.

(A) Levels of serum creatinine and blood urea nitrogen in liver-specific *Gcgr* KO (liver KO) and floxed control (Flox) mice. n = 5-8 mice per group; ***p < 0.001. **(B)** Levels of serum creatinine and blood urea nitrogen in global *Gcgr* knockout (global KO) and wild-type (wt) mice. n = 7-8 mice per group; ***p < 0.001. **(C)** Concentrations of urinary urea in global KO and wt mice. n = 10 mice per group; ***p < 0.001. **(D)** Total daily urinary urea excretion in global KO and wt mice. n = 10 mice per group. **(E)** Total daily urine volume in kidney-specific *Gcgr* KO (kidney KO) and floxed control (Flox) mice housed at 30^{o}C. n = 4 mice per group; *p < 0.05. **(F)** Plasma renin activity in kidney KO and Flox mice, as well as in global KO, Global *Gcgr* +/-, and wt mice. n = 6-10 mice per group. **(G)** Concentrations of and total daily excretion of urinary urea in liver KO and Flox mice. n = 7-8 mice per group. **(H)** Total daily water intake and urine output in liver KO and Flox mice. n = 10 mice per group. **(I)** QPCR analysis of kidney water channel (*Aqp*) gene expression in kidney KO and Flox mice. n = 6-7 mice per group; *p < 0.05. **(J)** The protein abundance of kidney AQP2 in kidney KO and Flox mice. (Left) Representative microphotographs of immunofluorescent staining (in red) with anti-AQP2 antibody of kidney sections from kidney KO and Flox mice. Nuclei were stained with DAPI (in blue). Scale bar, 100 μm. (Right) The immunoblot of AQP2 protein in kidney lysates from kidney KO and Flox mice. AQP2 band density was normalized as relative protein expression to β-actin. n = 5 mice per group; *p < 0.05. **(K)** Total daily urine output in global KO and wt mice. n = 8 mice per group; ***p < 0.001. **(L)** QPCR analysis of kidney water channel (*Aqp*) gene expression in global KO and wt mice. n = 5-6 mice per group; *p < 0.05, **p < 0.01, ***p < 0.001. **(M)** Total daily water intake in global KO and wt mice. n = 8 mice per group; ***p < 0.001.

Figure S4

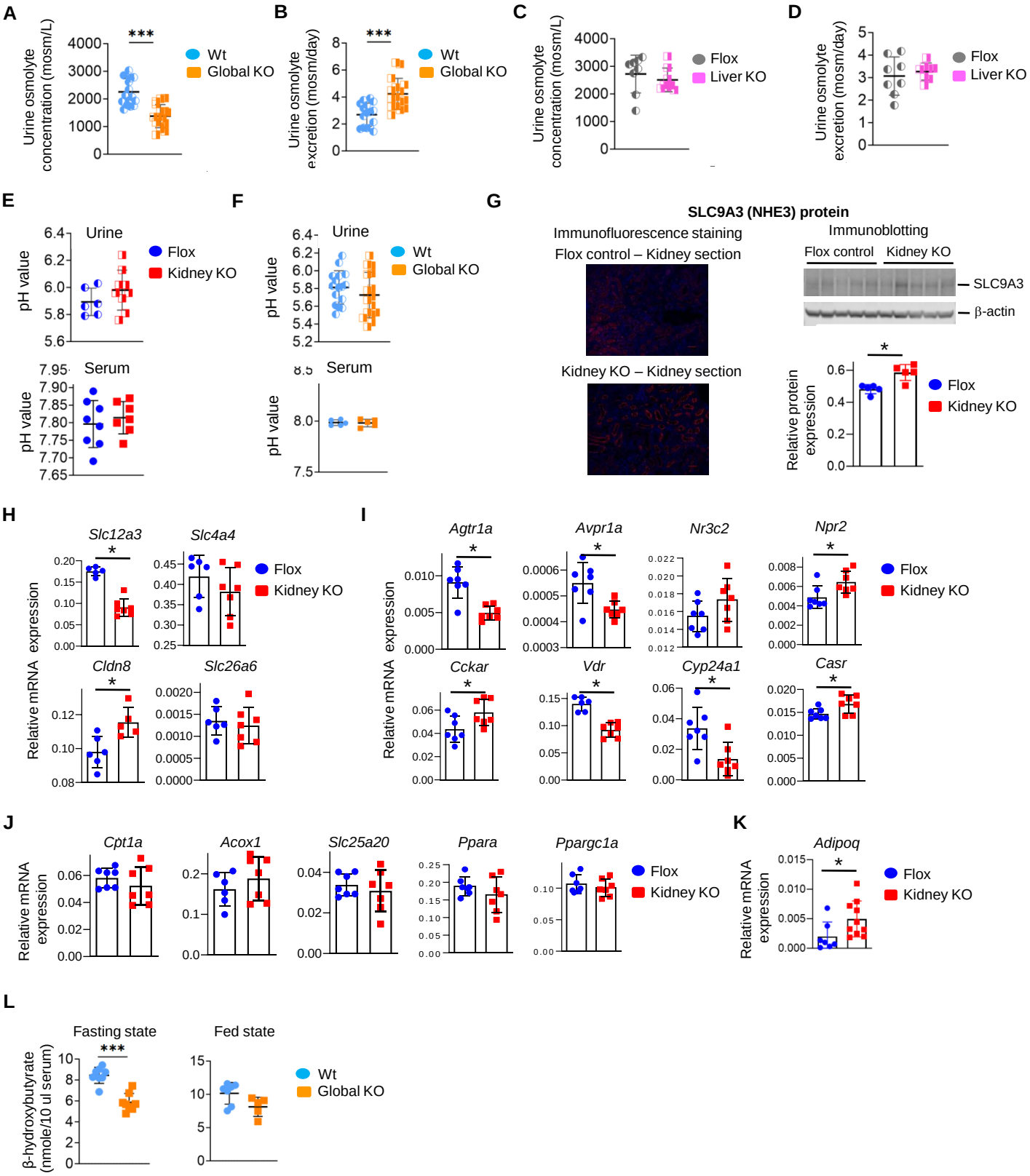
A
Urine osmolyte concentration (mosm/L)
***
Wt
Global KO
B
Urine osmolyte excretion (mosm/day)
***
Wt
Global KO
C
Urine osmolyte concentration (mosm/L)
Flox
Liver KO
D
Urine osmolyte excretion (mosm/day)
Flox
Liver KO
E
Urine
pH value
Flox
Kidney KO
Serum
pH value
F
Urine
pH value
Wt
Global KO
Serum
pH value
G
SLC9A3 (NHE3) protein
Immunofluorescence staining
Flox control – Kidney section
Kidney KO – Kidney section
Immunoblotting
Flox control
Kidney KO
SLC9A3
β-actin
Relative protein expression
Flox
Kidney KO
H
Slc12a3
Slc4a4
Cldn8
Slc26a6
Relative mRNA expression
Flox
Kidney KO
I
Agtr1a
Avpr1a
Nr3c2
Npr2
Cckar
Vdr
Cyp24a1
Casr
Relative mRNA expression
Flox
Kidney KO
J
Cpt1a
Acox1
Slc25a20
Ppara
Ppargc1a
Relative mRNA expression
Flox
Kidney KO
K
Adipoq
Relative mRNA expression
Flox
Kidney KO
L
Fasting state
Fed state
β-hydroxybutyrate (nmole/10 ul serum)
***
Wt
Global KO

Figure S4. Effect of *Gcgr* inactivation on systemic electrolyte balance, on kidney lipid metabolism-related gene expression, and on circulating ketone levels in mice. Related to Figure 3 and Table 1. **(A)** Concentrations of urinary osmolytes in global *Gcgr* knockout (Global KO) and wild-type (wt) mice. n = 12 mice per group; ***p < 0.001. **(B)** Total daily urinary osmolyte excretion in global KO and wt mice. n = 12 mice per group; ***p < 0.001. **(C)** Concentrations of urinary osmolytes in liver-specific *Gcgr* KO (liver KO) and floxed control (Flox) mice. n = 7-8 mice per group. **(D)** Total daily urinary osmolyte excretion in liver KO and Flox mice. n = 7-8 mice per group. **(E)** Urine and serum pH in kidney-specific *Gcgr* KO (kidney KO) and Flox mice. n = 6-8 mice per group. **(F)** Urine and serum pH in global KO and wt mice. n = 5-8 mice per group. **(G)** The protein abundance of kidney SLC9A3 (NHE3) in kidney KO and Flox mice. (Left) Representative microphotographs of immunofluorescent staining (in red) with anti-SLC9A3 antibody of kidney sections from kidney KO and Flox mice. Nuclei were stained with DAPI (in blue). Scale bar, 50 μm. (Right) The immunoblot of SLC9A3 protein in kidney lysates from kidney KO and Flox mice. SLC9A3 band density was normalized as relative protein expression to β-actin. n = 5 mice per group; *p < 0.05. **(H)** QPCR analysis of kidney transporter gene expression in kidney KO and Flox mice. *Slc12a3*, sodium-chloride cotransporter Ncc; *Slc4a4*, sodium-bicarbonate cotransporter Nbc1; *Cldn8*, claudin-8; *Slc26a6*, chloride-formate exchanger Cfex. n = 5-7 mice per group; *p < 0.05. **(I)** QPCR analysis of kidney signal transducer gene expression in kidney KO and Flox mice. *Agtr1a*, angiotensin II receptor; *Avpr1a*, arginine vasopressin receptor 1A; *Nr3c2*, mineralocorticoid receptor; *Npr2*, natriuretic peptide receptor 2; *Cckar*, cholecystokinin A receptor; *Vdr*, vitamin D receptor; *Cyp24a1*, 1,25-dihydroxyvitamin D(3) 24-hydroxylase; *Casr*, calcium-sensing receptor. n = 5-7 mice per group; *p < 0.05. **(J)** QPCR analysis of kidney fatty acid oxidation, transporter, and regulator gene expression in kidney-specific *Gcgr* KO (kidney KO) and floxed control (Flox) mice. Housekeeping gene 36b4 was used for normalization of gene transcript levels. *Cpt1a*, carnitine O-palmitoyltransferase 1a; *Acox1*, acyl-coenzyme A oxidase 1; *Slc25a20*, carnitine/acylcarnitine carrier protein; *Ppara*, peroxisome proliferator-activated receptor alpha; *Ppargc1a*, peroxisome proliferator-activated receptor gamma coactivator 1-alpha. n = 6-7 mice per group. **(K)** QPCR analysis of renal adiponectin (*Adipoq*) gene expression in kidney KO and Flox mice. n = 7-10 mice per group; *p < 0.05. **(L)** Levels of circulating ketone β-hydroxybutyrate in global *Gcgr* knockout (global KO) and wild-type (wt) mice in the fasting and fed states. n = 5-8 mice per group; ***p < 0.001.

Figure S5

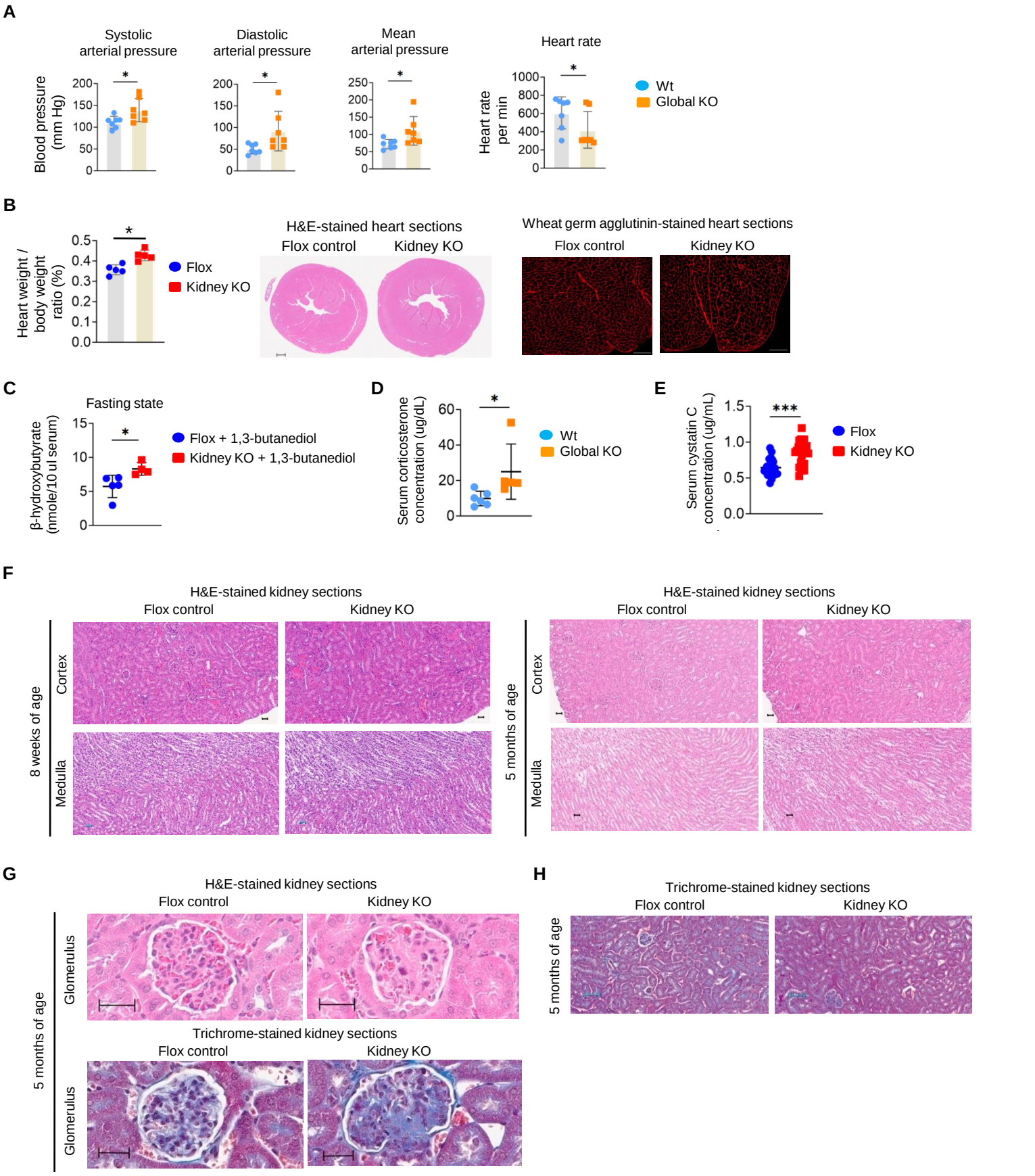
A
Systolic arterial pressure
Diastolic arterial pressure
Mean arterial pressure
Heart rate
Blood pressure (mm Hg)
Heart rate per min
Wt
Global KO
B
Heart weight / body weight ratio (%)
Flox
Kidney KO
H&E-stained heart sections
Flox control
Kidney KO
Wheat germ agglutinin-stained heart sections
Flox control
Kidney KO
C
Fasting state
β-hydroxybutyrate (nmole/10 ul serum)
Flox + 1,3-butanediol
Kidney KO + 1,3-butanediol
D
Serum corticosterone concentration (ug/dL)
Wt
Global KO
E
Serum cystatin C concentration (ug/mL)
Flox
Kidney KO
F
H&E-stained kidney sections
Flox control
Kidney KO
8 weeks of age
5 months of age
Cortex
Medulla
G
H&E-stained kidney sections
Flox control
Kidney KO
5 months of age
Glomerulus
Trichrome-stained kidney sections
Flox control
Kidney KO
Glomerulus
H
Trichrome-stained kidney sections
Flox control
Kidney KO
5 months of age

Figure S5. Effect of *Gcgr* inactivation on blood pressure, on various serum parameters and on heart and kidney tissue structure in mice. Related to Figure 4.

(A) Arterial blood pressure and resting heart rate in global *Gcgr* knockout (global KO) and wild-type (wt) mice. n = 6-7 mice per group; *p < 0.05. **(B)** Heart-to-body weight ratios, and hematoxylin and eosin (H&E)- and wheat germ agglutinin-stained heart sections in kidney-specific *Gcgr* KO (kidney KO) and floxed control (Flox) mice. Scale bar, 100 μm. n = 5 mice per group; *p < 0.05. **(C)** Levels of circulating ketone β-hydroxybutyrate in kidney KO and Flox mice in the fasting states, following 4-week treatment of 1,3-butanediol. n = 5 mice per group; *p < 0.05. **(D)** Serum levels of corticosterone in global KO and wt mice. n = 5-6 mice per group; *p < 0.05. **(E)** Serum concentrations of cystatin C in kidney KO and Flox mice. n = 16 mice per group; ***p < 0.001. **(F)** Representative microphotographs of cortical and medullary regions in H&E-stained kidney sections from kidney KO and Flox mice aged 8 weeks and 5 months. Scale bar, 30 μm. **(G)** Representative microphotographs of glomerular regions in H&E- or trichrome-stained kidney sections from 5-month-old kidney KO and Flox mice. Scale bar, 30 μm. **(H)** Representative microphotographs of trichrome-stained kidney sections from 5-month-old kidney KO and Flox mice. Scale bar, 60 μm.

Figure S6

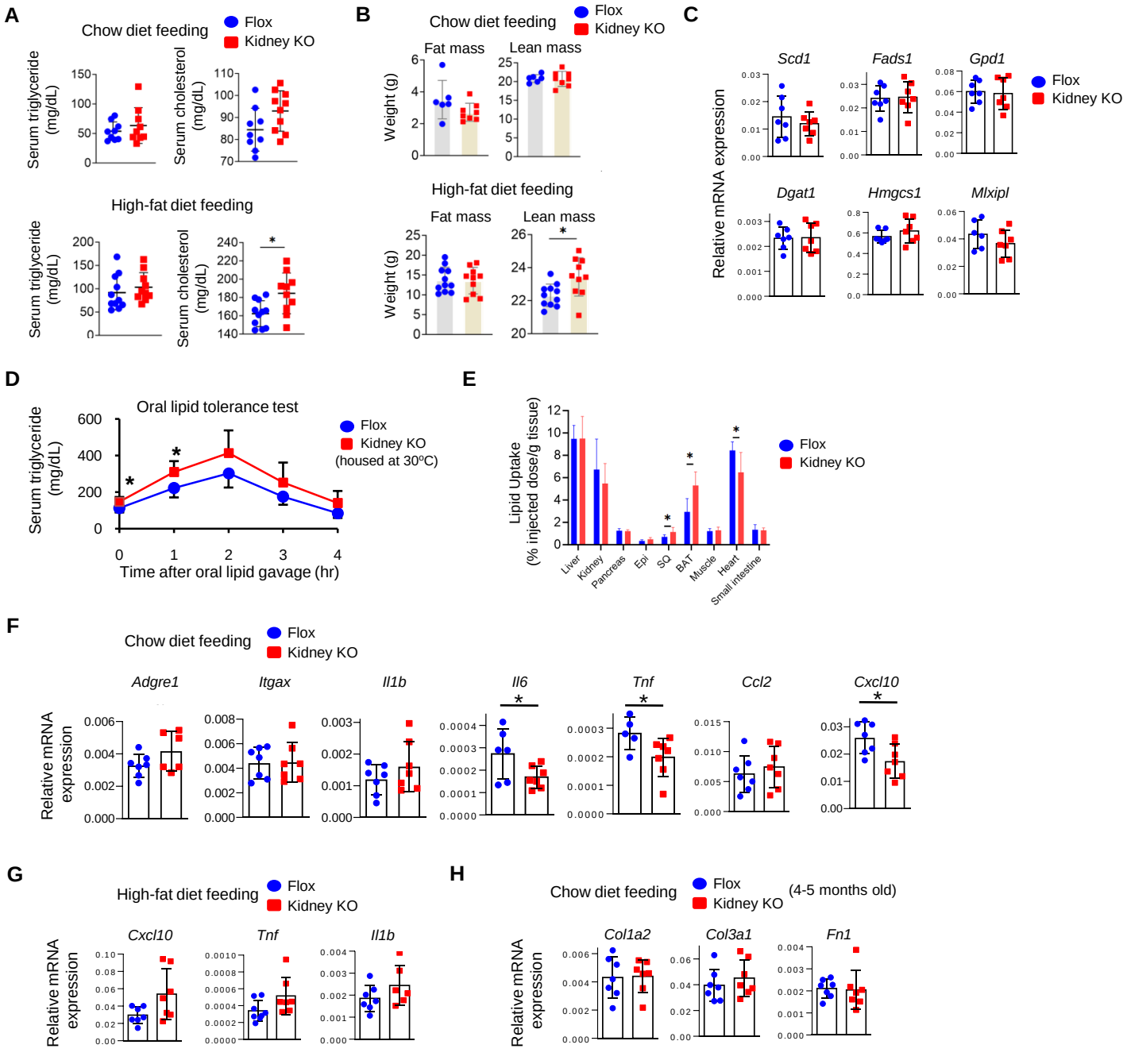
A
Chow diet feeding
Flox
Kidney KO
Serum triglyceride (mg/dL)
Serum cholesterol (mg/dL)
High-fat diet feeding
B
Chow diet feeding
Fat mass
Lean mass
Weight (g)
High-fat diet feeding
C
Scd1
Fads1
Gpd1
Dgat1
Hmgcs1
Mlxipl
Relative mRNA expression
D
Oral lipid tolerance test
Serum triglyceride (mg/dL)
Kidney KO (housed at 30ºC)
Time after oral lipid gavage (hr)
E
Lipid Uptake (% injected dose/g tissue)
Liver
Kidney
Pancreas
Epi
SQ
BAT
Muscle
Heart
Small intestine
F
Chow diet feeding
Adgre1
Itgax
Il1b
Il6
Tnf
Ccl2
Cxcl10
Relative mRNA expression
G
High-fat diet feeding
Cxcl10
Tnf
Il1b
Relative mRNA expression
H
Chow diet feeding
(4-5 months old)
Col1a2
Col3a1
Fn1
Relative mRNA expression

Figure S6. Lipid-related metabolic parameters and gene expression in kidney-specific *Gcgr* KO and control mice. Related to Figures 5 and 6.

(A) Serum levels of lipids in chow diet- or high fat diet-fed kidney-specific *Gcgr* KO (kidney KO) and floxed control (Flox) mice. n = 8-11 mice per group; *p < 0.05. **(B)** Fat and lean body mass of chow diet- or high fat diet-fed kidney KO and Flox mice. n = 6-11 mice per group; *p < 0.05. **(C)** QPCR analysis of renal lipid metabolism-related gene expression in kidney KO and Flox mice. *Scd1*, stearoyl-Coenzyme A desaturase 1; *Fads1*, fatty acid desaturase 1; *Gpd1*, glycerol-3-phosphate dehydrogenase; *Dgat1*, diacylglycerol O-acyltransferase 1; *Hmgcs1*, hydroxymethylglutaryl-CoA synthase; *Mlxipl*, carbohydrate-responsive element-binding protein. n = 6-7 mice per group. **(D)** Serum triglyceride levels during oral lipid tolerance tests in kidney KO and Flox mice housed at 30^{o}C. n = 7 mice per group; *p < 0.05. **(E)** Tissue accumulation (uptake) of radioactive ^{3}H in kidney KO and Flox mice after a lipid load with ^{3}H-labeled triolein as a tracer. Epi, epididymal adipose tissue; SQ, subcutaneous adipose tissue; BAT, brown adipose tissue. n = 7-8 mice per group; *p < 0.05. **(F)** QPCR analysis of kidney immune- and inflammatory-related gene expression in chow diet-fed kidney KO and Flox mice. *Adgre1*, cell surface glycoprotein F4/80; *Itgax*, integrin alpha-X; *Il1b*, interleukin-1 beta; *Il6*, interleukin-6; *Tnf*, tumor necrosis factor; *Ccl2*, C-C motif chemokine 2; *Cxcl10*, C-X-C motif chemokine 10. n = 5-7 mice per group; *p < 0.05. **(G)** QPCR analysis of kidney immune- and inflammatory-related gene expression in high fat diet-fed kidney KO and Flox mice. *Cxcl10*, C-X-C motif chemokine 10; *Tnf*, tumor necrosis factor; *Il1b*, interleukin-1 beta. n = 5-7 mice per group. **(H)** QPCR analysis of renal profibrotic gene expression in 4- to 5-month-old kidney-specific *Gcgr* KO (kidney KO) and floxed control (Flox) mice fed a chow diet. *Col1a2*, collagen type I alpha 2; *Col3a1*, collagen type III alpha 1; *Fn1*, fibronectin 1. n = 5-7 mice per group.

Supplemental Tables

Table S1. Serum and urine electrolyte parameters in global *Gcgr* knockout and wild-type control mice. Related to Figure 3 and Table 1.

	Wild-type control	Global knockout
	Electrolyte concentration[a]	
Serum sodium (mM)	149.9±3.2	146.7±3.3
Serum potassium (mM)	6.1±0.6	6.9±0.7[b]
Serum calcium (mg/dL)	10.6±0.3	10.9±0.2[b]
Serum chloride (mM)	111.9±2.8	110.3±3.0
Serum phosphate (mg/dL)	9.8±0.7	9.6±0.8
Urine sodium (mM)	132.1±16.0	93.2±24.7[b]
Urine potassium (mM)	251.5±51.6	171.2±67.6[b]
Urine calcium (mg/dL)	5.3±1.3	6.6±2.5
Urine chloride (mM)	236.4±47.0	184.7±71.3[b]
Urine phosphate (mg/dL)	219.3±75.1	172.6±82.4
	Daily electrolyte excretion[a]	
Urine sodium (mmol/day)	0.17±0.06	0.25±0.11[b]
Urine potassium (mmol/day)	0.30±0.10	0.40±0.11[b]
Urine calcium (mg/day)	0.07±0.03	0.18±0.10[b]
Urine chloride (mmol/day)	0.30±0.10	0.43±0.11[b]
Urine phosphate (mg/day)	2.54±0.87	4.06±1.52[b]

[a] Values are expressed as mean ± SD; n = 8 mice per group.
[b] $p < 0.05$ vs. wild-type control.

Table S2. QPCR primer sequences. Related to STAR Methods.

Organism	Target	Forward Sequence (5' - 3')	Reverse Sequence (5' - 3')
Mus musculus	36B4	CGACCTGGAAGTCCAACTAC	ATCTGCTGCATCTGCTTG
Mus musculus	*Gcgr*	TGCTGTTTGTCATCCCCTGG	GCAGGATCCACCAGAATCCC
Mus musculus	*Adcy6*	TGAGTCTTCTAGCCAGCTCTG	CAGCACCAAGTAGGTGAACCC
Mus musculus	*Creb1*	AGCAGCTCATGCAACATCATC	AGTCCTTACAGGAAGACTGAACT
Mus musculus	*Itpr2*	CCTCGCCTACCACATCACC	TCACCACTCTCACTATGTCGT
Mus musculus	*Prkar2b*	CCAGTAAGGGTGTCAACTTCG	GGACTCTGCATCGTCTTCCTC
Mus musculus	*Insr*	ATGGGCTTCGGGAGAGGAT	GGATGTCCATACCAGGGCAC
Mus musculus	*Pcx*	CTGAAGTTCCAAACAGTTCGAGG	CGCACGAAACACTCGGATG
Mus musculus	*Pck1*	CTGCATAACGGTCTGGACTTC	CAGCAACTGCCCGTACTCC
Mus musculus	*Fbp1*	CACCGCGATCAAAGCCATCT	AGGTAGCGTAGGACGACTTCA
Mus musculus	*G6pc*	CGACTCGCTATCTCCAAGTGA	GTTGAACCAGTCTCCGACCA
Mus musculus	*Slc2a2*	TCAGAAGACAAGATCACCGGA	GCTGGTGTGACTGTAAGTGGG
Mus musculus	*Slc2a1*	CAGTTCGGCTATAACACTGGTG	GCCCCCGACAGAGAAGATG
Mus musculus	*Slc5a2*	ATGGAGCAACACGTAGAGGC	ATGACCAGCAGGAAATAGGCA
Mus musculus	*Slc3a2*	TGATGAATGCACCCTTGTACTTG	GCTCCCCAGTGAAAGTGGA
Mus musculus	*Slc6a19*	CAGGTGCTCAGGTCTTCTACT	CGATCACAGAATCCATCTCACAA
Mus musculus	*Slc7a7*	CACCACCAAGTATGAAGTGGC	CCCTTAGGGGAGACAAAGATGC
Mus musculus	*Slc7a8*	TGTGACTGAGGAACTTGTGGA	GTGGACAGGGCAACAGAAATG
Mus musculus	*Slc7a9*	GAGGAGACGGAGAGAGGATGA	CCCCACGGATTCTGTGTTG
Mus musculus	*Slc16a10*	GAGGTGGAGCTGACGAGGT	CATGGACACGAAGAGCACCC
Mus musculus	*Slc43a2*	TGCACCGCTGTGTTGGAAA	CCGTGCTGTTAGTGACATTCTC
Mus musculus	*Agxt2*	TCACCTGAGAAATACCAGTCCC	CAAAGAGCCACTCCATGTGTC
Mus musculus	*Asl*	CTATGACCGGCATCTGTGGAA	AGCAACCTTGTCCAACCCTTG
Mus musculus	*Ass1*	ACACCTCCTGCATCCTCGT	GCTCACATCCTCAATGAACACCT
Mus musculus	*Gcat*	GGACAGCGAACTGGAAGGG	AGTTATTGGCACAGAAGTTGAGG
Mus musculus	*Got2*	GGACCTCCAGATCCCATCCT	GGTTTTCCGTTATCATCCCGGTA
Mus musculus	*Oat*	GGAGTCCACACCTCAGTCG	CCACATCCCACATATAAATGCCT
Mus musculus	*Pah*	TTGTCCTGGAGAACGGAGTC	CTGGATTCAATGTGTGTCAGGTT
Mus musculus	*Prodh2*	GTGGGGCCTTCCATGTCAAG	CCTGAAACGCTAGTCCATGAGT
Mus musculus	*Uta1*	GACAGTGAGACGCAGTGAAG	ACGGTCTCAGAGCTCTCTTC
Mus musculus	*Uta2*	TTTCTCCAGTCCTATCTGAG	ACGGTCTCAGAGCTCTCTTC
Mus musculus	*Uta3*	ACGGTCTCAGAGCTCTCTTC	AGAGTGGAGGCCACACGGAT
Mus musculus	*Utab*	TCTTCTCAAACAAGGGCGAC	TTGCTGAGCACGGAGCTCAA
Mus musculus	*Aqp11*	CTATGCAGGAGGGAGCCTCA	AAAGTGCAGAGAAAGTGCCAG
Mus musculus	*Avpr2*	TGACCGAGACCCGCTGTTA	CGACCCCGTCGTATTAGGG
Mus musculus	*Aplnr*	GGTTACAACTACTATGGGGCTGA	AGCTGAGCGTCTCTTTTCGC
Mus musculus	*Slc9a3*	TGAAAAGCAGGACAAGGAAATCT	TTGGCCGCCTTCTTATTCTGG
Mus musculus	*Slc12a1*	TCATTGGCCTGAGCGTAGTTG	TTTGTGCAAATAGCCGACATAGA
Mus musculus	*Scnn1a*	CCTTCTCCTTGGATAGCCTGG	CAGACGGCCATCTTGAGTAGC
Mus musculus	*Scnn1b*	GGCCCAGGCTACACCTACA	AGCAGCGTAAGCAGGAACC
Mus musculus	*Scnn1g*	GCACCGACCATTAAGGACCTG	GCGTGAACGCAATCCACAAC
Mus musculus	*Sgk1*	CTGCTCGAAGCACCCTTACC	TCCTGAGGATGGGACATTTTCA
Mus musculus	*Atp1a1*	GGGGTTGGACGAGACAAGTAT	CGGCTCAAATCTGTTCCGTAT
Mus musculus	*Atp1b1*	GCTGCTAACCATCAGTGAACT	GGGGTCATTAGGACGGAAGGA
Mus musculus	*Fxyd2*	TCTGTCAGCGAACAGTGGTG	TTCATAGTCGTACTCGAAGGGAT
Mus musculus	*Sik1*	TCATGTCGGAGTTCAGTGCG	ACCTGCGTTTTGGTGACTCG
Mus musculus	*Slc12a4*	ATGCCTCACTTCACCGTGG	GTTACCCTGTCCGTCCGAG
Mus musculus	*Clcnka*	GCATCAGAGGGGGCCTAGA	CCGATAGCAAAGTTCATGGCA
Mus musculus	*Clcnkb*	TGGGGCCTTTATGTTCCACC	GAAAGTCCGCTGGCTGTAGT
Mus musculus	*Slc26a4*	AAGAGAGCCTTTGGTGTGGTA	CAGGGCATAAGCCATCCCTTG
Mus musculus	*Slc8a1*	CTTCCCTGTTTGTGCTCCTGT	AGAAGCCCTTTATGTGGCAGTA
Mus musculus	*TrpV5*	ATGGGGGCTAAAACTCCTTGG	CCTCTTTGCCGGAAGTCACA
Mus musculus	*Atp2b1*	AGATGGAGCTATTGAGAATCGCA	CCCTGTAACACGGATTTTTCCTT
Mus musculus	*Acadm*	AGGGTTTAGTTTTGAGTTGACGG	CCCCGCTTTTGTCATATTCCG
Mus musculus	*Slc27a2*	GCTGACATCGTGGGACTGGT	TTCGACCCTCATGACCTGGC
Mus musculus	*Cd36*	ATGGGCTGTGATCGGAACTG	GTCTTCCCAATAAGCATGTCTCC

Mus musculus	*Cpt2*	CAGCACAGCATCGTACCCA	TCCCAATGCCGTTCTCAAAAT
Mus musculus	*Acads*	TGGCGACGGTTACACACTG	GTAGGCCAGGTAATCCAAGCC
Mus musculus	*Acadl*	TCTTTTCCTCGGAGCATGACA	GACCTCTCTACTCACTTCTCCAG
Mus musculus	*Hk1*	CACCGGCAGATTGAGGAAAC	CTCAGCCCCATTTCCATCTCT
Mus musculus	*Pfkl*	CTGCTGGTGATTGGTGGCTTTG	TTGCTGATGGTGGCTGGGATG
Mus musculus	*Pfkp*	GGGCATAACCAATCTGTGCG	GAAGTCCGCTCCACTCCTTT
Mus musculus	*Pkm*	ATGTGGCTCGGCTGAATTTCTC	GTGATCTTCAGAGTGGCTCCC
Mus musculus	*Mpc1*	ATGAGTACGCACTTCTGGGG	CGCCCACTGATAATCTCTGGA
Mus musculus	*Slc16a1*	TGTTAGTCGGAGCCTTCATTTC	CACTGGTCGTTGCACTGAATA
Mus musculus	*Slc16a7*	GCTGGGTCGTAGTCTGTGC	ATCCAAGCGATCTGACTGGAG
Mus musculus	*Slc16a3*	TCACGGGTTTCTCCTACGC	GCCAAAGCGGTTCACACAC
Mus musculus	*Bdh1*	ACAAGACACACGCTGTTGTTT	CTCTTCAAGCTGTCCAGTTCC
Mus musculus	*Oxct1*	CATAAGGGGTGTGTCTGCTACT	GCAAGGTTGCACCATTAGGAAT
Mus musculus	*Sod1*	AACCAGTTGTGTTGTCAGGAC	CCACCATGTTTCTTAGAGTGAGG
Mus musculus	*Hmox1*	AAGCCGAGAATGCTGAGTTCA	GCCGTGTAGATATGGTACAAGGA
Mus musculus	*Prdx5*	GGCTGTTCTAAGACCCACCTG	GGAGCCGAACCTTGCCTTC
Mus musculus	*Txn1*	CATGCCGACCTTCCAGTTTTA	TTTCCTTGTTAGCACCGGAGA
Mus musculus	*Ucp2*	ATGGTTGGTTTCAAGGCCACA	CGGTATCCAGAGGGAAAGTGAT
Mus musculus	*Pm20d1*	CTTCTCTTTTTCGCTACGGTCT	CACCTTTCAGCGCCTCTTTTAT
Mus musculus	*Atf4*	ATGGCGCTCTTCACGAAATC	ACTGGTCGAAGGGGTCATCAA
Mus musculus	*Nrf2*	TCTTGGAGTAAGTCGAGAAGTGT	GTTGAAACTGAGCGAAAAAGGC
Mus musculus	*Hsd11b1*	CAGAAATGCTCCAGGGAAAGAA	GCAGTCAATACCACATGGGC
Mus musculus	*Hsd11b2*	GGTTGTGACACTGGTTTTGGC	AGAACACGGCTGATGTCCTCT
Mus musculus	*Kim1*	ACATATCGTGGAATCACAACGAC	ACAAGCAGAAGATGGGCATTG
Mus musculus	*Lcn2*	TGGCCCTGAGTGTCATGTG	CTCTTGTAGCTCATAGATGGTGC
Mus musculus	*Sostdc1*	CCTGCCATTCATCTCTCTCTCA	CCGGGACAGGTTTAACCACA
Mus musculus	*Wt1*	GAGAGCCAGCCTACCATCC	GGGTCCTCGTGTTTGAAGGAA
Mus musculus	*Nphs1*	ATGGGAGCTAAGGAAGCCACA	GATGGAGAGGATTACGCTGGG
Mus musculus	*Podxl*	GCCACCAAAGTGCCACAAC	CGGCATAGATGGAGATTGGGTT
Mus musculus	*Ym1*	GGGCATACCTTTATCCTGAG	CCACTGAAGTCATCCATGTC
Mus musculus	*Arg1*	ATGGAAGAGACCTTCAGCTAC	GCTGTCTTCCCAAGAGTTGGG
Mus musculus	*Mrc1*	TGTGGTGAGCTGAAAGGTGA	CAGGTGTGGGCGCAGGTAGT
Mus musculus	*Nos2*	AGCTGAACTTGAGCGAGGAG	TGCCCCATAGGAAAAGACTG
Mus musculus	*Il4r*	AGGCCCCAGTACAGAATGTG	TCTCAGGTGACATGCTCAGG
Mus musculus	*Fasn*	GGAGGTGGTGATAGCCGGTAT	TGGGTAATCCATAGAGCCCAG
Mus musculus	*Acaca*	ATGGGCGGAATGGTCTCTTTC	TGGGGACCTTGTCTTCATCAT
Mus musculus	*Acly*	ACCCTTTCACTGGGGATCACA	GACAGGGATCAGGATTTCCTTG
Mus musculus	*Acsm2*	TGGGGGAATGAGATTTCCTGC	CTTCACTCAGTTCTCGGAAGC
Mus musculus	*Hmgcr*	AGCTTGCCCGAATTGTATGTG	TCTGTTGTGAACCATGTGACTTC
Mus musculus	*Srebp1a*	TGACCCGGCTATTCCGTGA	CTGGGCTGAGCAATACAGTTC
Mus musculus	*Srebp1c*	GGAGCCATGGATTGCACATT	GCTTCCAGAGAGGAGGCCAG
Mus musculus	*Icam1*	GTGATGCTCAGGTATCCATCCA	CACAGTTCTCAAAGCACAGCG
Mus musculus	*Cdh1*	CAGGTCTCCTCATGGCTTTGC	CTTCCGAAAAGAAGGCTGTCC
Mus musculus	*Cd68*	CAGCTGCCTGACAAGGGACA	GGAGGACCAGGCCAATGATG
Mus musculus	*Cxcl15*	CAAGGCTGGTCCATGCTCC	TGCTATCACTTCCTTTCTGTTGC
Mus musculus	*Nlrp3*	ATTACCCGCCCGAGAAAGG	TCGCAGCAAAGATCCACACAG
Mus musculus	*Il18*	GACTCTTGCGTCAACTTCAAGG	CAGGCTGTCTTTTGTCAACGA
Mus musculus	*Cd11b*	AGATCGTCTTGGCAGATGCT	GACTCAGTGAGCCCCATCAT
Mus musculus	*Il6*	CCGGAGAGGAGACTTCACAG	CAGAATTGCCATTGCACAAC
Mus musculus	*Ccl2*	TTAAAAACCTGGATCGGAACCAA	GCATTAGCTTCAGATTTACGGGT
Mus musculus	*Cxcl2*	ACTAGCTACATCCCACCCACAC	GCACACTCCTTCCATGAAAGCC
Mus musculus	*Adgre1*	AACTCTGTCCTCCTTGCCTGG	CAGCAACCTCGTGTCCTTGAG
Mus musculus	*Col1a1*	GCTCCTCTTAGGGGCCACT	CCACGTCTCACCATTGGGG
Mus musculus	*Acta2*	GTCCCAGACATCAGGGAGTAA	TCGGATACTTCAGCGTCAGGA
Mus musculus	*Timp1*	GCAACTCGGACCTGGTCATAA	CGGCCCGTGATGAGAAACT
Mus musculus	*Mmp2*	CAAGTTCCCCGGCGATGTC	TTCTGGTCAAGGTCACCTGTC
Mus musculus	*Dcn*	TCTTGGGCTGGACCATTTGAA	CATCGGTAGGGGCACATAGA
Mus musculus	*Tgfb1*	CTCCCGTGGCTTCTAGTGC	GCCTTAGTTTGGACAGGATCTG
Mus musculus	*Ctgf*	GGGCCTCTTCTGCGATTTC	ATCCAGGCAAGTGCATTGGTA

Mus musculus	*Col1a2*	GTAACTTCGTGCCTAGCAACA	CCTTTGTCAGAATACTGAGCAGC
Mus musculus	*Col3a1*	CTGTAACATGGAAACTGGGGAAA	CCATAGCTGAACTGAAAACCACC
Mus musculus	*Fn1*	ATGTGGACCCCTCCTGATAGT	GCCCAGTGATTTCAGCAAAGG
Mus musculus	*Col4a1*	CTGGCACAAAAGGGACGAG	ACGTGGCCGAGAATTTCACC
Mus musculus	*Tgfbr1*	TCTGCATTGCACTTATGCTGA	AAAGGGCGATCTAGTGATGGA
Mus musculus	*Aqp1*	AGGCTTCAATTACCCACTGGA	GTGAGCACCGCTGATGTGA
Mus musculus	*Aqp2*	ATGTGGGAACTCCGGTCCATA	ACGGCAATCTGGAGCACAG
Mus musculus	*Aqp3*	GCTTTTGGCTTCGCTGTCAC	TAGATGGGCAGCTTGATCCAG
Mus musculus	*Aqp4*	CTTTCTGGAAGGCAGTCTCAG	CCACACCGAGCAAAACAAAGAT
Mus musculus	*Aqp6*	GTGTAGCAGGGCTTACCTTCT	GATGGCGATCTGGAGCACA
Mus musculus	*Aqp7*	AATATGGTGCGAGAGTTTCTGG	ACCCAAGTTGACACCGAGATA
Mus musculus	*Slc12a3*	ACACGGCAGCACCTTATACAT	GAGGAATGAATGCAGGTCAGC
Mus musculus	*Slc4a4*	GATGCCACCGACAACATGC	TCAAGATGGTAAGCGGTTGAC
Mus musculus	*Cldn8*	GCAACCTACGCTCTTCAAATGG	TTCCCAGCGGTTCTCAAACAC
Mus musculus	*Slc26a6*	GTGGCGAACTTGGTTCCGAT	AGCCATTCACGCACAGGATAC
Mus musculus	*Agtr1a*	AACAGCTTGGTGGTGATCGTC	CATAGCGGTATAGACAGCCCA
Mus musculus	*Avpr1a*	GCTGGCGGTGATTTTCGTG	GCAAACACCTGCAAGTGCT
Mus musculus	*Nr3c2*	GAAAGGCGCTGGAGTCAAGT	TGTTCGGAGTAGCACCGGAA
Mus musculus	*Npr2*	TGCTGCCAGAACACAACCTG	TTCGGAGCTGACAAACCGC
Mus musculus	*Cckar*	CTTTTCTGCCTGGATCAACCT	ACCGTGATAACCAGCGTGTTC
Mus musculus	*Vdr*	ACCCTGGTGACTTTGACCG	GGCAATCTCCATTGAAGGGG
Mus musculus	*Cyp24a1*	CTGCCCCATTGACAAAAGGC	CTCACCGTCGGTCATCAGC
Mus musculus	*Casr*	CTGACCAGCGAGCCCAAAA	GCTGCTACTCCAAAATGGATAGG
Mus musculus	*Cpt1a*	CTCCGCCTGAGCCATGAAG	CACCAGTGATGATGCCATTCT
Mus musculus	*Acox1*	TAACTTCCTCACTCGAAGCCA	AGTTCCATGACCCATCTCTGTC
Mus musculus	*Slc25a20*	GACGAGCCGAAACCCATCAG	AGTCGGACCTTGACCGTGT
Mus musculus	*Ppara*	AGAGCCCCATCTGTCCTCTC	ACTGGTAGTCTGCAAAACCAAA
Mus musculus	*Ppargc1a*	TCACACCAAACCCACAGAAA	CTTGGGGTCATTTGGTGACT
Mus musculus	*Adipoq*	TGTTCCTCTTAATCCTGCCCA	CCAACCTGCACAAGTTCCCTT
Mus musculus	*Scd1*	GGCCTGTACGGGATCATACTG	GGTCATGTAGTAGAAAATCCCGAAGA
Mus musculus	*Fads1*	AGCACATGCCATACAACCATC	TTTCCGCTGAACCACAAAATAGA
Mus musculus	*Gpd1*	ATGGCTGGCAAGAAAGTCTG	CGTGCTGAGTGTTGATGATCT
Mus musculus	*Dgat1*	TCCGTCCAGGGTGGTAGTG	TGAACAAAGAATCTTGCAGACGA
Mus musculus	*Hmgcs1*	AACTGGTGCAGAAATCTCTAGC	GGTTGAATAGCTCAGAACTAGCC
Mus musculus	*Mlxipl*	ACTCAGGGAATACACGCCTACAG	TCTTGGTCTTAGGGTCTTCAGGAA
Mus musculus	*Itgax*	ACGTCAGTACAAGGAGATGTTGGA	ATCCTATTGCAGAATGCTTCTTTACC
Mus musculus	*Il1b*	GCAACTGTTCCTGAACTCAACT	ATCTTTTGGGGTCCGTCAACT
Mus musculus	*Tnf*	CCCCAAAGGGATGAGAAGTT	CACTTGGTGGTTTGCTACGA
Mus musculus	*Cxcl10*	CTCAGGCTCGTCAGTTCTAAGT	CCCTTGGGAAGATGGTGGTTAA
Canis lupus familiaris	*Gcgr*	TGCTCTTTGTCGTCCCCTGGG	GTAGGATCCACCAGAACCCC
Canis lupus familiaris	*Acta2*	GCCCCAGACATCAGGGAGTGA	TCGGGTACTTCAAGGTCAGGA
Canis lupus familiaris	*Col1a1*	GCTCCTCTTAGCGGCCACC	TCCATACGTCTCGGTCATAG
Canis lupus familiaris	*Fn1*	ATGTGGACCCCCCCTGAGAGC	GTCCGGTGACTTCCGCGAAGG
Canis lupus familiaris	*B2M*	ATCCACCAGAGATTGAAATTG	GCTAAACTCATCCTGCTCATTG